An organism-wide atlas of hormonal signaling based on the mouse lemur single-cell transcriptome

Shixuan Liu[1, 2, 3], Camille Ezran[2, 3], Michael F. Z. Wang[4], Zhengda Li[1], The Tabula Microcebus Consortium[11], Jonathon Z. Long[5, 6], Iwijn De Vlaminck[4], Sheng Wang[7], Christin Kuo[8], Jacques Epelbaum[9,10], Jeremy Terrien[9], Mark A. Krasnow[2, 3]*, James E. Ferrell, Jr.[1, 2]*

1. Department of Chemical and Systems Biology, Stanford University School of Medicine, Stanford, CA, USA;
2. Department of Biochemistry, Stanford University School of Medicine, Stanford, CA, USA;
3. Howard Hughes Medical Institute, Stanford University School of Medicine, Stanford, CA, USA;
4. Meinig School of Biomedical Engineering, Cornell University, Ithaca, NY, USA;
5. Department of Pathology, Stanford University School of Medicine, Stanford, CA, USA;
6. Stanford ChEM-H, Stanford University, Stanford, Stanford, CA, USA;
7. Paul G. Allen School of Computer Science & Engineering, University of Washington, Seattle, WA, USA;
8. Department of Pediatrics, Stanford University School of Medicine, Stanford, CA, USA;
9. Unité Mécanismes Adaptatifs et Evolution (MECADEV), UMR 7179, CNRS, Museum National d'Histoire Naturelle, Brunoy, France;
10. Unité Mixte de Recherche en Santé 894 INSERM, Centre de Psychiatrie et Neurosciences, Université Paris Descartes, Sorbonne, Paris, France;
11. See the full list of the consortium members and their affiliations at the end of the manuscript.

*Corresponding authors, james.ferrell@stanford.edu, krasnow@stanford.edu

Abstract

Hormones coordinate long-range cell-cell communication in multicellular organisms and play vital roles in normal physiology, metabolism, and health. Using the newly-completed organism-wide single cell transcriptional atlas of a non-human primate, the mouse lemur (*Microcebus murinus*), we have systematically identified hormone-producing and -target cells for 87 classes of hormones, and have created a browsable atlas for hormone signaling that reveals previously unreported sites of hormone regulation and species-specific rewiring. Hormone ligands and receptors exhibited cell-type-dependent, stereotypical expression patterns, and their transcriptional profiles faithfully classified the discrete cell types defined by the full transcriptome, despite their comprising less than 1% of the transcriptome. Although individual cell types generally exhibited the same characteristic patterns of hormonal gene expression, a number of examples of similar or seemingly-identical cell types (e.g., endothelial cells of the lung versus of other organs) displayed different hormonal gene expression patterns. By linking ligand-expressing cells to the cells expressing the corresponding receptor, we constructed an organism-wide map of the hormonal cell-cell communication network. The hormonal cell-cell network was remarkably densely and robustly connected, and included classical hierarchical circuits (e.g. pituitary → peripheral endocrine gland → diverse cell types) as well as examples of highly distributed control. The network also included both well-known examples of feedback loops and a long list of potential novel feedback circuits. This primate hormone atlas provides a powerful resource to facilitate discovery of regulation on an organism-wide scale and at single-cell resolution, complementing the single-site-focused strategy of classical endocrine studies. The network nature of hormone regulation and the principles discovered here further emphasize the importance of a systems approach to understanding hormone regulation.

Introduction

Hormones are chemical messengers that circulate through the bloodstream and control and coordinate functions of both nearby and distant cells. Since the discovery of secretin over a hundred years ago[1], about 100 mammalian hormones have been identified[2]. Over the decades, these hormones have been purified, sequenced, and synthesized, their receptors have been identified, and the intracellular signaling pathways they regulate have been explored[3]. Hormones regulate diverse biological processes ranging from growth and development, reproduction, metabolism, and immune responses, to mood and behavior. Many hormones are also therapeutically significant. For example, the discovery of insulin[4] changed type I diabetes from an inevitably-fatal disease to a manageable one. Likewise, corticosteroids, a class of small molecule adrenal hormones, are used to treat diverse pathological conditions, including the inflammation attendant to COVID-19, where corticosteroids reduce the death rate in severe cases by ~30%[5,6].

The classical endocrine hormones are produced by secretory cells residing in one of the nine endocrine glands. However, it is now clear that other cell types, like fat cells and leukocytes, secrete global regulators into the circulatory system[7]. In addition, some endocrine functions, like menstrual cycles in human females, depend upon the interplay and feedback between multiple hormones and multiple cell types[8]. For these reasons, a complete understanding of endocrine physiology requires comprehensive, global approaches. Variations in hormone regulation and function in different species further complicate the situation. Although comparative studies have shown that many hormones are highly conserved across vertebrates, the hormone-producing and -receiving cells are sometimes rewired for different functions[3].

The grey mouse lemur (*Microcebus murinus*) is a small non-human primate with a lifespan of 5-13 years. Because of its small size, rapid reproduction, and close genetic proximity to humans, the mouse lemur is an appealing model organism for studies of primate biology, behavior, aging, and disease[9–13]. With the advances in single-cell RNA-sequencing (scRNAseq) techniques, we have recently created a molecular cell atlas of the mouse lemur by profiling transcripts from ~225,000 cells from 27 mouse lemur organs and tissues of 4 individuals[14] (https://tabula-microcebus.ds.czbiohub.org/). This organism-wide dataset provides an unprecedented opportunity to study global hormone regulation at single cell resolution in a non-human primate.

In this study, we present a comprehensive analysis of primate hormone signaling based on the information in the mouse lemur molecular cell atlas[14]. We systematically mapped hormone-producing and target cells for 87 hormone classes, and created a browsable atlas that depicts gene expression of hormone ligands, modulators, and receptors. This systematic analysis detected both canonical and unreported sites of hormone secretion and action, and identified several examples of species-specific rewiring. We also analyzed the global expression patterns of hormone ligands and receptors, constructed and characterized an organism-wide cell communication network for hormone signaling, and systematically searched the network for feedback circuits. This analysis revealed a few remarkable principles of hormone signaling and a long list of potentially novel feedback mechanisms.

The hormone atlas provides a useful resource and a general approach to study hormone regulation on an organism-wide scale and at single-cell resolution, complementing the more reductionistic strategies typical in classical endocrine studies. The network nature of hormone

regulation and principles discovered here further emphasize the importance of a systems approach in understanding hormone regulation.

Results

A comprehensive table of genes involved in the biosynthesis and sensing of human and mouse lemur hormones

Although many hormones have been studied for decades, there is not a well-annotated database of hormone ligands, synthases, processing enzymes, and receptors. Therefore, we integrated multiple sources to compile a comprehensive gene table for human hormone signaling (**Table 1**). For the hormone list, we mainly referenced the *Handbook of Hormones*[2], the Wikipedia *List of human hormones*, and the *Handbook of Biologically Active Peptides*[15], and added newly discovered hormones including asprosin[16] and the endocrine fibroblast growth factors FGF21, FGF19, and FGF23[17]. To collect the genes involved in hormone production, we manually assembled the ligand genes for peptide and protein hormones and the hormone synthesis genes for small molecule hormones. Maturation or activation of many hormones requires specific enzymes such as angiotensin-converting enzyme (ACE) for angiotensin, the deiodinases DIO1/2 for thyroid hormones, and prohormone processing enzymes (e.g., PCSK1, PCSK2, CPE) for many peptide hormones[15]. In addition, hormone function may involve endocrine modulators such as IGF binding proteins (IGFBPs) for IGF1/2. Accordingly, we added these processing enzymes and modulators for the corresponding hormones. Next, we collected the hormone receptor genes that are responsible for signaling in the target cells. We searched ligand-receptor databases[18,19] for the receptor genes of protein and peptide hormones, and manually added the receptor genes for the small molecule hormones. Most hormones have characterized ligands and receptors with a few exceptions in which the genes remain unidentified (e.g., endomorphin ligand and irisin receptor). In total, we collected information for 87 groups of hormones including 106 ligand genes, 38 synthases, 24 processing enzymes/modulators, and 164 receptor genes.

When a hormone group included multiple ligand, receptor, synthase, or processing enzyme genes, we incorporated AND/OR logic gates among the genes (**Table 1**). Sometimes two or more of the genes were required for signaling; this AND gate logic was designated by an ampersand (&). For example, amylin receptors are heterodimeric complexes of CALCR and RAMP proteins, and both subunits are required for function; thus, CALCR and RAMP were connected by an AND symbol. Similarly, AND gates were applied among hormone synthases that catalyze different steps, and between hormone ligands and the corresponding processing enzymes. On the other hand, some receptor subtypes function independently. For example, there are nine different adrenergic receptor genes, and none of these receptors require any of the others for function. Genes like these were linked by OR gates, designated by a vertical line (|).

We next looked up the mouse lemur orthologs of the human hormone genes in the most up-to-date mouse lemur genome assembly (Mmur_3.0) with both NCBI and Ensembl ortholog databases (**Table 2**). Almost all (99.1%, 329/332) of the human hormone-related genes were annotated in the mouse lemur genome. The three genes without mouse lemur orthologs (LHB,

136 GALP, and INSL4) may result from incomplete annotation of the mouse lemur genome. For
137 example, LHB encodes the beta subunit of luteinizing hormone, which is thought to be expressed
138 in the gonadotrophs of the pituitary gland across all vertebrates. The mouse lemur atlas includes
139 a small number of gonadotrophs that might be expected to express the LHB transcripts.
140 Therefore, we searched for transcripts expressed in the gonadotrophs and identified a candidate
141 gene region[20], currently unannotated in NCBI and Ensembl, with high sequence similarity to
142 human and macaque LHB. The putative LHB region is located next to the RUVBL2 gene, as in
143 humans and mice[21]. The gene region also is selectively expressed in the expected cell type,
144 gonadotrophs (**Fig. S1-luteinizing hormone**). We therefore conclude that the identified region is
145 a likely candidate of the mouse lemur LHB gene. For GALP and INSL4, the atlas lacked the
146 tissue or cell type that is known to express the genes. INSL4, a primate-only paralog of relaxin,
147 is expressed by the placenta in humans[22]. GALP was reported to be secreted by certain
148 hypothalamic neurons[2]. Neither the placenta nor the hypothalamic neurons were surveyed in the
149 mouse lemur cell atlas[14]. Thus, taken together, at least 330/332 (99.4%), and possibly all, of the
150 human hormone-related genes are present in the mouse lemur. For comparison, the mouse
151 genome lacks five human hormone-related genes (98.5% present, 327/332), and four are known
152 to have been lost (GNRH2, MCHR2, MLN, MLNR) (**Table 2**). The percentages of human
153 hormone-related orthologs present in mouse lemur or mouse genomes were higher than the
154 percentage of protein-coding genes (>99.1% vs. 89.5% in the mouse lemur genome, and 98.5%
155 vs. 89.8% in the mouse genome). Most (86.3%) human hormone-related proteins were more
156 similar in sequence to their mouse lemur orthologs than their mouse homologs (**Fig. S2**). These
157 findings underscore the close relationship between human and mouse lemur hormone-related
158 genes.

159

160 **Organism-wide identification of hormone-producing and target cells**

161 We systematically identified the source cells and target cells for the 87 known hormone groups
162 by examining the expression of genes involved in hormone synthesis and sensing across 739 cell
163 types profiled by 10x droplet-based single cell RNA sequencing from 27 different tissues
164 included in the mouse lemur cell atlas[14]. Source cells were defined as cell types with positive
165 expression of the ligand (for protein/peptide hormones) or synthase(s) (for small molecule
166 hormones) and any necessary modulator genes. Target cells were defined as the cell types with
167 positive expression of the hormone receptor genes. We generated a browsable set of figures that
168 depict the global expression profiles of the hormone-related genes for each of the 87 hormone
169 groups as well as one set of figures for prohormone processing enzymes and one for endocrine
170 secretory proteins (**Fig. S1**). **Fig. 1** shows the cell-type specific expression of four representative
171 examples of hormones (in red) and their receptor(s) (in blue) across the five, color-coded cell
172 compartment types (1. epithelial/neural/germ cells; 2. endothelial cells; 3. stromal cells; 4.
173 lymphoid cells; and 5. myeloid cells). This systematic review identified many canonical sites of
174 hormone secretion and targets, affirming the validity of the single-cell transcriptomic
175 measurements and analysis approach. The analysis also revealed many less-recognized or
176 unreported hormone source/target cells and interesting global patterns of hormone signaling.
177 Below, we highlight a few examples of well-known, lesser-known, and previously unknown
178 sources and target cells. We also showcase examples where hormone signaling is likely rewired
179 in the mouse lemur versus humans or mice.

180 **Prolactin (PRL).** The first example is a classical endocrine hormone, prolactin. Prolactin was
181 one of the first hormones discovered[23] and has been studied in depth over the decades. Prolactin
182 is secreted by the lactotrophs of the anterior pituitary gland, the master endocrine organ.
183 Although prolactin was originally regarded as a female-specific hormone that promotes milk
184 secretion, it is now clear that prolactin plays pleiotropic roles in both sexes[2]. These roles include
185 regulation of water and electrolyte balance in the kidney, and control of skin cell proliferation
186 and hair/feather growth and shedding[24]. Prolactin also plays a major role in energy homeostasis
187 by regulating cell growth and metabolism in the liver, adipose tissues, and pancreas in both
188 sexes[25], and may be involved in the immune response[26]. These sex-non-specific functions are
189 conserved, not just among milk-producing mammals, but across all vertebrates.

190 As expected, prolactin transcripts were selectively expressed in the lactotrophs of the mouse
191 lemur pituitary gland, and were not detected in other tissues (**Fig. 1, Fig. S1-prolactin**). The
192 prolactin receptor (PRLR) was found in both male and female lemurs in the expected cell types,
193 including kidney nephron tubule cells, skin epithelial cells, pancreatic ductal and acinar cells,
194 hepatocytes, intestinal epithelial cells, adipocytes, reticular cells, plasma cells, choroid plexus
195 cells, and the neighboring TSH-secreting thyrotrophs and FSH/LH-secreting gonadotrophs in the
196 pituitary gland (**Fig. 1, Fig. S1-prolactin**). Thus, single-cell RNA sequencing confirms that
197 prolactin signaling is similar in mouse lemurs and other animals.

198 **Adiponectin (ADIPOQ) and leptin (LEP).** Mouse lemurs undergo dramatic seasonal changes
199 in body weight and fat reserves[27–29]. Adipocytes were originally regarded only as nutrient storage
200 cells, but it is now clear that they also serve an endocrine role[30]. Adiponectin and leptin are two
201 important metabolic hormones secreted by adipocytes[31,32]. Surprisingly, leptin transcripts were
202 almost undetectable in the adipocytes captured in the atlas (see detailed discussion in the
203 accompanying Tabula Microcebus manuscript 2) (**Fig. S1-leptin**).

204 However, adiponectin was abundantly and specifically expressed in mouse lemur adipocytes
205 captured from multiple tissues, including four adipose depots (subcutaneous, mesenteric,
206 interscapular brown, and perigonadal), as well as kidney, limb muscle, pancreas, and bone (**Fig.**
207 **1**, **Fig. S1-adiponectin**). Both UCP1-low white-like and UCP1-high brown-like adipocytes
208 highly expressed ADIPOQ.

209 Previous research has characterized tissue-specific functions of adiponectin in the liver,
210 pancreas, skeletal muscle, endothelial cells, macrophages, and adipocytes[33]. While we indeed
211 observed expression of the adiponectin receptor ADIPOR1 in these tissues in the mouse lemur,
212 we also found ADIPOR1 to be abundantly expressed in almost all lemur cell types (**Fig. 1**). The
213 ubiquitous expression of this receptor suggests that adiponectin exerts an organism-wide effect
214 through ADIPOR1.

215 In comparison, ADIPOR2, the other adiponectin receptor, was expressed more selectively, most
216 notably in the male germ cells and adipocytes. Interestingly, the mouse lemur expression pattern
217 of ADIPOR2 differs from that of the mouse in which ADIPOR2 is reported to be most highly
218 expressed in the liver and almost undetectable in the testis[34], suggesting differential ADIPOR2
219 effects in the two species.

220 **Motilin (MLN).** Comparing expression patterns of the mouse lemur to that of the mouse and
221 human, we identified interesting cases of hormone network rewiring. A telling example is

motilin, canonically considered to be a gastrointestinal hormone secreted by enteroendocrine cells to regulate gastrointestinal smooth muscle movement[15]. Mice lack both the motilin and the motilin receptor genes (**Table 2**). Indeed, genome comparative studies reported that motilin signaling is conserved in vertebrates but is lost in rodents[35]. The lack of motilin signaling in mice and rats has hampered progress on further characterizing motilin function as well as the development of motilin agonists for the treatment of gastroparesis[36]. In the mouse lemur, we observed motilin expression in enteroendocrine cells in the small intestine but not colon (**Fig. 1A**), which is consistent with the canonical view. However, there was also a broad range of other motilin-expressing cell types, including kidney nephron tubule cells, chemosensory tuft cells from both the airway (lung and trachea) and small intestine, certain brain neurons, adipocytes (higher in UCP1-high brown-like adipocytes than in white-like adipocytes), mesothelial cells, and the majority of the CD4+CD8-CCL5- helper T cells (**Fig. 1**, **Fig. S1-motilin**). The receptor was found to be most highly expressed in pancreatic delta cells and several epithelial cell types of the skin (e.g., sweat gland cells). Together, this expression pattern suggests that motilin is involved in a diverse array of mouse lemur physiological functions in addition to the regulation of gut motility.

Resistin (RETN). We also noted interesting species differences in resistin signaling. Resistin is a phylogenetically recent hormone, present only in mammals[2]. It is expressed mainly by adipocytes in mice but by macrophages, monocytes, and neutrophils in humans[37,38]. In the mouse lemur, we found that resistin is highly expressed in macrophages, monocytes, and neutrophils, and nearly absent from adipocytes (**Fig. 1, Fig. S1-resistin**), as it is in humans. Interestingly, resistin is also highly expressed in many of the vascular endothelial cell types and in metastatic uterine tumor cells, suggesting additional sources for this hormone.

Prohormone processing enzymes. Prohormone processing enzymes are required for the maturation of many peptide hormones, including insulin, adrenocorticotropic hormone (ACTH), gastric inhibitory polypeptide (GIP), and somatostatin[15]. The required processing enzymes have been identified for some but not all hormones[39,40]. In this study, we considered both the ligand and the known or suggested processing enzymes when determining if a cell type was a hormone source. Selective expression of the processing enzymes can help distinguish hormones that share the same precursor gene. For example, proglucagon (GCG) is the precursor for both glucagon and glucagon-like peptide-1 (GLP-1). GCG was expressed in both pancreatic α cells and intestinal enteroendocrine cells, but the two cell types expressed different processing enzymes: α cells expressed only PCSK2 which is required for glucagon synthesis, and enteroendocrine cells expressed only PCSK1 which is required for GLP-1 synthesis (**Fig. S1-glucagon**). Thus, as is the case in mice and humans [41], α cells are sources of glucagon and enteroendocrine cells are sources of GLP-1 in the mouse lemur.

Interestingly, we noticed that some cell types in the mouse lemur transcribed prohormone genes without expressing the respective processing enzymes. For example, proopiomelanocortin (POMC) is the precursor of multiple hormones including ACTH, melanocyte-stimulating hormone (MSH), β-endorphin, and lipotropin, and the first step in POMC processing is carried out by PCSK1[42]. As expected, ACTH-secreting corticotrophs expressed both POMC and the necessary processing enzymes, but mouse lemur male germ cells expressed abundant POMC without PCSK1 (**Fig. S1-proopiomelanocortin-derived hormones**). Similarly, male germ cells expressed GIP, which also requires PCSK1 processing. We also found renin (REN) expression in

266 the intestinal and airway tuft cells without the necessary PCSK1, oxytocin (OXT) expression in
267 kidney proximal tubule epithelium without the required carboxypeptidases E (CPE), and
268 neuropeptide Y (NPY) expression in bladder urothelial cells without the necessary CPE (**Fig.**
269 **S1**). These results suggest several possible hypotheses: different peptidases are involved, the
270 prohormone transcripts are not translated, the prohormone proteins may function without
271 proteolysis, or the processing enzymes may be expressed below detection levels in the animals
272 that were sampled.

273 In summary, we have depicted the organism-wide, single-cell expression patterns for hormones,
274 synthases, hormone modulators, and receptors from 87 hormone groups, and have systematically
275 identified their sources and targets (**Fig. S1**). This global analysis detected canonical cell types
276 underlying hormone secretion and target functions while also revealing previously unreported
277 sources and targets. This organism-wide single-cell hormone atlas should facilitate the
278 systematic study of hormone regulation in an unbiased, global manner, paving the way for the
279 discovery of novel aspects of hormone regulation and function.

280

281 **Hormone-related gene expression faithfully classifies cell type**

282 Next, we clustered mouse lemur cell types based on the transcriptional profiles of only the
283 hormone-related genes (**Fig. 2A-B**). We organized the cell types into 75 clusters and summarized
284 the hormones and hormone receptors that were expressed in the majority of the cell types for
285 each cluster in **Table 3**. We noted that cells of the same type almost always clustered closely
286 irrespective of their tissue of origin, and different cell types were well-separated in the cluster
287 dendrogram (**Fig. 2A**). For example, all lymphatic endothelial cells clustered closely and showed
288 characteristic IGF1 expression despite their coming from nine different tissues and four
289 individuals (cluster 53, **Fig. 3B**, **Fig. S1-insulin-like growth factor, Table 3**). Schwann cells
290 from nine tissues clustered into myelinating and non-myelinating subtypes (cluster 40 and 37).
291 Adipocytes sampled from four adipose depots and six other tissues formed one cluster (cluster
292 13, **Table 3**). Skeletal muscle stem cells from the limb muscle and tongue clustered together
293 (cluster 17, **Table 3**). Mesothelial cells sampled from eight visceral organs formed a cluster
294 distant from other stromal cells and showed distinctive expression of NPR1, CFB, PTGIS,
295 ITGB3, and PNMT (cluster 44, **Fig. 2A-B, Fig. S4A, Table 3**). Although the analysis only
296 examined the transcripts of 329 hormone-related genes, ~1% of all detected genes, these results
297 suggest that hormone-related gene expression is indicative of the overall transcriptome among
298 different cell types.

299 To further test this hypothesis, three comparative analyses were performed. First, we projected
300 the high-dimensional transcriptional profiles of the mouse lemur cell types into two-dimensional
301 uniform manifold approximation and projection (UMAP) representations, which illustrate cell
302 type similarity in the space of the selected genes. We compared the spatial relationship of cell
303 types in two UMAPs: one constructed based on only the 329 hormone-related genes (**Fig. 2B**),
304 the other based on all genes excluding the hormone genes (>30,000 genes) (**Fig. S3**). In each
305 case, the data points represent cell types rather than individual cells (**Fig. 2B, Fig. S3, Fig. S4**).
306 The two UMAPs showed remarkable similarity and cell types were similarly clustered with only
307 minor differences (see **Fig. S4C** for comparison). One such difference was the chemosensory tuft
308 cells that reside in the epithelium of both the airway (lung, trachea) and small intestine. In the

space of hormone-related genes, tuft cells from all three tissues formed a cluster (cluster 21) with distinctive expression of renin (REN), cyclooxygenase 1 (PTGS1), arachidonate 5-lipoxygenase-activating protein (ALOX5AP, required for leukotriene production), and motilin (MLN) (**Fig. 2B, Fig. S1, Table 3**). However, in the space of all genes, the lung, trachea, and intestinal tuft cells were separated from each other (labeled as 21*A, 21*B, and 21*C in **Fig. S3**). Another notable exception was skin melanocytes (cluster 38), which clustered closely with oligodendrocytes (cluster 39) when using only the hormone-related genes (**Fig. 2B**) but clustered with skin epithelial cell types (cluster 36) in the space of all genes (**Fig. S3**). These differences notwithstanding, the hormone-gene and transcriptome-based cell type UMAPs were qualitatively similar and shared an overall clustering pattern.

We then compared the transcriptional distances between pairs of cell types for either just the hormone-related genes (hormone-based distances) or the non-hormonal transcriptome (transcriptome-based distances) (**Fig. 2C, Fig. S5A-B**). The two distances were positively correlated, with a Pearson correlation coefficient (r) of 0.70 (p < 1E-15). Similarly, we compared hormone-based transcriptional distances between pairs of cell types to a Cell Ontology-based distance. Cell Ontology distances represent a canonical view of the relatedness of cell types[43] and were calculated as the mean of the Cell Ontology embedding-based distances from the Cell Ontology graph and the text-based distances from the text descriptions of the Cell Ontology terms[44]. These two distances were also significantly correlated, with r=0.45 (p < 1E-15) (**Fig. 2D, Fig. S5A and C**). Taken together, these analyses support the notion that the small number of hormone-related genes faithfully classifies most of the cell types of the mouse lemur.

We then examined if the expression of hormone ligands or receptors alone could distinguish cell types (**Fig. S4**). Interestingly, for most cell type clusters, hormone ligands or receptors alone classified cell types similarly. This suggests that most cell types have stereotypical expression of proteins involved in both incoming and outgoing hormonal signaling. A small fraction of clusters were segregated from other clusters mainly by only the ligands or receptors. For example, clusters of pituitary neuroendocrine cells (cluster 7) and tuft cells (cluster 21) are distinguished mainly by hormone ligands, whereas clusters of the skeletal muscle stem cells (cluster 17) and lung endothelial cells (cluster 51) are mostly based on differences in hormone receptor expression.

In summary, we found that cells generally show stereotypical and cell-type-specific expression of hormone ligands and receptors. Thus, hormone secretion and sensing essentially labels the identity of the cells.

Hormonal regulation nevertheless does sometimes differ in related cell types

Although cells of the same type tended to have similar hormonal expression patterns, we identified a number of interesting exceptions where closely related cell types differed in their hormone signaling. Below we highlight several such examples in which we identified changes in hormonal signaling among cells at different development stages (spermatogenesis), cells from different tissue origins (vascular endothelial cells), cell types that are not discretely segregated but form a continuous gradient (kidney nephron and vasa recta), cells of different molecular subtypes (hepatocytes), and primary vs. metastatic tumor cells (**Fig. 3**).

351 **Spermatogenesis.** Spermatogenesis is a tightly regulated process that happens asynchronously
352 and continuously in the male testis[45]. Therefore, sampling the testis at one fixed time point can
353 capture snapshots of the entire process. The atlas includes seven sperm and sperm progenitor cell
354 types that are at different spermatogenesis stages as indicated by the expression of known stage
355 markers[14]. Interestingly, these cells exhibited spermatogenesis-stage-dependent hormone
356 signaling (**Fig. 3A**). The seven cell types fall into three major stages: the undifferentiated
357 spermatogonia, the spermatocytes (which undergo meiosis), and the haploid spermatids that
358 elongate and form mature sperms. Comparing hormone-related gene expression among these
359 three major stages (cluster 1, 2, 8), over 50 hormone ligands, enzymes, and receptors were
360 differentially expressed (**Fig. 3A**), suggesting an extensive shift in hormone signaling. Previous
361 studies on spermatogenesis have mainly focused on testosterone and on the supporting cells
362 rather than sperms and sperm progenitors[46,47]. The present data suggest that sperms and sperm
363 progenitor cells are not only differentially regulated by a variety of hormones but may also
364 secrete a changing array of signaling molecules as they mature. Some of these molecules have
365 been recently suggested to be involved in sperm functions. For example, progesterone was
366 known to activate a sperm-specific calcium channel prior fertilization to induce Ca^{2+} influx, but
367 the underlying progesterone receptor(s) remained unidentified[48]. Two non-classical progesterone
368 membrane receptors (PAQR5/9) were highly expressed in the lemur spermatids and therefore
369 may mediate the process (**Fig. 3A**). Interestingly, two additional membrane progesterone
370 receptors (PAQR8, PGRMC1) were specifically expressed in the undifferentiated spermatogonia
371 (**Fig. 3A**), suggesting that they may contribute to regulation of early spermatogenesis by
372 progesterone[49]. Insulin-like factor 6 (INSL6), a member of the secretory relaxin family, was
373 selectively expressed in the lemur spermatocytes (**Fig. 3A**). Supporting a function in these cells,
374 knockout of INSL6 arrests spermatogenesis at late meiotic prophase in mice[50]. This analysis
375 suggests that sperms and sperm progenitor cells may be directly engaged in hormone signaling
376 with surrounding and potentially distant cells to affect spermatogenesis and sperm functions.

377 **Vascular endothelium.** Endothelial cells, including artery, vein, capillary, and lymphatic cells,
378 line the surface of the circulatory system and are all derived from a developmentally uniform
379 lineage[51]. The mouse lemur cell atlas includes a large number of endothelial cells captured from
380 different organs, providing an opportunity for cross-organ comparison. Although vascular
381 endothelial cells in general shared similar transcriptional profiles (**Fig. 2A-B, Fig. S3**), the lung
382 and brain vascular endothelial cells exhibited unique hormone signaling signatures (**Fig. 3B**).

383 Endothelial cells of artery, vein, and capillary in the mouse lemur lung showed higher expression
384 of hormone receptors VIPR1, CALCRL, and RAMP1 (**Fig. 3B**) compared to endothelial cells
385 from other organs. VIPR1 is a receptor for vasoactive intestinal peptide (VIP), a strong
386 bronchodilator and one of the most abundant signaling peptides in the lung[52]. Similar expression
387 of VIPR1 is also observed in human but not mouse lung endothelial cells[53,54]. RAMP1 forms
388 heterodimeric receptors with CALCR or CALCRL that are regulated by several hormone ligands
389 including CGRP, adrenomedullin, amylin, and calcitonin, all of which have been reported to
390 have vasodilatory effects[2]. Interestingly, RAMP1 is expressed in the lung endothelium of the
391 mouse lemur but not in mice or humans, whereas RAMP2 is expressed in all three species and
392 RAMP3 is only expressed in humans (**Fig. S1-adrenomedullin**)[53,54] (also see accompanying
393 Tabula Microcebus manuscripts 1[14] and 2). These results suggest that lung vascular endothelium
394 is a unique hormonal target in comparison to vasculature elsewhere, possibly because of the
395 distinctive nature of the pulmonary circulation (e.g., high volume, low pressure) compared to the

396 systemic circulation. The lung endothelium also shows species variation in the hormone
397 signature, perhaps reflecting the relatively recent appearance of lungs in evolution compared to
398 other visceral organs.

399 In contrast, brain vascular endothelium was found to express higher levels of a few hormone
400 ligands/synthases. Endothelin-3 (ET-3), a member of the vasoconstricting endothelin family, was
401 selectively expressed in the brain vascular endothelium (**Fig. 3B**). ET-3 peptide has been
402 detected at various brain locations in rodents, but it remained unsettled what cells secreted the
403 peptide and what physiological role it played[55]. Our results suggest that ET-3 is synthesized by
404 the endothelial cells in the brain, which could target the nearby EDNRB-expressing SLC7A10+
405 astrocytes and the EDNRA-expressing vascular smooth muscle cells and pericytes of the brain
406 (**Fig. S1-endothelin**). Additionally, the brain endothelium also expressed high levels of PTGES
407 and PTGS2/COX-2 (**Fig. 3B**), which are the synthases for prostaglandin E2 (PGE2). PGE2 has
408 been suggested to regulate inflammation-induced fever in mice[56,57]. Interestingly, brain
409 endothelial cells also selectively lacked expression of IGFBP4, which was abundantly expressed
410 in the endothelium of all other tissues (**Fig. 3B**).

411 The expression of the detected hormone signature genes (RAMP1, CALCRL, and VIPR1 in
412 lung, and EDN3, PTGES, and PTGS2 in the brain) was higher in endothelial cells than other cell
413 types from the same organ (**Fig. S1**). Thus, it is unlikely that these organ-specific endothelial
414 expression patterns resulted from cross-contamination (signal spreading). Altogether, lung and
415 brain endothelial cells exhibited organ-specific hormone signaling which likely regulates organ-
416 specific physiological functions.

417 **Kidney nephron and vasa recta.** Although discrete cell types were common in the mouse lemur
418 cell atlas, there were clear examples of spatially continuous cell types that displayed a continuum
419 of gene expression. These were the kidney nephron epithelium and the vasa recta endothelium[14],
420 and these cells also displayed gradients of hormone signaling along their spatial axes (**Fig. 3C-**
421 **D**).

422 Nephrons are single-cell layered, one-directional tubules that serve as the structural and
423 functional units of the kidney. We identified a large number of hormone-related genes that are
424 specific to different sections of the nephron epithelium (**Fig. 3C**). Some of these hormones target
425 specific nephron sections to regulate urine formation. For example, vasopressin is well known
426 for its antidiuretic effect, promoting water reabsorption in the collecting duct principal cells[2].
427 Indeed, the vasopressin receptor AVPR2 was expressed exclusively in the collecting duct
428 principal cells. Interestingly, the collecting duct intercalated cells expressed another vasopressin
429 receptor, AVPR1A (**Fig. 3C**), which has been recently reported to mediate the regulation of acid
430 homeostasis by vasopressin[58]. Although the kidney epithelium is not commonly considered to be
431 an endocrine tissue, many hormone ligands/synthases were also expressed in different nephron
432 sections, including angiotensin (AGT), adrenomedullin 2 (ADM2), motilin (MLN), and
433 neuropeptide Y (NPY). This suggests that nephron epithelium may play multifaceted roles in
434 hormone production in addition to urine formation.

435 We also identified interesting differences in hormone signaling in the vascular endothelium of
436 different regions of the mouse lemur kidney. In particular, we identified a gradual shift in
437 hormone signaling along the arteriole-to-venule-axis of the vasa recta endothelium (**Fig. 3D**).

438 The vasa recta align parallel to the nephron tubules in the kidney medulla and function
439 collaboratively with the nephrons in urine formation[59]. **Fig. 3D** shows the hormone-related genes
440 that are significantly differentially expressed along the vasa recta axis. Notably, several genes
441 involved in IGF signaling were differentially expressed: IGF1, which was expressed in the
442 lymphatic endothelial cells but almost absent from other vascular endothelial types (**Fig. 3B, Fig.**
443 **S1-IGF**), was highly expressed at the venule end of the vasa recta; IGF2 and IGF1R exhibited
444 the opposite pattern with higher expression in the arteriole end; and four IGFBPs (IGFBP3-6),
445 which modulate IGF signaling, exhibited axis-dependent expression patterns. This spatial
446 organization of IGF signaling may be evolutionarily conserved, as a recent study on mouse
447 kidney vasculature development shows a similar pattern of IGF1 expression in the mouse vasa
448 recta[60].

449 **Hepatocyte subtypes.** The mouse lemur cell atlas identified multiple novel molecular subtypes
450 of known cell types[14]. For example, the liver hepatocytes of the mouse lemur clustered into two
451 discrete subtypes, APOB+ hepatocytes and PHYH+ hepatocytes. These two hepatocyte subtypes
452 are likely independent of the known zonal heterogeneity, and a similar subtype division was
453 observed in mouse hepatocytes[14]. Interestingly, a number of hormone-related genes were among
454 the most highly differentially expressed genes in the two hepatocyte subtypes in both the mouse
455 lemur and mouse (**Fig. 3E**)[14]. Hormones including glucagon, androgens, and prolactin appear to
456 selectively target the APOB+ hepatocytes as indicated by differential expression of the
457 corresponding receptors (GCGR, AR, PRLR). In addition, angiotensin (AGT), a canonical
458 hepatic hormone, was expressed at a much higher level in the APOB+ hepatocytes, whereas no
459 subtype difference was detected in the expression of hepcidin (HAMP) or IGF1, two other
460 hormones abundantly produced by the liver. Hepatocytes are known to show sex-dependent
461 hormone regulation[61]; however, the subtype differences in hormone gene expression were not
462 sex-dependent (**Fig. S6**).

463 Liver is a central organ of metabolism and plays important roles in hormonal regulation. The
464 detected heterogeneity in hormone signaling suggests potentially important functional
465 divergence between the hepatocyte subtypes in both the mouse lemur and mouse. A deeper
466 understanding of the mechanisms and regulation of hepatocyte hormone heterogeneity would be
467 particularly relevant to the study of mouse lemur-specific physiology, like hibernation/torpor and
468 seasonal body weight changes[28].

469 **Metastatic vs. primary tumor cells.** The atlas also contains cells that are pathologic, including
470 cells from the lung tissue of one female mouse lemur that were hypothesized by gene signature
471 analysis and confirmed by histology to be metastatic tumor cells of endometrial cancer origin
472 (also see accompanying Tabula Microcebus manuscripts 1[14] and 2). The tumor cells clustered
473 with the epithelial cells of the uterus from a second female individual (also, as it happened, with
474 confirmed endometrial cancer), particularly the MUC16+ non-ciliated uterus epithelial cells
475 which are likely primary tumor cells according to signature gene expression (see accompanying
476 Tabula Microcebus manuscript 2). The metastatic and primary tumor cell types shared
477 characteristic expression of oxytocin receptor (OXTR) and inhibin beta B subunit (INHBB) (**Fig.**
478 **3F, Fig. 2A-B, Fig. S3, Table 3**), suggesting that the metastatic tumor in the lung originated
479 from cells resembling the primary MUC16+ uterine tumor cells. However, certain aspects of
480 hormone signaling were likely to have been rewired in the metastatic tumor (**Fig. 3F**). Notably,
481 the tumor cells showed a loss of estrogen receptors (ESR1), a change associated with high grade

482 and advanced stage endometrial cancers in humans[62] and more often reported in high mortality
483 type 2 human endometrial cancers[63].

484 Interestingly, the metastatic tumor cells also acquired new abilities in hormone production. For
485 example, elevated expression of prostaglandin E2 synthase (PTGES2) was present in metastatic
486 cells (**Fig. 3F**). PGE2 has been suggested to be a tumorigenic factor in many cancers[64]. A recent
487 study identified that the PGE2 synthase PTGES2 was elevated in human endometrial cancer
488 tissues and found that PGE2 promotes cell proliferation and invasion in *in vitro* cell assays[65].
489 Resistin was also found to be highly expressed in the metastatic cells (**Fig. 3F**). Resistin has been
490 reported to promote invasiveness of breast cancer cells *in vitro*[66]. Thus, endometrial tumors may
491 utilize autocrine resistin signaling to promote metastasis. The shift in hormone signaling
492 identified in the lemur metastatic endometrial tumor is similar overall to that reported in the
493 human. This suggests that the rewiring of hormone signaling may be an important step in tumor
494 development and metastasis. Mouse lemurs may serve as a useful animal model to study human
495 cancers that are not well modeled in mice such as endometrial cancers (see more in
496 accompanying Tabula Microcebus manuscript 2).

497 In summary, we have highlighted five examples where closely related cells differ in their
498 hormone signaling. These closely related cells usually share the same developmental origin but
499 diverge during cell differentiation or development. Cells likely undergo changes in hormone
500 signaling during the process to interact with other cells and accommodate their specific
501 functional requirements.

502

503 **The hormonal cell communication network is densely connected**

504 Long-range hormonal signaling connects both nearby and distant cells through the bloodstream
505 and enables cross-organ communication. By linking the source cells that produce a hormone
506 ligand to the target cells that express the corresponding receptor, we constructed a global cell
507 communication network for mouse lemur hormone signaling (**Fig. 4A**). Nodes of the network are
508 cell types and edges are directed from hormone source to target cells.

509 The hormone network was remarkably densely connected; 51% of all possible directed edges
510 were found to be present. In fact, in the graphical depiction of the network (**Fig. 4A**), individual
511 edges are hardly distinguishable because the edges are so dense. The density of the hormone
512 network is comparable to that of the cytokine network[67], but much higher than the densities of
513 other characterized biological networks. For example, the network densities of the yeast, fly, and
514 human protein-protein interaction networks are all estimated to be ~0.1%[68–70], and the yeast
515 genetic interaction network density is ~3%[71]. The dense connection between cell types by
516 hormonal regulation is also highly robust: 67% of all existing edges are connected by more than
517 one ligand-receptor pair, and the network maintains high density connection when randomly
518 removing 10% of the ligand-receptor pairs (**Fig. S7A**).

519 The density of the hormone network is largely due to the fact that multiple hormone ligands and
520 receptors are expressed in most cell types (**Fig. 4B**). On average, cell types expressed 17.0 ± 7.9
521 (mean ± S.D.) receptors or receptor complexes. In comparison, fewer hormone ligands were

522 expressed (2.8 ± 2.5, mean ± S.D.). Only a few cell types expressed 10 or more hormone ligands
523 (e.g., enteroendocrine cells, pancreatic endocrine cells, certain neurons, and certain fibroblasts),
524 and 38.3% of cell types expressed a single ligand or no ligand. This indicates that cells in general
525 respond to more hormones than they produce.

526 The five neuroendocrine cell types of the anterior pituitary—corticotrophs, thyrotrophs,
527 gonadotrophs, lactotrophs, and somatotrophs—play a vital role in endocrinology. These cells are
528 components of regulatory cascades, and classically they are regarded as receiving regulatory
529 signals from one or a few hormones produced in the hypothalamus, and in turn producing one or
530 a few hormones to regulate a peripheral endocrine gland. Yet even these cells were found to
531 express numerous receptors, ranging from 17 (corticotrophs) to 29 (gonadotrophs and
532 somatotrophs) (**Table 4**). These cells appeared to be regulated by growth factors, neuropeptides,
533 peripheral and classical hypothalamic hormones, as well as neurotransmitters (e.g., dopamine)
534 that were not on our hormone list. Likewise, they were found to express genes for several
535 hormones in addition to the classical hormones (**Table 4**). For example, corticotrophs expressed
536 galanin (GAL), gastrin (GAS), and cortistatin (CORT), as well as the ACTH precursor (POMC)
537 and its processing enzymes PCSK1, PCSK2, and CPE.

538 Taken together, this analysis suggests that virtually all cell types across the body are extensively
539 engaged in cell communication via hormonal signaling and that the connections are likely
540 evolutionarily robust to random mutations that disturb hormone regulation. The dense connection
541 of the network resulted in a large number of highly connected nodes and no obvious network
542 cores (**Fig. 4A, Fig. S8**). This differs from the commonly studied scale-free networks, which are
543 dominated by a small number of highly-connected hub nodes[72]. Studies on hormone regulation
544 usually focus on one specific site of secretion and/or target; our analysis emphasizes the
545 importance of a systems view in understanding hormone regulation.

546

547 **A small number of hormones are global regulators**

548 We next examined properties of the hormone network edges. In contrast to the protein-protein
549 interaction network and the genetic interaction network, the edges of the hormone
550 communication network are directional and can be distinguished into different types according to
551 the specific ligand-receptor pairing. The hormone network contained 332 different edge types
552 that are selected pairings of 128 ligands and 166 receptors. A ligand or receptor may contain
553 multiple genes as required for ligand synthesis/maturation and in receptor complexes (see **Table**
554 **1**).

555 Some ligands and receptors were expressed in highly specific cell types while others were more
556 broadly expressed. We therefore quantified for each ligand or receptor a generality score to
557 evaluate the range of its expression across different cell types in the atlas (**Fig. 4D-E, Fig. S9,**
558 **Table 5**). Strikingly, a small number of hormone receptors were globally expressed. For
559 example, the top ranking receptor, adiponectin receptor 1 (ADIPOR1), was expressed in 93.4%
560 of the cell types. Other broadly expressed hormone receptors included the renin receptor
561 ATP6AP2 (90.4%), the membrane-associated progesterone receptor PGRMC1 (84.1%), the
562 cortisol receptor NR3C1 (73.7%), the resistin receptor CAP1 (72.9%), the IGF1 receptor IGF1R

563 (69.5%), the opioid growth factor receptor OGFR (65.9%), and the thyroid hormone receptor
564 THRA in complex with RXRB (54.3%). While it has been recognized that some of these
565 hormones exert organism-wide effects, our results suggest that they target not only a broad range
566 of tissues but likely regulate a large portion or perhaps majority of the cells of the body.

567 In comparison, most hormone ligands and receptors were expressed in specific cell types; ~85%
568 of the hormone ligands and ~60% of the hormone receptors were detected in less than 5% of the
569 cell types. Certain hormones like follicle stimulating hormone (FSHB and CGA) were only
570 detected in a single cell type. Only a few hormone ligands were relatively broadly expressed,
571 including adrenomedullin (ADM, 18.6%), acylation stimulating protein (C3, 18.1%), IGF2
572 (17.9%), and resistin (RETN, 15.4%). The generality score followed a power-law distribution
573 toward the tail where a small number of globally expressed receptors dominated the distribution
574 (**Fig. S9B-C**). This resulted in a bimodal distribution of the network node outdegree (abundance
575 of outgoing edges/downstream regulation) (**Fig. 4A and C, Fig. S8**). Cells expressing hormone
576 ligand(s) to the high-generality receptors (e.g., adipocytes which secrete adiponectin) sent
577 globally connected outgoing edges, and other cells that only expressed ligand(s) to specific
578 receptors sent a much smaller number of outgoing edges. In contrast, the nodes' indegree
579 (abundance of incoming edges/upstream regulation) was more homogeneously distributed
580 because of the higher specificity of hormone ligand expression and large number of hormone
581 receptors expressed in the cells (**Fig. 4A-C, Fig. S8**).

582

583 **Receptors for the same hormone tend to be expressed in mutually exclusive cell types**

584 Many hormones have more than one receptor, which may mediate different functions (**Table 1**).
585 We therefore examined if receptors for the same ligand tend to be co-expressed or if their
586 expression is mutually exclusive across different cell types. To quantitatively compare the target
587 cell type profiles, we calculated a Jaccard index (JI, intersection over union) for each qualifying
588 receptor pair, namely the ratio of cell types that co-expressed both receptors to the cell types that
589 expressed either of the receptors. This analysis revealed that the majority of the receptor pairs
590 had extremely low JIs: 25% (41/161) of the receptor pairs had a JI equaling zero, meaning no
591 overlap in their target cell types, and 57% (92/161) of the receptor pairs had a JI of less than 5%
592 (**Fig. 4F**). A telling case is the adrenoceptors; although epinephrine (adrenaline) targets many
593 cell types, different adrenoceptor subtypes were selectively employed in different cell types (**Fig.
594 4F, Fig. S1-epinephrine/norepinephrine**). For example, adrenoceptors ADRA1D and ADRB3
595 shared no target cell types; ADRA1D was expressed broadly in vascular smooth muscle cells and
596 pericytes of multiple organs, certain glial cells, and leptomeningeal cells, whereas ADRB3
597 mainly targeted adipocytes. Vasopressin receptors AVPR1A and AVPR2 also had less than 3%
598 overlap in their target cell types; AVPR2 was predominantly expressed in the kidney collecting
599 duct principal cells, while AVPR1A was highly expressed in the kidney collecting duct
600 intercalated cells and broadly expressed in many stromal cell types (**Fig. S1-vasopressin**).

601 A few receptor pairs showed a tendency toward co-expression, suggesting possible interactions
602 in cell signaling. Supporting the notion, one top ranked pair was the IGF receptors IGF1R and
603 IGF2R (JI=0.40), which are known to interact in IGF2 signaling. IGF2R internalizes after IGF2
604 binding and clears IGF2 from the cell surface, and therefore functions as a competitive inhibitor

605 of IGF2-IGF1R signaling[73,74]. Two other top ranked pairs were NPY1R/NPY5R (JI=0.49),
606 receptors for neuropeptide Y, peptide YY and pancreatic polypeptide[75], and
607 ADIPOR1/ADIPOR2 (0.39), receptors for adiponectin. Coexpression of NPY1R and NPY5R
608 has been identified in rodent brain, and recent studies indicate that the two GPCRs may form
609 heterodimers, resulting in modulated agonist binding properties[76,77]. Similarly, biochemical
610 studies on ADIPOR1 and ADIPOR2 in cell culture systems have shown that the two receptors
611 can form heterodimers promoting membrane expression of ADIPOR2[78,79].

612 Taken together, this analysis showed that the expression of distinct receptors for the same
613 hormone tends to be mutually exclusive, suggesting functional divergence and specification
614 among hormone receptor subtypes. The rare cases of co-expressed receptors appear to involve
615 functional interaction or cross-regulation between the receptor pairs.

616

617 **Feedback circuits are widespread in the hormonal cell communication network**

618 Hormone regulation often involves feedback control. We therefore searched the mouse lemur
619 hormone cell communication network to systematically identify potential feedback regulation.
620 For simplicity, we focused on two-node feedback circuits, namely cell type pairs that are
621 connected by edges in both directions (**Fig. 5A**). This systematic search revealed a vast number
622 of feedback circuits; 29% of all node pairs formed feedback circuits, showing that feedback
623 control is widespread in the hormone network (**Table 6**). We then tested if feedback circuits are
624 enriched in the hormone network, i.e. more prevalent than would be expected by chance. We
625 applied degree-preserving random rewiring[80] to randomly permute edge connections without
626 changing node degree (i.e., network edge number and distribution). **Fig. 5B** shows the
627 distribution of the feedback circuit counts from such randomly permuted networks (n = 1000).
628 The number of feedback circuits in the permuted networks was consistently lower than in the
629 original hormone network. However, the difference was small (on average, only ~0.2%).
630 Additionally, we randomly removed 10% of ligand-receptor pairs to test how perturbations to
631 ligand-receptor binding affect feedback distribution of the network. This analysis revealed that
632 the network feedback circuits remained abundant despite edge removal as cell connections
633 usually involved multiple ligand-receptor pairs (**Fig. S7B, Fig. 4B**). Taken together, this analysis
634 suggests that feedback circuits are abundantly and robustly distributed as a result of the dense
635 connection of the hormone network. Evolution may have further enriched feedback circuits in
636 hormone regulation as suggested by the random rewiring analysis.

637 We next reviewed selected feedback circuits between endocrine cell types (**Fig. 5C-L**) to
638 compare with literature reports on hormonal feedback regulation. The analysis successfully
639 detected well-known feedback regulation. For example, **Fig. 5C** shows the feedback loop
640 between gonadotrophs in the anterior pituitary and the estrogen-producing granulosa cells of the
641 ovary (fortuitously obtained from female perigonadal fat), a classical example of hormonal
642 feedback control that is evolutionarily conserved across vertebrates[81]. Consistent with this
643 scheme, mouse lemur gonadotrophs expressed two highly-conserved gonadotropins, follicle
644 stimulating hormone (FSH, a dimer of FSHB and CGA) and luteinizing hormone (LH,
645 LHB/CGA dimer), which target granulosa cells through the corresponding receptors FSHR and
646 LHCGR. Granulosa cells, in turn, expressed key synthases required for the production of sex

647 hormones, which feed back to gonadotrophs through androgen and estrogen receptors (AR,
648 ESR1). Additional feedback regulation from granulosa cells to gonadotrophs was also mediated
649 through anti-Müllerian hormone (AMH) and inhibin/activin signaling. We also detected the well-
650 established feedback loop between somatotrophs in the anterior pituitary and hepatocytes in the
651 liver, which was mediated through growth hormone (GH), IGF1[2,82], and potentially hepcidin and
652 FGF21 signaling[83] (**Fig. 5D**). Additionally, in the pancreas, we detected the known feedback
653 circuits between pancreatic α and β cells through glucagon and insulin signaling and between α
654 and δ cells through glucagon and somatostatin signaling (**Fig. 5E-F**)[84]. The detection of these
655 various known feedback loops supports the validity of the comprehensive scRNAseq approach.

656 The analysis also revealed a long list of potential endocrine feedback circuits that have not been
657 reported, or have been reported recently but are not yet widely appreciated. For example, we
658 detected a feedback loop between pancreatic α cells and hepatocytes with one leg from α cells to
659 hepatocytes mediated by glucagon and the other leg from hepatocytes to α cells through IGF1
660 and FGF21 (**Fig. 5G**). Regulation of hepatocyte glycogenolysis and gluconeogenesis by
661 glucagon is well-established[85]. Previous work on the fasting-induced hormone FGF21 has shown
662 that injection of glucagon increases plasma FGF21 in humans[86] and injection of FGF21 reduces
663 glucagon in mice[87]. A recent study also observed that plasma IGF1 and glucagon levels are
664 negatively correlated in non-diabetic humans and found that IGF1 negatively modulates
665 glucagon secretion in an α cell culture model[88]. Considering that the liver is a major source of
666 circulating IGF1 and FGF21, our results and the literature reports suggest that α cells likely form
667 a negative feedback loop with hepatocytes in maintaining metabolic homeostasis.

668 Additionally, adipocytes, through adiponectin, formed feedback loops with pituitary
669 neuroendocrine cells, including the growth hormone secreting somatotrophs, the prolactin
670 secreting lactotrophs, and the ACTH secreting corticotrophs (**Fig. 5H-J**). It has been established
671 that growth hormone, prolactin, and ACTH reduce adiponectin secretion in adipocytes[89–91], but
672 much less is known about the effect of adiponectin on pituitary neuroendocrine cells.
673 Interestingly, a recent study using cultured primary pituitary cells from two non-human primate
674 species found that adiponectin decreases growth hormone and ACTH release and increases
675 prolactin release[92]. This suggests that adipocytes form a negative feedback loop with lactotrophs
676 which possibly stabilizes prolactin and adiponectin levels, and form double-negative feedback
677 loops with somatotrophs and corticotrophs, possibly functioning as bistable switches[93]. It
678 remains to be characterized how adiponectin affects pituitary hormone secretion, what are the
679 physiological functions of the pituitary-adipocyte feedback control, and whether this regulation
680 is specific to primates.

681 We also detected feedback circuits of intestinal enteroendocrine cells with pancreatic β cells and
682 adipocytes (**Fig. 5K-L**). It is known that enteroendocrine cells secrete GIP, which induces
683 glucose-dependent insulin secretion in β cells after eating and exposure of the intestinal lumen to
684 nutrients[2]. Despite the important physiological role of GIP in insulin secretion and glucose
685 homeostasis, there is limited research on the potential feedback regulation of GIP secretion by
686 insulin. García-Martínez et al. reported that insulin induces prolonged GIP expression in an
687 enteroendocrine cell line[94] , suggesting a positive feedback regulation and synergistic effects
688 between the two hormones in maintaining glucose homeostasis under a surge of blood glucose
689 after eating.

690 Taken together, this analysis identified an extensive list of potential feedback circuits in the
691 global hormonal cell communication network (**Table 6**), providing a rich resource for generating
692 hypotheses on endocrine regulations and to compare hormonal regulatory mechanisms in
693 different species.

694

695 **Exploring hormonal regulation of the circannual rhythms that control organismal biology**

696 Lastly, the mouse lemur hormone atlas may bring new insights to the study of mouse lemur
697 physiology, such as circannual rhythms[29,95], social interactions[96], and aging[11–13,97]. As an
698 adaptation to seasonal environmental changes, mouse lemurs have evolved striking seasonal
699 rhythms in metabolism, behavior, and reproduction throughout their 5–10-year lifespan. Mouse
700 lemurs build fat reserves in preparation for the winter and enter daily torpor, a hypometabolic
701 state, to preserve energy, while in the summer the animals maintain a lean body and regrow their
702 reproductive organs for mating. The global nature of these phenotypic changes suggests that they
703 may be hormonally mediated. To date, only 12 circulating hormones have been measured in
704 mouse lemurs, but all showed dramatic seasonal changes (**Fig. 6A, Table 7**). This suggests that
705 hormones are likely the key messengers coordinating and driving various seasonal changes
706 among different organs. The hormone atlas suggests that these seasonally changing hormones
707 target a broad array of cells and tissues; 95% of the cell types possessed receptors for at least one
708 of these 12 hormones. This finding suggests that seasonal rhythms engage not only tissues that
709 demonstrate obvious morphological changes (e.g., adipose tissues and gonads), but involve
710 global shifts in cellular metabolism and physiology (**Fig. 6B**).

711 Discussion

712 Hormonal signaling is vital to multicellular life, allowing cells to communicate with both
713 surrounding cells and remote cells in other tissues. In this study, we systematically mapped
714 hormone-producing and -target cells across the 739 cell types from 27 different tissues from the
715 mouse lemur molecular cell atlas. We generated a browsable atlas that depicts gene expression of
716 ligands, modulators, and receptors for 87 hormone classes (**Fig. S1, Fig. 1**). This dataset
717 complements the scale and resolution of classical endocrine studies and brings a cellular and
718 molecular foundation for studying novel aspects of hormone regulation. The mouse lemur
719 hormone atlas represents a primate model of hormone signaling and should be useful in future
720 organism-wide cross-species comparisons.

721 The hormone atlas also provides an opportunity to extract global principles of hormone
722 signaling. The hormone-related genes exhibited cell-type-dependent, stereotypical expression
723 patterns, and their transcriptional profiles faithfully classified cell types, despite their constituting
724 less than 1% of the transcriptome (**Fig. 2, Fig. S3, Fig. S5**). Ligands alone and receptors alone
725 also clustered cell types well, with certain clusters mostly defined by their ligands and others by
726 their receptors (**Fig. S4**). It is remarkable, perhaps, how well a cell's intercellular communication
727 repertoire encapsulates the cell's identity.

728 There were, however, some exceptions to this general rule. For example, sperms and sperm
729 progenitor cells exhibited dramatic changes in hormone gene expression during spermatogenesis

730 despite their close developmental connection (**Fig. 3A**). In addition, vascular endothelial cells
731 from lung and brain exhibited hormone signatures that were distinct from those of other vascular
732 endothelial cells (**Fig. 3B**). Hormone signaling varied in an orderly and graded fashion along the
733 epithelium and vasa recta endothelium of the nephron (**Fig. 3C and D)**. Hepatocytes were found
734 to fall into two molecular subtypes with differential hormonal gene expression (**Fig. 3E, Fig.**
735 **S6**), suggesting different physiological roles. And finally, metastatic endometrial tumor cells
736 exhibited different hormonal signaling from that seen in their likely cells of origin in the uterus
737 (**Fig. 3F**), suggesting possible rewiring of hormone signaling during tumor development and
738 metastasis.

739 The cell-type specific gene expression data allowed us to construct an organism-wide cell
740 communication network for mouse lemur hormone signaling, by connecting the hormone-
741 producing cells to the corresponding target cells (**Fig. 4**). This hormone network was
742 exceptionally dense and robust to deletion of individual edges (**Fig. 4A, Fig. S7A**), which mainly
743 resulted from two network features. First, most cells in the network expressed multiple hormone
744 receptors and/or ligands, though in general cells were regulated by more hormones than they
745 produced (**Fig. 4B**). Second, although most hormone ligands and receptors were expressed in
746 specific cell types, a small fraction of hormone receptors were nearly ubiquitously expressed
747 (e.g., adiponectin receptors, a membrane progesterone receptor, the IGF1 receptor, the thyroid
748 hormone receptor, and the cortisol receptor), resulting in almost global connection of the relevant
749 hormone-producing cells to the other cells of the body (**Fig. 4C-E, Fig. S8, Fig. S9**).
750 Interestingly, despite the density of the hormone signaling network, subtypes of hormone
751 receptors that bind to the same ligand were generally expressed in a mutually exclusive fashion,
752 supporting the notion that different hormone receptor subtypes usually mediate different
753 physiological functions through separate target cells (**Fig. 4F**). The dense connection of the
754 network indicates extensive hormonal communication among the cells and contributes to a large
755 number of highly connected nodes and no obvious network cores. Whereas regulatory circuits of
756 individual hormones may be hierarchical, as classically viewed, the overall decentralized
757 network architecture of the hormone interactome highlights the importance of taking a
758 comprehensive approach to the understanding of global hormonal function.

759 Feedback regulation was widespread in hormonal signaling, and it was robust to network
760 perturbations (**Fig. 5B, Fig. S7B**). The analysis identified well-known feedback circuits among
761 several endocrine cell pairs and detected additional, previously unreported, hormones involved in
762 feedback control (**Fig. 5C-F**). We also identified many novel feedback circuits (**Fig. 5G-L**)
763 which may be involved in adaptation or homeostasis (negative feedback circuits) or in generating
764 switch-like responses (positive and double-negative feedback circuits). This hypothesis-
765 generating analysis provided an extensive list of potential feedback circuits (**Table 6**) to guide
766 future functional validation and characterization studies. Our findings may also inform studies of
767 the systems biology and network topology of hormone signaling (see for example Karin et al.[98]).

768 Mouse lemurs display dramatic seasonal changes in body weight, hibernation propensity, and
769 reproductive activities[29,95,99]. Such seasonal rhythms are likely regulated, at least in part, by
770 seasonally-varying hormones that coordinate the changes across different organs of the body
771 (**Fig. 6A**). The hormone atlas shows that almost all (95%) of the mouse lemur cell types are
772 regulated by seasonally varying hormones (**Fig. 6B**). This suggests that most, if not all, mouse
773 lemur cells across all organs of the body experience seasonal changes in metabolism, growth,

774 and function. By systematic mapping of hormone secreting and target cells, the atlas also points
775 to candidate cell types and signaling to explore the upstream and downstream regulation for each
776 of the seasonally varying hormones. Circannual rhythms are widespread in nature[100,101] and
777 humans display seasonally varying hormone levels and cellular transcriptomes[102–104]. The
778 findings of the present study may apply to species beyond the mouse lemur, and may bring new
779 insights for season-associated human diseases[105–107] because of the close genetic proximity of
780 mouse lemurs and humans.

781 Single-cell RNA sequencing is a powerful tool for assaying cellular function and activity, but
782 there are limitations. Although the technique has improved rapidly in sensitivity, accuracy, and
783 efficiency, scRNAseq still faces low capture efficiency and high transcript dropout[108]. With the
784 large number of cells assayed in the mouse lemur molecular cell atlas, we averaged gene
785 expression across cells of the same cell type to smooth the noise in individual cells from dropout.
786 In the analysis of hormone regulation, genes involved in hormone production, such as ligands
787 and modulators, tend to be abundantly expressed; but certain hormone receptor proteins may be
788 low in copy number and slow in turnover, and therefore may result in false-negative errors. In
789 addition, there can be false-positive errors caused by contamination from other cells in the same
790 sample (i.e., signal spreading). This is most notable for abundantly expressed ligand genes and
791 tissues affected by endogenous digestive enzymes (e.g., pancreas). In this study, we scored
792 positive expression of a hormone ligand only when both the ligand gene and the necessary
793 modulators (such as prohormone processing enzymes) were present. This approach mitigated
794 false-positive detection of highly abundant ligands. Lastly, scRNAseq has low capture efficiency
795 for certain cells such as neurons and large sized adipocytes. Nevertheless, the mouse lemur cell
796 atlas included several neuronal subtypes from the brain cortex, brainstem, and retina, as well as
797 both UCP1-high and UCP1-low adipocytes from multiple tissues[14]. Although not yet a complete
798 sampling, the mouse lemur cell atlas is one of the most comprehensive and accurately-annotated
799 organism-wide scRNAseq datasets reported to date. Other organism-wide scRNAseq atlases
800 have been created or are being created for other species, including mouse[54,109,110], ascidian[111],
801 cynomolgus monkey[112], and human[113], bringing exciting resources to the study of the evolution
802 of hormone signaling, as well as the cellular and molecular mechanisms and interactions
803 underlying hormone-regulated biology.

804 Traditionally, biologists focus on one particular cell type and/or organ system. However,
805 hormone signaling by its very nature connects different cell types and organs. The emerging
806 organism-wide atlases open a new door in understanding the cross-organ communication
807 systems that allow organisms to function as a reliable robust whole.

808

809

810 Methods

811 **Mapping and counting transcript reads**: The single-cell gene expression matrix of the mouse
812 lemur cell atlas was obtained from The Tabula Microcebus[14] where methods and parameters to
813 extract the transcript counts can be found. In this study, we used only the 10x droplet-based
814 sequencing derived data for all analysis. In brief, the *Microcebus murinus* genome assembly

815 (Mmur 3.0, NCBI) was used to create a genome FASTA file. Sequencing reads were processed
816 with Cell Ranger (version 2.2, 10x Genomics) to generate cell barcodes and the gene expression
817 matrix. We additionally counted reads for three genes (MC1R, SCT, LHB) that are unannotated
818 in Mmur 3.0, NCBI. For MC1R and SCT, we used their annotation in the Ensembl *Microcebus*
819 *murinus* genome. For LHB, we used the uTAR-scRNA-seq pipeline described by Wang et al.[20]
820 to first predict its chromosome location in the mouse lemur genome. In brief, the pipeline
821 employs the approach of groHMM[114] to detect transcriptionally active regions (TARs) from
822 aligned sequencing data and annotates these TARs as unannotated (uTARs) or annotated
823 (aTARs) based on their overlap with the existing annotation. For the LHB_uTAR counts, we
824 uncovered uTARs from the mouse lemur pituitary and hypothalamus dataset and used
825 BLASTn[115,116] to find nucleotide sequence homology of all uTARs against human LHB. We
826 found one uTAR at position NC_033681.1:19143249-19145949 with high sequence homology
827 to human and macaque LHB. The LHB_uTAR is highly differentially expressed in the expected
828 cell type (gonadotroph). The LHB_uTAR is located next to gene RUVBL2, in conservation with
829 the co-location pattern of the two genes in humans and mice[21]. We therefore conclude that the
830 identified LHB_uTAR is the likely coding region of the mouse lemur LHB gene. We then used
831 Drop-seq tools[117] to extract transcript counts for the three genes (MC1R, SCT, LHB_uTAR).

832

833 **Protein sequence analysis**: We compared the sequence similarity between orthologs of human
834 and mouse or lemur. Protein sequences were retrieved from NCBI according to protein RefSeq
835 using the Matlab built-in function getgenpept. Conversion between gene ID and protein Refseq
836 identifier was performed using bioDBnet (https://biodbnet.abcc.ncifcrf.gov/db/db2db.php). We
837 aligned ortholog protein sequences and used the maximal scores in the cases of one-to-multi or
838 multi-to-multi ortholog mapping. Global alignment was carried out using the Needleman-
839 Wunsch algorithm and default parameters of the function nwalign.

840

841 **Identification of hormone-producing and target cells**: The functional concentration is
842 different for different proteins, so we applied adaptive thresholding to determine if a gene is
843 positively expressed in a cell type, where cell type is defined as a unique combination of the
844 cells' annotation and tissue of origin, as described in the accompanying Tabula Microcebus
845 manuscript 1[14]. For example, vein cells of the lung and brain were considered two different cell
846 types. Cell types that were of low quality (low gene count or transcript count) or annotated as
847 technical doublets were removed from the analysis. For each gene, two cell type parameters were
848 used, average expression level and percentage of nonzero cells. Single-cell expression levels
849 were first normalized by total transcript counts, multiplied by 10,000, averaged across all cells in
850 the cell type, then natural log transformed (i.e., log(1+AverageUMIcountPer10KTranscripts);
851 note that 1 is added to the average so that genes with zero transcripts will yield zero rather than
852 negative infinity). To determine positive expression at the cell type level, we first applied a low-
853 level absolute threshold on average expression level (0.037) and percent of nonzero cells (5%)
854 below either of which we considered the expression to be negative. Second, we calculated a
855 "maximal" expression level of the gene by searching the high-expression levels across the atlas.
856 Specifically, we considered the 99th percentile of the cells that passed the first thresholding to be
857 the maximum to increase the robustness of the analysis. Lastly, we applied relative thresholding
858 of the "maximal" level (for ligand genes at 20% and other gene types at 5%). Cell types that

859 passed all thresholding criteria were considered to have functional expression of the gene. We
860 used a higher relative threshold for the ligand genes because 1) ligands are secreted into the
861 circulation so a highly expressing source outshadows a low expressing source, whereas non-
862 ligand products of other genes (e.g., receptors, synthases, processing enzymes) function inside
863 individual cells; 2) we noted that ligand genes were usually expressed at higher levels and were
864 more easily affected by cross-contamination (signal spreading) inside a tissue. For hormone
865 ligands and receptors that included multiple genes, we applied AND or OR logic gates as
866 indicated in **Table 1** to determine if a cell type expressed the ligand or receptor. For an AND
867 logic gate, a functional cell type should express all its components above the functional level;
868 while for an OR logic gate, expression of any of its components would suffice.

869

870 **Cell type distances, clustering, and visualization**: We performed hierarchical clustering of the
871 cell types included in the mouse lemur atlas based on the transcriptional profiles of hormone
872 ligand, synthase, modulator, and receptor genes. Analysis was carried out at the cell type level
873 and relative average gene expression levels were used to calculate cell-type pairwise distances.
874 To test consistency of hormone-related gene expression among mouse lemur individuals, we
875 separated cells from different lemurs. Because circulating immune cells sampled from different
876 tissues were already kept as different cell types, immune cell types were not separated for
877 different lemurs to avoid overcrowding of the data. We found that this simplification only
878 slightly influenced the clustering results of individual cell types and did not affect the overall
879 clustering pattern. Next, cell types were filtered to remove potentially low quality cell types that
880 were: 1) low in cell number, 2) technical doublets, or 3) low in transcript and/or gene count. We
881 also manually corrected for notable cross-contamination in certain cell types. For example,
882 almost all non-endocrine cell types of the pancreas showed high expression of insulin (INS) and
883 proglucagon (GCG), probably caused by cross-contamination due to autolysis in the pancreas
884 during tissue processing. We therefore removed INS and GCG expression from all non-
885 endocrine pancreatic cell types. Similarly, we corrected contamination of GUCA2A, GUCA2B,
886 GIP, NTS, and SST from stromal, endothelial, and immune cells of the intestine (small intestine
887 and colon). Matlab built-in functions were used in the hierarchical clustering analysis. We used
888 cosine distances to calculate cell type pairwise distances and then applied average-linkage to
889 construct the dendrogram (cophenetic correlation coefficient = 0.80). Cell type clusters were then
890 divided at a threshold of 0.49 with minor manual inputs to further divide certain large clusters or
891 merge an apparently close neighboring leaf. We obtained 75 total clusters and numbered them
892 according to their sequence in the dendrogram shown in **Fig. 2A**. We also named the clusters
893 according to the shared characteristics of its cell types. Cell types included in each cluster are
894 listed in **Table 3** with the list of hormones, hormone receptors, and hormone-related genes that
895 were expressed in the majority ($\geq$ 50%) of the cell types for each cluster.

896 In addition to visualizing the cell type clustering via dendrogram, we also applied uniform
897 manifold approximation and projection (UMAP)[118] to embed the high dimensional expression
898 data to 2D using a Matlab UMAP package[119]. Cell type pairwise cosine distances were used as
899 input when generating the UMAPs.

900 For comparative analysis, we additionally calculated distances between cell types by either the
901 non-hormonal transcriptome or by Cell Ontology[43]. Transcriptome-based distances were

902 calculated similarly as the hormone-based distances were, with relative expression levels of non-
903 hormonal genes used to calculate pairwise cosine distances. For Cell Ontology distances, each
904 cell type was assigned a Cell Ontology term during cell type annotation as described in the
905 accompanying Tabula Microcebus manuscript 1[14]. Cell Ontology distances were calculated as
906 the mean of Cell Ontology embedding-based distances and text-based distances[44]. Cell Ontology
907 embedding-based distances represent distances between cell types in the Cell Ontology graph.
908 Text-based distances were calculated using an adapted version of Sentence-BERT[44,120].

909 To estimate the quality of the clustering results, we calculated silhouette values and compared
910 cluster average silhouette values based on only the hormone ligand genes, hormone receptor
911 genes, or the non-hormonal transcriptome. Silhouette values for a cell type i is from the equation
912 $s(i) = \frac{b(i)-a(i)}{max\{b(i),a(i)\}}$, for cell types belonging to a cluster with more than one member. $a(i)$ is the
913 mean in-cluster distance, namely the mean distance between cell type i and all other cell types in
914 the same cluster. $b(i)$ is the minimal out-cluster distance, namely the minimal mean distance
915 between cell type i and members of other clusters.

916

917 **Vasa recta trajectory analysis**: Analysis was performed independently for kidney samples from
918 three mouse lemur individuals using an in-house program written in Matlab. To detect the
919 arteriole-to-venule trajectory, data were first pre-processed following the standard procedure as
920 in Seurat[121]. In brief, single cell transcript counts for all sequenced genes were normalized to
921 total transcript counts, log transformed, and linearly scaled so that each gene has a mean
922 expression of 0 and standard deviation of 1. Then genes with high dispersion (variance-to-mean
923 ratio) compared to other genes with the same mean expression were selected as highly variable
924 genes for principal component analysis (PCA). Following PCA, the top 20 principal components
925 that were not driven by extreme outlier data points or immediate early genes were used to
926 generate a 2D UMAP using cell-cell Euclidean distances as input[118]. To quantify the trajectory,
927 we detected the probability density ridge of the data points in the UMAP using automated image
928 processing. The direction of the trajectory was manually assigned according to marker gene
929 expression. Individual cells were aligned to the trajectory by finding the shortest connecting
930 point to the trajectory. Data points that were too distant from the trajectory were deemed outliers
931 and removed from the following analysis. To detect the hormone-related genes that follow a
932 trajectory dependent expression pattern, we calculated the Spearman correlation coefficient
933 between the gene expression level and 20 unimodal patterns. These preassigned patterns have
934 their data smoothly changing along the trajectory and have a single peak. We let the 20 patterns
935 have their peaks uniformly distributed from 0 to 1. This analysis tested, for each gene, whether
936 its distribution along the trajectory follows one or more of the 20 unimodal patterns. All p values
937 were then multi-testing corrected to detect significant genes and their associated patterns. Lastly,
938 we compared results from the three kidney samples and kept the genes that showed consistent
939 patterns in all three samples.

940

941 **Identification of differentially expressed genes**: We used the Wilcoxon rank-sum test to detect
942 differentially expressed hormone genes among cell populations. Genes that were expressed
943 above functional level in any of the analyzed cell populations were included in the analysis. For

944 hormone-related genes differentially expressed during spermatogenesis, we tested whether each
945 gene is differentially expressed in one of the three sperm cell clusters compared to the other two
946 clusters. For the analysis of endothelial cells, we tested whether each gene is differentially
947 expressed in the lung or brain endothelial cells compared to all other endothelial cells. For the
948 kidney nephron analysis, we tested whether each gene is differentially expressed in one of the
949 nephron clusters compared to the rest of the nephron epithelial cells. For the hepatocyte analysis,
950 we tested whether each gene is differentially expressed in one subtype compared to the other in
951 both the mouse lemur and the mouse. The mouse hepatocyte data was obtained from the Tabula
952 Muris Senis[54] smartseq2 plate-based sequencing of mouse hepatocytes. For the tumor cell
953 analysis, we tested whether each gene is differentially expressed in the metastatic cells versus the
954 MUC16+ non-ciliated uterus epithelial cells. All *p* values were multi-testing corrected, and then
955 all genes with corrected *p* values less than 0.05 were examined to confirm consistent expression
956 of the gene in all relevant cell types and mouse lemur individuals.

957

958 **Constructing and analyzing the hormonal cell communication network**: Cells with the same
959 annotation name and tissue of origin were grouped as a cell type/node. Data from different lemur
960 individuals were merged in the analysis. Cell types that were likely low quality were removed.
961 Edge connections were determined independently for all possible cell type pairs. For example, if
962 cell type A expressed a hormone ligand and cell type B expressed the corresponding hormone
963 receptor(s), a directed edge from A to B was drawn. Note that this allows self-loops on any cell
964 type that expresses both the ligand and corresponding receptor. When multiple directed edges
965 connected two cell types, they were merged for the purpose of edge counting.

966 Network density is defined as the number of edges divided by the number of possible edges in
967 the network. Because the hormone network is directed, its network density is calculated as $\frac{N_{edges}}{N_{nodes}^2}$.
968 For comparison, the density of an undirected network (e.g., protein interaction network) is
969 calculated as $\frac{2*N_{edges}}{N_{nodes}\cdot(N_{nodes}+1)}$ if it allows self-loops, or $\frac{2*N_{edges}}{N_{nodes}\cdot(N_{nodes}-1)}$ if it does not allow self-
970 loops.

971 Outdegree and indegree are node features and defined as the relative number of outgoing edges
972 (node expressing a ligand) and incoming edges (node expressing a receptor). Edge counts were
973 normalized by cell type abundance so that node degrees range from 0-100% and represent the
974 fraction of the cell types that the node connects with by outgoing or incoming edges. To
975 normalize the node degrees, we used a weighted cell type abundance determined by the
976 clustering so that each cluster contributes the same weight. This is because certain cell types like
977 circulating immune cells are likely over-represented in the network as they appear in multiple
978 tissues and would be categorized as different "cell types" by our definition. We did not merge
979 circulating cell types from different tissues because it is challenging for some cell types like T
980 cells to determine whether they are circulating or potentially tissue specific or tissue-resident.
981 We also tried simply normalizing the node degree by the total number of nodes; similar
982 conclusions were reached using either method.

983

984 **Calculating generality scores for hormone ligands and receptors**: To calculate generality
985 scores for the hormone ligands and receptors, we counted the cell types that express the ligand or
986 receptor. Cell types that were likely low quality were removed from the analysis. Cell type
987 counts were normalized by cell type abundances similarly as was the node degree, so that the
988 generality score was not dominated by over-represented cell types. In comparison, we also
989 counted the cell type clusters that express the hormone ligands and receptors. Here we defined
990 that a gene was expressed in a cell type cluster if more than 50% of the cell types in the cluster
991 positively expressed the gene. For hormone ligands and receptor complexes that contained
992 multiple genes, we applied the AND or OR logic gates indicated in **Table 1** to determine positive
993 expression in cell type clusters.

994 To analyze the distribution of generality scores, we tested if the distribution followed normal,
995 exponential, lognormal, or gamma distributions. We first performed parametric distribution
996 fitting and then performed Kolmogorov–Smirnov tests comparing the fitted versus data
997 cumulative distribution functions. This analysis used Matlab built-in functions fitdist and kstest.
998 Additionally, we tested if the data followed a power law distribution using plfit and plpva
999 functions[122].

1000

1001 **Calculating target cell Jaccard indices for different receptors that bind to the same ligand**:
1002 We calculated Jaccard indices for pairs of receptors that 1) can bind to the same ligand as
1003 described in **Table 1**, and 2) were both expressed in at least one atlas cell type. Jaccard index
1004 here is calculated as the number of cell types that express both receptors divided by the number
1005 of cell types that express either of the receptors. Cell types that were likely low quality were
1006 removed from the analysis. Data from different mouse lemur individuals were merged in the
1007 analysis.

1008

1009 **Network perturbation analysis**: We performed two types of network perturbations: degree-
1010 preserving random rewiring and random edge removal. For degree-preserving random rewiring,
1011 we applied the algorithm developed by Maslov and Sneppen[80]. The algorithm starts with the
1012 original network and performs repeated rewiring steps. For each rewiring, it randomly identifies
1013 two edges (e.g., A→B and C→D) and swaps the connections (i.e., A→D and C→B). This allows
1014 constructing a random network while preserving the node indegree and outdegree of the original
1015 network. For the perturbation by edge removal, we randomly selected 10% of the edge types
1016 (ligand-receptor pairs) and removed these edges from the original network. Note for this
1017 analysis, multiple directed edges connecting the same cell type pairs were not merged. Therefore,
1018 the connection between two cell types would be removed only if all of its redundant edges (of
1019 different ligand-receptor pairs) were selected to be removed.

1020

1021 **Hormone assays**: Cortisol concentrations (ng/ml) were measured in duplicates from urine
1022 samples by Cortisol Urine ELISA (LDN®, catalog no. MS E-5100). Urine creatinine (mg/ml)
1023 was measured using MicrovueTM Creatinine Elisa kit (Quidel R Corporation, catalog no. 8009).
1024 Creatinine concentration was used to normalize urine measurements as an indicator of renal

filtration activity. Cortisol measurements are thus expressed in ng/mg creatine. Thyroxine (T4, nmol/L) was assayed in plasma samples using T4 ELISA kit (LDN®, catalog no. TF E-2400) and the 6-point standard curve was adapted from 0 to 100 nmol/L.

Acknowledgments

We are grateful to Sandra Schmid, Uri Alon, Chaitan Khosla, the Krasnow lab, and the Ferrell lab for helpful discussions and comments on the manuscript. This work is supported by NIH grant R35 GM131792 to J. E. Ferrell, funding from Wall Center to M. A. Krasnow, and a fellowship from the Wu Tsai Neurosciences Institute to S. Liu. M. A. Krasnow is an investigator of the Howard Hughes Medical Institute.

Author Contributions

S. Liu, M.A. Krasnow, and J.E. Ferrell conceived the project. S. Liu designed and performed all the analysis with input from C. Ezran, Z. Li, C. Kuo, J. Epelbaum, J. Terrien, M.A. Krasnow, and J.E. Ferrell. S. Liu, C. Kuo, and J. Long assembled the hormone list. M.F.Z. Wang and I.D. Vlaminck performed uTAR analysis on the candidate lemur LHB gene. S. Wang calculated the cell ontology distances. S. Liu, J. Epelbaum, and J. Terrien analyzed the seasonally oscillating hormones. The Tabula Microcebus Consortium constructed the mouse lemur molecular cell atlas. S. Liu and J.E. Ferrell wrote the manuscript with input from all authors.

Figure legends

Fig. 1. **Expression of selected hormone ligands and receptors across the mouse lemur cell atlas.** Four exemplary sets of hormone ligands and receptors are shown: prolactin (PRL, PRLR), adiponectin (ADIPOQ, ADIPOR1, ADIPOR2), motilin (MLN, MLNR), and resistin (RETN, CAP1, DCN, ROR1, TLR4). Cell types are arranged by compartment: epithelial/neural/germ cells (**A**), stromal cells (**B**), endothelial cells (**C**), lymphoid cells (**D**), and myeloid cells (**E**). Within each panel, rows are cell types ordered by tissue of origin. Cell type names are labeled on the right, tissue of origin on the left, and gene symbols on the top (red for ligand genes, blue for receptor genes). Dots represent average gene expression (circle color) and percent of cells positive for the gene (circle size). The red/blue circle edges highlight the cell types deemed positive for the ligand or receptor gene expression (see **Methods**). Cell types that are potentially low quality (e.g., low cell count) are excluded from this plot. A complete set of figures that display ligand and receptor gene expression for all 87 hormone classes can be found in **Fig. S1**.

1059 **Fig. 2. Hormone-related gene expression faithfully classifies cell type. A**. Clustering of mouse
1060 lemur cell types by hormone-related genes. At the top is a dendrogram of the hierarchical
1061 clustering. Clusters of cell types are color-coded, and cluster numbers are labeled as space
1062 allows. Cell types included in each cluster are listed in **Table 3**. The lower part of the panel
1063 shows the heatmap of the relative gene expression levels for the hormone-related genes. Cluster-
1064 specific hormone genes are ordered based on the cluster with the highest expression level, with
1065 the genes preferentially expressed in the left-hand cell type clusters on the top. Broadly
1066 expressed genes (expressed in more than 35% of cell types) are placed in the bottom and ordered
1067 from least to most broadly expressed. **B**. UMAP visualization of mouse lemur cell types based
1068 on the expression of hormone-related genes. Circles are cell types (unique combination of
1069 annotation name and tissue of origin) and color-coded by cell type compartment types (epithelial,
1070 neural, germ, stromal, endothelial, lymphoid, and myeloid). Dashed lines circumscribe the cell
1071 type clusters as in panel A (also see **Table 3**), and cluster IDs and names were labeled nearby. As
1072 UMAPs qualitatively display relationships among data points, the extremely distant clusters (i.e.,
1073 cluster 44. mesothelial cells) were shifted up in UMAP-2 towards the center of the figure for
1074 display purposes. **C, D**. Scatter plots showing positive correlation (*p*-values < 1E-15) between
1075 cell type pairwise distances based on hormone-related gene expression versus the non-hormonal
1076 transcriptome (**C**) or Cell Ontology descriptors (**D**). Red lines show linear fitting of the data.

1077

1078 **Fig. 3. Hormonal regulation sometimes differs in closely related cell types.** Panels show
1079 expression of the hormone ligand, synthase, modulator, and receptor genes that are differentially
1080 expressed during spermatogenesis (**A**), endothelial cells of the lung and brain (**B**), epithelial cells
1081 along the spatial axis of the kidney nephron tubule (**C**), endothelial cells along the arteriole-to-
1082 venule axis of the kidney vasa recta (**D**), two molecular subtypes of hepatocytes (**E**), and
1083 between metastatic tumor cells in the lung of lemur L2 and the putative cell type of metastatic
1084 origin (MUC16+ non-ciliated uterus epithelial cells) sampled from L3 (**F**). **A-C, E and F** are dot
1085 plots showing average gene expression and percent of positive cells of the indicated genes and
1086 cell types, merging data from different mouse lemur individuals. In **A**, cell types are arranged
1087 along the course of the spermatogenesis. In **B**, endothelial cells are arranged by tissue of origin.
1088 In **C**, cell types are arranged according to their spatial distribution along the kidney nephron
1089 tubule. In **D**, on the top are a schematic representation of the kidney nephron and vasa recta and
1090 the UMAP visualization of the vasa recta cells based on expression of all genes. The black line
1091 shows the detected arteriole-to-venule trajectory with the arrow pointing in the direction of blood
1092 flow. Cells are color-coded according to the cell type annotation names in the atlas. Grey lines
1093 show the alignment of the individual cells to the trajectory. The bottom portion of the panel
1094 shows single cell scatter plots of gene expression levels along the arteriole-to-venule trajectory
1095 for the endothelial markers and hormone genes that are differentially expressed. Shown here is
1096 vasa recta data from one animal. Similar results were obtained from two other lemurs. **PCT**:
1097 proximal convoluted tubule. **PT**: proximal tubule. **PST**: proximal straight tubule (also called
1098 loop of Henle thick descending limb). **LHd**: loop of Henle thin descending limb. **LHa1**: loop of
1099 Henle thin ascending limb. **LHa2**: loop of Henle thick ascending limb. **DCT**: distal convoluted
1100 tubule. **MD**: macula densa. **CDp**: collecting duct principal cell. **CDiα**: collecting duct α
1101 intercalated cell. **CDiβ**: collecting duct β intercalated cell. **D** shows the fitted arteriole-to-venule
1102 trajectory of the kidney vasa recta capillary network (upper panel) and single-cell gene
1103 expression levels along the trajectory for the endothelial markers and differentially expressed

1104 hormone-related genes. Shown here are representative results from one of three lemur vasa recta
1105 samples. **VRD**: vasa recta descending section. **VRA**: vasa recta ascending section.

1106

1107 **Fig. 4. The hormonal cell-cell communication network**. **A.** A representation of the network as
1108 constructed by force-directed graph drawing. Nodes (cell types) are color-coded according to the
1109 node outdegree (% of cells connected to the current node by outgoing edges) and the node circle
1110 size shows the node indegree (% of cells connected to the current node by incoming edges).
1111 Network edges are directed and connect nodes expressing a hormone ligand to all nodes
1112 expressing the corresponding hormone receptor. **B.** Number of ligand and receptor types
1113 expressed by the network nodes (cell types), ranked from most to fewest. **C.** Indegree and
1114 outdegree of the network nodes (cell types), ranked from high to low values. Node degree is
1115 normalized to the total number of nodes and cluster size and measures the percentage of cell
1116 types connected from or to a network node. **D.** Generality score of all hormone ligands and
1117 receptors ranked from the most generally expressed to most selectively expressed. Generality
1118 score is defined as the percentage of nodes (cluster size normalized) positively expressing the
1119 gene(s) involved in ligand synthesis or receptor binding. Also see **Fig. S9A** for generality score
1120 defined as the number of cell type clusters positively expressing the gene(s). **E.** Scatterplot
1121 showing generality scores of the hormone ligands and corresponding receptors. Each circle is a
1122 unique ligand-receptor pair. **F.** Ranking (left) and distribution (right) of Jaccard indices of
1123 receptor pairs binding to the same ligand across all hormone receptors. Jaccard index is
1124 calculated as the number of cell types co-expressing both receptors divided by the number of cell
1125 types expressing either of the receptors.

1126

1127 **Fig. 5. Feedback circuits in the hormonal cell-cell communication network. A.** Definition of
1128 two-node feedback circuits. **B**. Comparison of the number of 2-node feedback circuits identified
1129 in the hormonal cell-cell communication network (red dashed line) and that of permuted
1130 networks (n = 1000). Permutation preserved node outdegree and indegree. Note that none of the
1131 permuted networks has as many 2-node feedback circuits as in the original network. **C-H**.
1132 Examples of two-node feedback circuits identified in the network, focusing on the endocrine cell
1133 types. Solid black arrows indicate known regulation, dashed orange arrows indicate predicted
1134 regulation with partial literature support, and dotted red arrows predicted regulation without
1135 earlier knowledge. Parentheses are used to group multiple genes that are expressed in the
1136 relevant cell type that function either together (&) or independently (/).

1137

1138 **Fig. 6. Seasonality of hormone concentrations in the mouse lemur likely affects almost all**
1139 **cells and tissues. A**. Concentrations of twelve hormones measured in summer (long-
1140 photoperiod) and winter (short-photoperiod) in the mouse lemur. Bars represent fold changes in
1141 hormone concentration compared to average summer levels. Error bars represent 95%
1142 confidence intervals. *P*-values were calculated by 2-sample *t*-test. Data were listed in **Table 7**,
1143 collected from literature and supplemented with additional new measurements: estradiol[123,124],
1144 testosterone[125–127], thyroxine[123,128] (and additional data in Table 7), DHEA[124], cortisol[129] (and

1145 additional data in Table 7), IGF1[130], melatonin[131], and gut hormones (GIP, PPY, insulin, PYY,
1146 and GLP-1)[132,133]. **B.** Mouse lemur cell types targeted by any of these 12 seasonal hormones. Cell
1147 types are displayed in the same UMAP plot as in **Fig. 2B**. Circles are cell types and are color
1148 coded according to whether they express receptors for any of the 12 hormones. Dashed lines
1149 circumscribe the cell type clusters and are colored according to cell type compartments.

1150

1151 **Fig. S1. Ligand and receptor gene expression for 87 hormone classes across the mouse**
1152 **lemur cell atlas.** Each dot plot shows one of the 87 hormone groups and one of the five cell
1153 compartment types (1. epithelial/neural/germ cells; 2. endothelial cells; 3. stromal cells; 4.
1154 lymphoid cells; and 5. myeloid cells). The hormone group name and cell compartment type is
1155 indicated on the top right of the figure. The dot plots are arranged in a polar coordinate style.
1156 Radial lines represent individual cell types, with cell type names labeled inside the inner circle
1157 and the tissue source labeled outside the outer circle. Cell types are arranged by their tissue of
1158 origin. Circular lines represent the related genes for this hormone group (red for ligands or
1159 synthases, light red for processing enzymes and/or other modulator genes, and blue for receptor
1160 genes). The dark colored dots on the intersections of the radial lines and circular lines depict
1161 mean gene expression level (by dot shade) and percent of positive cells (by dot size) for the
1162 respective gene and cell type. The outermost red or blue dots indicate positive expression of one
1163 of the hormone(s) (red) or hormone receptor(s) (blue), or both (purple) for the hormone group by
1164 the respective cell type (see **Methods**). The outermost grey dots indicate potentially low-quality
1165 cell types (e.g., low cell number (<10) and pancreatic cells that show notable signal
1166 contamination) whether or not the cell type expresses one the hormone ligand(s) (red outline),
1167 receptor(s) (blue outline), both (purple outline), or neither (no outline).

1168

1169 **Fig. S2. Protein sequences of hormonal genes are generally more similar between human**
1170 **and mouse lemur than human and mouse.** Each circle is a hormone-related protein. Sequences
1171 were aligned by the Needleman-Wunsch algorithm and sequence identity was calculated as the
1172 percentage of identical amino acids. Points below the red line are proteins more similar between
1173 human and mouse lemur than between human and mouse.

1174

1175 **Fig. S3. UMAP visualization of mouse lemur cell types based on the non-hormonal**
1176 **transcriptome.** Circles (cell types) are color-coded by cell compartment types (epithelial, neural,
1177 germ, stromal, endothelial, lymphoid, and myeloid). Dashed lines circumscribe cell type clusters
1178 as in **Fig. 2A-B** and cluster IDs and names are labeled next to the cell type clusters. Cell types
1179 that were clustered by the hormone-related genes but not the non-hormonal transcriptome are
1180 labeled with asterisks (*). Note some cell types that formed discrete clusters based on hormonal
1181 gene expression intermingled with other clusters when mapped based on the non-hormonal
1182 transcriptome (e.g., cluster 51-52 and 54-58), and therefore were annotated together.

1183

1184 **Fig. S4. Classification of mouse lemur cell types using only the hormone ligand genes (A) or**
1185 **the hormone receptor genes (B).** In panels **A** and **B**, cell types are displayed by the UMAP
1186 algorithm according to the cell type distances calculated with either the hormone
1187 ligands/modulators or the hormone receptors respectively. Circles (cell types) are color-coded by
1188 the cell compartment types (epithelial, neural, germ, stromal, endothelial, lymphoid, and
1189 myeloid). Dashed lines circumscribe cell type clusters as in **Fig. 2A-B** and cluster IDs are
1190 annotated nearby. Cell types that were clustered using all the hormone-related genes but not in
1191 this analysis are labeled with asterisks (*). As UMAPs qualitatively display relationships among
1192 data points, the extremely distant clusters in panel A (i.e., cluster 44. mesothelial cells by
1193 hormone ligand genes) were shifted towards the center of the figure for display purposes. **C.**
1194 Cluster averaged silhouette values of the 68 cell type clusters by both hormone ligand and
1195 receptor genes (black), only the hormone ligand genes (red), only the hormone receptor genes
1196 (blue), or the non-hormonal transcriptome (blank). The silhouette values are a measure of how
1197 well each cell type cluster was classified (see **Methods**).

1198

1199 **Fig. S5. Heatmap representation of cell type pairwise distances calculated by three**
1200 **different methods. A.** Hormone-gene transcriptional cosine distances. **B.** Non-hormonal gene
1201 transcriptional cosine distances. **C.** Cell Ontology-based distances. Cell types were ordered by
1202 cluster as in **Fig. 2A**, and cluster IDs were labeled along the diagonal for large clusters.

1203

1204 **Fig. S6. Dot plot showing the differentially expressed hormone ligands/synthases and**
1205 **receptors separately in the hepatocytes of male and female animals** (in comparison to **Fig.**
1206 **3E**).

1207

1208 **Fig. S7. The hormonal cell-cell communication network is robust to edge removal.**
1209 Distribution of network density (**A**) and number of 2-node feedback circuits (**B**) in networks
1210 where 10% of ligand-receptor connections were randomly removed.

1211

1212 **Fig. S8. Node properties of the hormonal cell-cell communication network.** Heatmap of
1213 indegree, outdegree, number of hormone ligands and receptors expressed, and six node centrality
1214 measurements (hubs, authorities, incloseness, outcloseness, pagerank, and betweenness) for all
1215 nodes (cell types) of the hormonal cell-cell communication network. Because the scales of the
1216 node properties are different, shown here are normalized values linearly scaled by median and
1217 median-absolute-deviation. Cell types (columns) are ordered by the clustering of the hormone-
1218 related genes (as in **Fig. 2A**) and cluster numbers are labeled as space allowed. Node properties
1219 (rows) are ordered by hierarchical clustering of the normalized values.

1220

1221 **Fig. S9. Generality scores for the hormone ligands and receptors. A.** Generality score,
1222 defined as the number of clusters with positive expression of the ligand or receptor (see **Fig. 4C**

for comparison), ranked from most generally expressed to most selectively expressed. **B-C**. Fitting the distribution of the ligand and receptor generality scores. Normal, exponential, log-normal, and gamma distributions failed to fit the distribution (**B**). The tail of the distribution can be approximated by a power law distribution *prob*(x) ~ $x^{-\alpha}$ for x ≥ xmin (**C**).

Supplemental Tables

Table 1. Genes involved in the biosynthesis and sensing of 87 classes of hormones. Rows show hormones and columns show the hormone class name, hormone name(s), type of hormones, symbol of the genes involved in biosynthesis (Ligand/Enzyme Gene(s)) and sensing (Receptor Gene(s)), whether the hormone synthesis or maturation requires coordination of multiple tissues, years discovered, classical sites of secretion and targets, and approximate plasma concentrations in humans. Genes in the table are human genes.

Table 2. Mouse lemur and mouse orthologs of the human hormone-related genes in Table 1. Rows show genes and columns show gene type, symbols of human, lemur, and mouse genes respectively. Special cases such as unknown/missing orthologs were highlighted and labeled with *.

Table 3. Clusters of mouse lemur cell types according to expression of hormone-related genes. Rows show clusters and columns show cluster ID, name, cell types included in the cluster, and the hormones, receptors, and hormone-related genes that were positively expressed in the majority (≥50%) of the cluster cell types.

Table 4. Hormones that regulate or are produced by the anterior pituitary neuroendocrine cells. Rows show the hormones and hormone receptors expressed in individual pituitary neuroendocrine cell types. Columns show the corresponding genes, hormone names, and upstream/downstream cell types.

Table 5. Generality scores of the hormone ligands, modulators and receptors. Rows show hormone ligands, modulators, or receptors. Columns show entry types, symbols of human and mouse lemur genes, whether the entry includes a single or multiple genes, and generality scores calculated as the percentage of positive cell types and the number of positive clusters.

Table 6. Two node feedback circuits detected from the mouse lemur hormone cell-cell communication network. Rows show the detected circuits and columns show the two cell types and hormone signaling that connects the cell types.

Table 7. Individual measurements of concentrations of mouse lemur seasonally-changing hormones. Rows show individual measurements and columns show the season of measurements, concentration, and hormone names.

References

1. W. M. Bayliss, E. H. S. The mechanism of pancreatic secretion. *J. Physiol.* **28**, 325 (1902).
2. Takei, Y., Ando, H. & Tsutsui, K. *Handbook of Hormones: Comparative Endocrinology for Basic and Clinical Research*. (Academic Press, 2015).
3. Tata, J. R. One hundred years of hormones. *EMBO Rep.* **6**, 490 (2005).
4. Lewis, G. F. & Brubaker, P. L. The discovery of insulin revisited: lessons for the modern era. *J. Clin. Invest.* **131**, (2021).
5. Horby, P. *et al.* Dexamethasone in Hospitalized Patients with Covid-19. *N. Engl. J. Med.* **384**, (2021).
6. Sterne, J. A. C. *et al.* Association Between Administration of Systemic Corticosteroids and Mortality Among Critically Ill Patients With COVID-19: A Meta-analysis. *JAMA* **324**, (2020).
7. Scheja, L. & Heeren, J. The endocrine function of adipose tissues in health and cardiometabolic disease. *Nat. Rev. Endocrinol.* **15**, 507–524 (2019).
8. Jabbour, H. N., Kelly, R. W., Fraser, H. M. & Critchley, H. O. D. Endocrine regulation of menstruation. *Endocr. Rev.* **27**, 17–46 (2006).
9. Ezran, C. *et al.* The Mouse Lemur, a Genetic Model Organism for Primate Biology, Behavior, and Health. *Genetics* **206**, 651–664 (2017).
10. Bons, N., Rieger, F., Prudhomme, D., Fisher, A. & Krause, K. H. Microcebus murinus: a useful primate model for human cerebral aging and Alzheimer's disease? *Genes Brain Behav.* **5**, (2006).
11. Languille, S. *et al.* The grey mouse lemur: a non-human primate model for ageing studies. *Ageing Res. Rev.* **11**, (2012).
12. Kraska, A. *et al.* Age-associated cerebral atrophy in mouse lemur primates. *Neurobiol. Aging* **32**, 894–906 (2011).
13. Pifferi, F. *et al.* Promoting healthspan and lifespan with caloric restriction in primates. *Commun Biol* **2**, 107 (2019).
14. The Tabula Microcebus Consortium. Tabula Microcebus: A transcriptomic cell atlas of mouse lemur, an emerging primate model organism. *bioRxiv* 2021.12.12.469460 (2021) doi:10.1101/2021.12.12.469460.
15. Kastin, A. *Handbook of Biologically Active Peptides*. (Academic Press, 2013).
16. Romere, C. *et al.* Asprosin, a Fasting-Induced Glucogenic Protein Hormone. *Cell* **165**, 566–579 (2016).
17. Itoh, N., Ohta, H. & Konishi, M. Endocrine FGFs: Evolution, Physiology, Pathophysiology, and Pharmacotherapy. *Front. Endocrinol.* **6**, 154 (2015).
18. Ramilowski, J. A. *et al.* A draft network of ligand–receptor-mediated multicellular signalling in human. *Nature Communications* vol. 6 (2015).
19. Armstrong, J. F. *et al.* The IUPHAR/BPS Guide to PHARMACOLOGY in 2020: extending

1300 immunopharmacology content and introducing the IUPHAR/MMV Guide to MALARIA
1301 PHARMACOLOGY. *Nucleic Acids Res.* **48**, D1006–D1021 (2020).
1302 20. Wang, M. F. Z. *et al.* Uncovering transcriptional dark matter via gene annotation independent single-
1303 cell RNA sequencing analysis. *Nat. Commun.* **12**, 1–10 (2021).
1304 21. Parfait, B. *et al.* Human TIP49b/RUVBL2 gene: genomic structure, expression pattern, physical link
1305 to the human CGB/LHB gene cluster on chromosome 19q13.3. *Ann. Genet.* **43**, 69–74 (2000).
1306 22. Wilkinson, T. N., Speed, T. P., Tregear, G. W. & Bathgate, R. A. D. Evolution of the relaxin-like
1307 peptide family. *BMC Evol. Biol.* **5**, 14 (2005).
1308 23. Riddle, O., Bates, R. W. & Dykshorn, S. W. THE PREPARATION, IDENTIFICATION AND
1309 ASSAY OF PROLACTIN—A HORMONE OF THE ANTERIOR PITUITARY. *American Journal*
1310 *of Physiology-Legacy Content* vol. 105 191–216 (1933).
1311 24. Bole-Feysot, C., Goffin, V., Edery, M., Binart, N. & Kelly, P. A. Prolactin (PRL) and its receptor:
1312 actions, signal transduction pathways and phenotypes observed in PRL receptor knockout mice.
1313 *Endocr. Rev.* **19**, 225–268 (1998).
1314 25. Tovar, S. & Diéguez, C. Prolactin and energy homeostasis: pathophysiological mechanisms and
1315 therapeutic considerations. *Endocrinology* vol. 155 659–662 (2014).
1316 26. Paré, P. *et al.* Molecular evolutionary insights from PRLR in mammals. *Gen. Comp. Endocrinol.*
1317 **309**, 113791 (2021).
1318 27. Giroud, S. *et al.* The Grey Mouse Lemur Uses Season-Dependent Fat or Protein Sparing Strategies
1319 to Face Chronic Food Restriction. *PLoS ONE* vol. 5 e8823 (2010).
1320 28. Terrien, J. *et al.* Metabolic and genomic adaptations to winter fattening in a primate species, the grey
1321 mouse lemur (Microcebus murinus). *International Journal of Obesity* vol. 42 221–230 (2018).
1322 29. Perret, M. & Aujard, F. Regulation by Photoperiod of Seasonal Changes in Body Mass and
1323 Reproductive Function in Gray Mouse Lemurs (Microcebus murinus): Differential Responses by
1324 Sex. *Int. J. Primatol.* **22**, 5–24 (2001).
1325 30. Galic, S., Oakhill, J. S. & Steinberg, G. R. Adipose tissue as an endocrine organ. *Molecular and*
1326 *Cellular Endocrinology* vol. 316 129–139 (2010).
1327 31. Maeda, K. *et al.* cDNA cloning and expression of a novel adipose specific collagen-like factor,
1328 apM1 (AdiPose Most abundant Gene transcript 1). *Biochem. Biophys. Res. Commun.* **221**, 286–289
1329 (1996).
1330 32. Zhang, Y. *et al.* Positional cloning of the mouse obese gene and its human homologue. *Nature* **372**,
1331 (1994).
1332 33. Ruan, H. & Dong, L. Q. Adiponectin signaling and function in insulin target tissues. *Journal of*
1333 *Molecular Cell Biology* vol. 8 101–109 (2016).
1334 34. Yamauchi, T. *et al.* Cloning of adiponectin receptors that mediate antidiabetic metabolic effects.
1335 *Nature* **423**, 762–769 (2003).
1336 35. He, J., Irwin, D. M., Chen, R. & Zhang, Y.-P. Stepwise loss of motilin and its specific receptor genes
1337 in rodents. *J. Mol. Endocrinol.* **44**, 37–44 (2010).
1338 36. Sanger, G. J., Wang, Y., Hobson, A. & Broad, J. Motilin: towards a new understanding of the
1339 gastrointestinal neuropharmacology and therapeutic use of motilin receptor agonists. *Br. J.*
1340 *Pharmacol.* **170**, 1323–1332 (2013).
1341 37. Hu, Q., Tan, H. & Irwin, D. M. Evolution of the Vertebrate Resistin Gene Family. *PLoS One* **10**,
1342 e0130188 (2015).
1343 38. Schwartz, D. R. & Lazar, M. A. Human Resistin: Found in Translation From Mouse to Man. *Trends*
1344 *Endocrinol. Metab.* **22**, 259 (2011).
1345 39. Zhang, X. *et al.* Neuropeptidomic Analysis Establishes a Major Role for Prohormone Convertase-2
1346 in Neuropeptide Biosynthesis. *J. Neurochem.* **112**, 1168 (2010).
1347 40. Seidah, N. G. The proprotein convertases, 20 years later. *Methods Mol. Biol.* **768**, 23–57 (2011).
1348 41. Sandoval, D. A. & D'Alessio, D. A. Physiology of proglucagon peptides: role of glucagon and GLP-
1349 1 in health and disease. *Physiol. Rev.* **95**, 513–548 (2015).
1350 42. Wardlaw, S. L. Hypothalamic proopiomelanocortin processing and the regulation of energy balance.

1351 *Eur. J. Pharmacol.* **660**, 213 (2011).
1352 43. Smith, B. *et al.* The OBO Foundry: coordinated evolution of ontologies to support biomedical data
1353 integration. *Nat. Biotechnol.* **25**, 1251–1255 (2007).
1354 44. Wang, S. *et al.* Unifying single-cell annotations based on the Cell Ontology. *Cold Spring Harbor*
1355 *Laboratory* 810234 (2020) doi:10.1101/810234.
1356 45. Griswold, M. D. Spermatogenesis: The Commitment to Meiosis. *Physiol. Rev.* **96**, 1–17 (2016).
1357 46. Smith, L. B. & Walker, W. H. The regulation of spermatogenesis by androgens. *Seminars in Cell &*
1358 *Developmental Biology* vol. 30 2–13 (2014).
1359 47. Ruwanpura, S. M., McLachlan, R. I. & Meachem, S. J. Hormonal regulation of male germ cell
1360 development. *Journal of Endocrinology* vol. 205 117–131 (2010).
1361 48. Lishko, P. V., Botchkina, I. L. & Kirichok, Y. Progesterone activates the principal Ca2+ channel of
1362 human sperm. *Nature* **471**, 387–391 (2011).
1363 49. Lue, Y. *et al.* Functional role of progestin and the progesterone receptor in the suppression of
1364 spermatogenesis in rodents. *Andrology* **1**, 308–317 (2013).
1365 50. Burnicka-Turek, O. *et al.* Inactivation of insulin-like factor 6 disrupts the progression of
1366 spermatogenesis at late meiotic prophase. *Endocrinology* **150**, 4348–4357 (2009).
1367 51. Dyer, L. A. & Patterson, C. Development of the endothelium: an emphasis on heterogeneity. *Semin.*
1368 *Thromb. Hemost.* **36**, 227–235 (2010).
1369 52. Groneberg, D. A., Springer, J. & Fischer, A. Vasoactive intestinal polypeptide as mediator of
1370 asthma. *Pulm. Pharmacol. Ther.* **14**, 391–401 (2001).
1371 53. Travaglini, K. J. *et al.* A molecular cell atlas of the human lung from single-cell RNA sequencing.
1372 *Nature* **587**, 619–625 (2020).
1373 54. Tabula Muris Consortium. A single-cell transcriptomic atlas characterizes ageing tissues in the
1374 mouse. *Nature* **583**, 590–595 (2020).
1375 55. Barnes, K. & Turner, A. J. The endothelin system and endothelin-converting enzyme in the brain:
1376 molecular and cellular studies. *Neurochem. Res.* **22**, 1033–1040 (1997).
1377 56. Wilhelms, D. B. *et al.* Deletion of prostaglandin E2 synthesizing enzymes in brain endothelial cells
1378 attenuates inflammatory fever. *J. Neurosci.* **34**, 11684–11690 (2014).
1379 57. Engström, L. *et al.* Lipopolysaccharide-induced fever depends on prostaglandin E2 production
1380 specifically in brain endothelial cells. *Endocrinology* **153**, 4849–4861 (2012).
1381 58. Giesecke, T. *et al.* Vasopressin Increases Urinary Acidification via V1a Receptors in Collecting Duct
1382 Intercalated Cells. *Journal of the American Society of Nephrology* vol. 30 946–961 (2019).
1383 59. Pannabecker, T. L. & Dantzler, W. H. Three-dimensional architecture of inner medullary vasa recta.
1384 *Am. J. Physiol. Renal Physiol.* **290**, F1355–66 (2006).
1385 60. Barry, D. M. *et al.* Molecular determinants of nephron vascular specialization in the kidney. *Nat.*
1386 *Commun.* **10**, 5705 (2019).
1387 61. Waxman, D. J. & O'Connor, C. Growth hormone regulation of sex-dependent liver gene expression.
1388 *Mol. Endocrinol.* **20**, 2613–2629 (2006).
1389 62. Backes, F. J. *et al.* Estrogen receptor-alpha as a predictive biomarker in endometrioid endometrial
1390 cancer. *Gynecol. Oncol.* **141**, 312–317 (2016).
1391 63. Shen, F., Gao, Y., Ding, J. & Chen, Q. Is the positivity of estrogen receptor or progesterone receptor
1392 different between type 1 and type 2 endometrial cancer? *Oncotarget* vol. 8 506–511 (2017).
1393 64. Nakanishi, M. & Rosenberg, D. W. Multifaceted roles of PGE2 in inflammation and cancer. *Semin.*
1394 *Immunopathol.* **35**, 123–137 (2013).
1395 65. Ke, J. *et al.* Prostaglandin E2 (PGE2) promotes proliferation and invasion by enhancing SUMO-1
1396 activity via EP4 receptor in endometrial cancer. *Tumour Biol.* **37**, 12203–12211 (2016).
1397 66. Lee, J. O. *et al.* Resistin, a fat-derived secretory factor, promotes metastasis of MDA-MB-231
1398 human breast cancer cells through ERM activation. *Sci. Rep.* **6**, 18923 (2016).
1399 67. Frankenstein, Z., Alon, U. & Cohen, I. R. The immune-body cytokine network defines a social
1400 architecture of cell interactions. *Biol. Direct* **1**, (2006).
1401 68. Giot, L. *et al.* A protein interaction map of Drosophila melanogaster. *Science* **302**, 1727–1736

(2003).
69. Yook, S. H., Oltvai, Z. N. & Barabási, A. L. Functional and topological characterization of protein interaction networks. *Proteomics* **4**, (2004).
70. Rolland, T. *et al.* A proteome-scale map of the human interactome network. *Cell* **159**, 1212–1226 (2014).
71. Costanzo, M. *et al.* The Genetic Landscape of a Cell. *Science* **327**, 425–431 (2010).
72. Barabási, A.-L. Scale-Free and Hierarchical Structures in Complex Networks. *AIP Conference Proceedings* (2003) doi:10.1063/1.1571285.
73. Iams, W. T. & Lovly, C. M. Molecular Pathways: Clinical Applications and Future Direction of Insulin-like Growth Factor-1 Receptor Pathway Blockade. *Clin. Cancer Res.* **21**, 4270–4277 (2015).
74. Ghosh, P., Dahms, N. M. & Kornfeld, S. Mannose 6-phosphate receptors: new twists in the tale. *Nat. Rev. Mol. Cell Biol.* **4**, 202–212 (2003).
75. Larhammar, D. & Salaneck, E. Molecular evolution of NPY receptor subtypes. *Neuropeptides* **38**, 141–151 (2004).
76. Kilpatrick, L. E., Humphrys, L. J. & Holliday, N. D. A G protein-coupled receptor dimer imaging assay reveals selectively modified pharmacology of neuropeptide Y Y1/Y5 receptor heterodimers. *Mol. Pharmacol.* **87**, (2015).
77. Gehlert, D. R., Schober, D. A., Morin, M. & Berglund, M. M. Co-expression of neuropeptide Y Y1 and Y5 receptors results in heterodimerization and altered functional properties. *Biochem. Pharmacol.* **74**, 1652–1664 (2007).
78. Almabouada, F. *et al.* Adiponectin Receptors Form Homomers and Heteromers Exhibiting Distinct Ligand Binding and Intracellular Signaling Properties. *J. Biol. Chem.* **288**, 3112–3125 (2013).
79. Keshvari, S. *et al.* Characterisation of the adiponectin receptors: the non-conserved N-terminal region of AdipoR2 prevents its expression at the cell-surface. *Biochem. Biophys. Res. Commun.* **432**, 28–33 (2013).
80. Maslov, S. & Sneppen, K. Specificity and stability in topology of protein networks. *Science* **296**, 910–913 (2002).
81. Dwyer, A. A. & Quinton, R. Anatomy and Physiology of the Hypothalamic-Pituitary-Gonadal (HPG) Axis. *Advanced Practice in Endocrinology Nursing* 839–852 (2019) doi:10.1007/978-3-319-99817-6_43.
82. Martín-Estal, I., de la Garza, R. G. & Castilla-Cortázar, I. Intrauterine Growth Retardation (IUGR) as a Novel Condition of Insulin-Like Growth Factor-1 (IGF-1) Deficiency. *Rev. Physiol. Biochem. Pharmacol.* **170**, 1–35 (2016).
83. Inagaki, T. *et al.* Inhibition of growth hormone signaling by the fasting-induced hormone FGF21. *Cell Metab.* **8**, 77–83 (2008).
84. Hartig, S. M. & Cox, A. R. Paracrine signaling in islet function and survival. *J. Mol. Med.* **98**, 451–467 (2020).
85. Habegger, K. M. *et al.* The metabolic actions of glucagon revisited. *Nat. Rev. Endocrinol.* **6**, 689–697 (2010).
86. Habegger, K. M. *et al.* Fibroblast growth factor 21 mediates specific glucagon actions. *Diabetes* **62**, 1453–1463 (2013).
87. Mu, J. *et al.* FGF21 analogs of sustained action enabled by orthogonal biosynthesis demonstrate enhanced antidiabetic pharmacology in rodents. *Diabetes* **61**, 505–512 (2012).
88. Mancuso, E. *et al.* Insulin-like growth factor-1 is a negative modulator of glucagon secretion. *Oncotarget* **8**, 51719–51732 (2017).
89. Kopchick, J. J., Berryman, D. E., Puri, V., Lee, K. Y. & Jorgensen, J. O. L. The effects of growth hormone on adipose tissue: old observations, new mechanisms. *Nat. Rev. Endocrinol.* **16**, 135–146 (2020).
90. Carré, N. & Binart, N. Prolactin and adipose tissue. *Biochimie* vol. 97 16–21 (2014).
91. Iwen, K. A. *et al.* Melanocortin crosstalk with adipose functions: ACTH directly induces insulin resistance, promotes a pro-inflammatory adipokine profile and stimulates UCP-1 in adipocytes. *J.*

1453 *Endocrinol.* **196**, (2008).
1454 92. Sarmento-Cabral, A. *et al.* Adipokines (Leptin, Adiponectin, Resistin) Differentially Regulate All
1455 Hormonal Cell Types in Primary Anterior Pituitary Cell Cultures from Two Primate Species. *Sci.*
1456 *Rep.* **7**, 43537 (2017).
1457 93. Ferrell, J. E., Jr. Self-perpetuating states in signal transduction: positive feedback, double-negative
1458 feedback and bistability. *Curr. Opin. Cell Biol.* **14**, 140–148 (2002).
1459 94. García-Martínez, J. M., Chocarro-Calvo, A., De la Vieja, A. & García-Jiménez, C. Insulin drives
1460 glucose-dependent insulinotropic peptide expression via glucose-dependent regulation of FoxO1 and
1461 LEF1/β-catenin. *Biochim. Biophys. Acta* **1839**, 1141–1150 (2014).
1462 95. Petter-Rousseaux, A. Age of Microcebus murinus at the onset of testicular development :
1463 Preliminary observations on photoperiodic effect. *Ann. Biol. anim. Bioch. Biophys.* **19**, 1801–1806
1464 (1979).
1465 96. Perret, M. Environmental and social determinants of sexual function in the male lesser mouse lemur
1466 (Microcebus murinus). *Folia Primatol.* **59**, 1–25 (1992).
1467 97. Epelbaum, J. & Terrien, J. Mini-review: Aging of the neuroendocrine system: Insights from
1468 nonhuman primate models. *Prog. Neuropsychopharmacol. Biol. Psychiatry* **100**, (2020).
1469 98. Karin, O. *et al.* A new model for the HPA axis explains dysregulation of stress hormones on the
1470 timescale of weeks. *Mol. Syst. Biol.* **16**, e9510 (2020).
1471 99. Perret, M. & Aujard, F. Daily hypothermia and torpor in a tropical primate: synchronization by 24-h
1472 light-dark cycle. *American Journal of Physiology-Regulatory, Integrative and Comparative*
1473 *Physiology* vol. 281 R1925–R1933 (2001).
1474 100. Gwinner, E. *Circannual Rhythms: Endogenous Annual Clocks in the Organization of Seasonal*
1475 *Processes*. (Springer, 2011).
1476 101. Lincoln, G. A brief history of circannual time. *J. Neuroendocrinol.* **31**, (2019).
1477 102. Tendler, A. *et al.* Hormone seasonality in medical records suggests circannual endocrine circuits.
1478 *Proc. Natl. Acad. Sci. U. S. A.* **118**, (2021).
1479 103. Sailani, M. R. *et al.* Deep longitudinal multiomics profiling reveals two biological seasonal patterns
1480 in California. *Nat. Commun.* **11**, 4933 (2020).
1481 104. Dopico, X. C. *et al.* Widespread seasonal gene expression reveals annual differences in human
1482 immunity and physiology. *Nat. Commun.* **6**, 7000 (2015).
1483 105. Moriyama, M., Hugentobler, W. J. & Iwasaki, A. Seasonality of Respiratory Viral Infections.
1484 *Annual review of virology* **7**, (2020).
1485 106. Marti-Soler, H. *et al.* Seasonal Variation of Overall and Cardiovascular Mortality: A Study in 19
1486 Countries from Different Geographic Locations. *PLoS One* **9**, e113500 (2014).
1487 107. Kurlansik, S. L. & Ibay, A. D. Seasonal affective disorder. *Am. Fam. Physician* **86**, (2012).
1488 108. Chen, G., Ning, B. & Shi, T. Single-Cell RNA-Seq Technologies and Related Computational Data
1489 Analysis. *Front. Genet.* **10**, 317 (2019).
1490 109. The Tabula Muris Consortium. Single-cell transcriptomics of 20 mouse organs creates a Tabula
1491 Muris. *Nature* **562**, 367–372 (2018).
1492 110. Han, X. *et al.* Mapping the Mouse Cell Atlas by Microwell-Seq. *Cell* **172**, (2018).
1493 111. Cao, C. *et al.* Comprehensive single cell transcriptome lineages of a proto-vertebrate. *Nature* **571**,
1494 349 (2019).
1495 112. Han, L. *et al.* Single-cell atlas of a non-human primate reveals new pathogenic mechanisms of
1496 COVID-19. *Cold Spring Harbor Laboratory* 2020.04.10.022103 (2020)
1497 doi:10.1101/2020.04.10.022103.
1498 113. Tabula Sapiens Consortium* *et al.* The Tabula Sapiens: A multiple-organ, single-cell transcriptomic
1499 atlas of humans. *Science* **376**, eabl4896 (2022).
1500 114. Chae, M., Danko, C. G. & Lee Kraus, W. groHMM: a computational tool for identifying
1501 unannotated and cell type-specific transcription units from global run-on sequencing data. *BMC*
1502 *Bioinformatics* **16**, 1–16 (2015).
1503 115. Johnson, M. *et al.* NCBI BLAST: a better web interface. *Nucleic Acids Res.* **36**, (2008).

1504 116. Altschul, S. F., Gish, W., Miller, W., Myers, E. W. & Lipman, D. J. Basic local alignment search
1505 tool. *J. Mol. Biol.* **215**, 403–410 (1990).
1506 117. Macosko, E. Z. *et al.* Highly Parallel Genome-wide Expression Profiling of Individual Cells Using
1507 Nanoliter Droplets. *Cell* **161**, 1202–1214 (2015).
1508 118. McInnes, L., Healy, J. & Melville, J. UMAP: Uniform Manifold Approximation and Projection for
1509 Dimension Reduction. (2018).
1510 119. Meehan, C., Ebrahimian, J., Moore, W. & Meehan, S. *Uniform Manifold Approximation and*
1511 *Projection (UMAP). MATLAB Central File Exchange.*
1512 *https://www.mathworks.com/matlabcentral/fileexchange/71902*. (2021).
1513 120. Reimers, N. & Gurevych, I. Sentence-BERT: Sentence Embeddings using Siamese BERT-Networks.
1514 (2019).
1515 121. Butler, A., Hoffman, P., Smibert, P., Papalexi, E. & Satija, R. Integrating single-cell transcriptomic
1516 data across different conditions, technologies, and species. *Nat. Biotechnol.* **36**, 411–420 (2018).
1517 122. Clauset, A., Shalizi, C. R. & Newman, M. E. J. Power-law distributions in empirical data. *SIAM Rev.*
1518 *Soc. Ind. Appl. Math.* **51**, 661–703 (2009).
1519 123. Noiret, A. *et al.* Sex-Specific Response to Caloric Restriction After Reproductive Investment in
1520 Microcebus murinus: An Integrative Approach. *Front. Physiol.* **11**, (2020).
1521 124. Perret, M. & Aujard, F. Aging and season affect plasma dehydroepiandrosterone sulfate (DHEA-S)
1522 levels in a primate. *Exp. Gerontol.* **40**, 582–587 (2005).
1523 125. Dal-Pan, A. *et al.* Caloric restriction or resveratrol supplementation and ageing in a non-human
1524 primate: first-year outcome of the RESTRIKAL study in Microcebus murinus. *Age* **33**, (2011).
1525 126. Petter-Rousseaux, A. & Picon, R. Annual variation in the plasma testosterone in Microcebus
1526 murinus. *Folia Primatol.* **36**, (1981).
1527 127. Schilling, A. & Perret, M. Removal of the olfactory bulbs modifies the gonadal responses to
1528 photoperiod in the lesser mouse lemur (Microcebus murinus). *Biol. Reprod.* **49**, 58–65 (1993).
1529 128. Petter-Rousseaux, A. Annual variations in the plasma thyroxine level in Microcebus murinus. *Gen.*
1530 *Comp. Endocrinol.* **55**, 405–409 (1984).
1531 129. Perret, M. & Predine, J. Effects of long-term grouping on serum cortisol levels in Microcebus
1532 murinus (Prosimii). *Horm. Behav.* **18**, 346–358 (1984).
1533 130. Aujard, F., Bluet-Pajot, M. T., Zizzari, P., Perret, M. & Epelbaum, J. IGF-1: a marker of individual
1534 life-span in a primate. *Ageing Research* **1**, (2010).
1535 131. Aujard, F. *et al.* Artificially accelerated aging by shortened photoperiod alters early gene expression
1536 (Fos) in the suprachiasmatic nucleus and sulfatoxymelatonin excretion in a small primate,
1537 Microcebus murinus. *Neuroscience* vol. 105 403–412 (2001).
1538 132. Giroud, S. *et al.* Gut hormones in relation to body mass and torpor pattern changes during food
1539 restriction and re-feeding in the gray mouse lemur. *J. Comp. Physiol. B* **179**, 99–111 (2009).
1540 133. Dal-Pan, A., Blanc, S. & Aujard, F. Resveratrol suppresses body mass gain in a seasonal non-human
1541 primate model of obesity. *BMC Physiol.* **10**, (2010).

1542

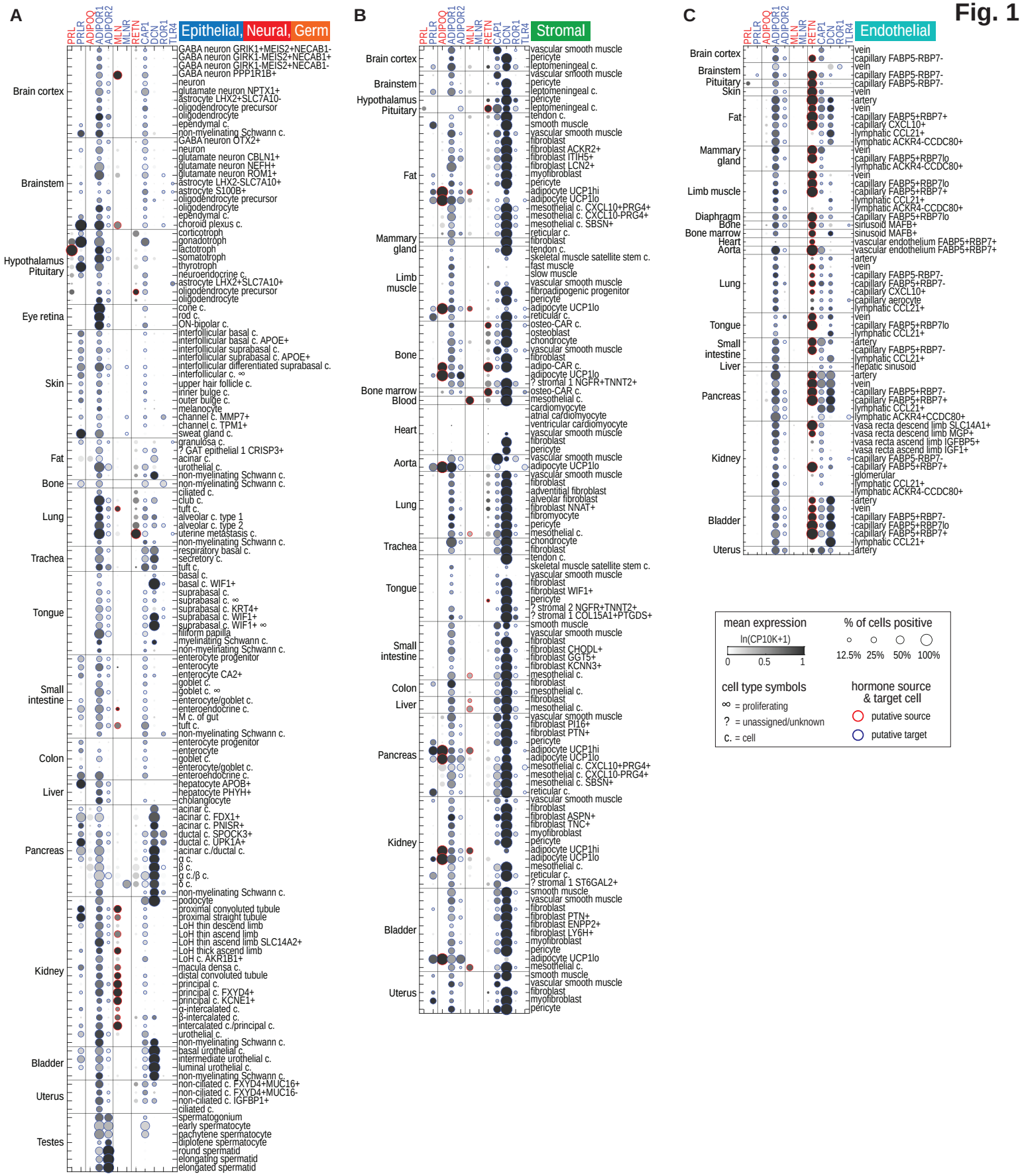
Fig. 1
A
Epithelial, Neural, Germ
PRL
PRLR
ADIPOQ
ADIPOR1
ADIPOR2
MLN
MLNR
RETN
CAP1
DCN
ROR1
TLR4
Brain cortex
Brainstem
Hypothalamus
Pituitary
Eye retina
Skin
Fat
Bone
Lung
Trachea
Tongue
Small intestine
Colon
Liver
Pancreas
Kidney
Bladder
Uterus
Testes
GABA neuron GRIK1+MEIS2+NECAB1-
GABA neuron GIRK1-MEIS2+NECAB1+
GABA neuron GIRK1-MEIS2+NECAB1-
GABA neuron PPP1R1B+
neuron
glutamate neuron NPTX1+
astrocyte LHX2+SLC7A10-
oligodendrocyte precursor
oligodendrocyte
ependymal c.
non-myelinating Schwann c.
GABA neuron OTX2+
neuron
glutamate neuron CBLN1+
glutamate neuron NEFH+
glutamate neuron ROM1+
astrocyte LHX2-SLC7A10+
astrocyte S100B+
oligodendrocyte precursor
oligodendrocyte
ependymal c.
choroid plexus c.
corticotroph
gonadotroph
lactotroph
somatotroph
thyrotroph
neuroendocrine c.
astrocyte LHX2+SLC7A10+
oligodendrocyte precursor
oligodendrocyte
cone c.
rod c.
ON-bipolar c.
interfollicular basal c.
interfollicular basal c. APOE+
interfollicular suprabasal c.
interfollicular suprabasal c. APOE+
interfollicular differentiated suprabasal c.
interfollicular c. ∞
upper hair follicle c.
inner bulge c.
outer bulge c.
melanocyte
channel c. MMP7+
channel c. TPM1+
sweat gland c.
granulosa c.
? GAT epithelial 1 CRISP3+
acinar c.
urothelial c.
non-myelinating Schwann c.
non-myelinating Schwann c.
ciliated c.
club c.
tuft c.
alveolar c. type 1
alveolar c. type 2
uterine metastasis c.
non-myelinating Schwann c.
respiratory basal c.
secretory c.
tuft c.
basal c.
basal c. WIF1+
suprabasal c.
suprabasal c. ∞
suprabasal c. KRT4+
suprabasal c. WIF1+
suprabasal c. WIF1+ ∞
filiform papilla
myelinating Schwann c.
non-myelinating Schwann c.
enterocyte progenitor
enterocyte
enterocyte CA2+
goblet c.
goblet c. ∞
enterocyte/goblet c.
enteroendocrine c.
M c. of gut
tuft c.
non-myelinating Schwann c.
enterocyte progenitor
enterocyte
goblet c.
enterocyte/goblet c.
enteroendocrine c.
hepatocyte APOB+
hepatocyte PHYH+
cholangiocyte
acinar c.
acinar c. FDX1+
acinar c. PNISR+
ductal c. SPOCK3+
ductal c. UPK1A+
acinar c./ductal c.
α c.
β c.
α c./β c.
δ c.
non-myelinating Schwann c.
podocyte
proximal convoluted tubule
proximal straight tubule
LoH thin descend limb
LoH thin ascend limb
LoH thin ascend limb SLC14A2+
LoH thick ascend limb
LoH c. AKR1B1+
macula densa c.
distal convoluted tubule
principal c.
principal c. FXYD4+
principal c. KCNE1+
α-intercalated c.
β-intercalated c.
intercalated c./principal c.
urothelial c.
non-myelinating Schwann c.
basal urothelial c.
intermediate urothelial c.
luminal urothelial c.
non-myelinating Schwann c.
non-ciliated c. FXYD4+MUC16+
non-ciliated c. FXYD4+MUC16-
non-ciliated c. IGFBP1+
ciliated c.
spermatogonium
early spermatocyte
pachytene spermatocyte
diplotene spermatocyte
round spermatid
elongating spermatid
elongated spermatid
B
Stromal
Brain cortex
Brainstem
Hypothalamus
Pituitary
Fat
Mammary gland
Limb muscle
Bone
Bone marrow
Blood
Heart
Aorta
Lung
Trachea
Tongue
Small intestine
Colon
Liver
Pancreas
Kidney
Bladder
Uterus
vascular smooth muscle
pericyte
leptomeningeal c.
vascular smooth muscle
pericyte
leptomeningeal c.
pericyte
leptomeningeal c.
tendon c.
smooth muscle
vascular smooth muscle
fibroblast
fibroblast ACKR2+
fibroblast ITIH5+
fibroblast LCN2+
myofibroblast
pericyte
adipocyte UCP1hi
adipocyte UCP1lo
mesothelial c. CXCL10+PRG4+
mesothelial c. CXCL10-PRG4+
mesothelial c. SBSN+
reticular c.
fibroblast
tendon c.
skeletal muscle satellite stem c.
fast muscle
slow muscle
vascular smooth muscle
fibroadipogenic progenitor
pericyte
adipocyte UCP1lo
reticular c.
osteo-CAR c.
osteoblast
chondrocyte
vascular smooth muscle
fibroblast
adipo-CAR c.
adipocyte UCP1lo
? stromal 1 NGFR+TNNT2+
osteo-CAR c.
mesothelial c.
cardiomyocyte
atrial cardiomyocyte
ventricular cardiomyocyte
vascular smooth muscle
fibroblast
pericyte
vascular smooth muscle
adipocyte UCP1lo
vascular smooth muscle
fibroblast
adventitial fibroblast
alveolar fibroblast
fibroblast NNAT+
fibromyocyte
pericyte
mesothelial c.
chondrocyte
fibroblast
tendon c.
skeletal muscle satellite stem c.
vascular smooth muscle
fibroblast
fibroblast WIF1+
pericyte
? stromal 2 NGFR+TNNT2+
? stromal 1 COL15A1+PTGDS+
smooth muscle
vascular smooth muscle
fibroblast
fibroblast CHODL+
fibroblast GGT5+
fibroblast KCNN3+
mesothelial c.
fibroblast
mesothelial c.
fibroblast
mesothelial c.
vascular smooth muscle
fibroblast PI16+
fibroblast PTN+
pericyte
adipocyte UCP1hi
adipocyte UCP1lo
mesothelial c. CXCL10+PRG4+
mesothelial c. CXCL10-PRG4+
mesothelial c. SBSN+
reticular c.
vascular smooth muscle
fibroblast
fibroblast ASPN+
fibroblast TNC+
myofibroblast
pericyte
adipocyte UCP1hi
adipocyte UCP1lo
mesothelial c.
reticular c.
? stromal 1 ST6GAL2+
smooth muscle
vascular smooth muscle
fibroblast
fibroblast PTN+
fibroblast ENPP2+
fibroblast LY6H+
myofibroblast
pericyte
adipocyte UCP1lo
mesothelial c.
smooth muscle
vascular smooth muscle
fibroblast
myofibroblast
pericyte
C
Endothelial
Brain cortex
Brainstem
Pituitary
Skin
Fat
Mammary gland
Limb muscle
Diaphragm
Bone
Bone marrow
Heart
Aorta
Lung
Tongue
Small intestine
Liver
Pancreas
Kidney
Bladder
Uterus
vein
capillary FABP5-RBP7-
vein
capillary FABP5-RBP7-
capillary FABP5-RBP7-
vein
artery
vein
capillary FABP5+RBP7+
capillary CXCL10+
lymphatic CCL21+
lymphatic ACKR4-CCDC80+
vein
capillary FABP5+RBP7lo
lymphatic ACKR4-CCDC80+
vein
capillary FABP5+RBP7lo
capillary FABP5+RBP7+
lymphatic CCL21+
lymphatic ACKR4-CCDC80+
capillary FABP5+RBP7lo
sinusoid MAFB+
sinusoid MAFB+
vascular endothelium FABP5+RBP7+
vascular endothelium FABP5+RBP7+
artery
vein
capillary FABP5-RBP7-
capillary FABP5+RBP7-
capillary CXCL10+
capillary aerocyte
lymphatic CCL21+
vein
capillary FABP5+RBP7lo
lymphatic CCL21+
artery
capillary FABP5+RBP7-
lymphatic CCL21+
hepatic sinusoid
artery
vein
capillary FABP5+RBP7-
capillary FABP5+RBP7+
lymphatic CCL21+
lymphatic ACKR4+CCDC80+
vasa recta descend limb SLC14A1+
vasa recta descend limb MGP+
vasa recta ascend limb IGFBP5+
vasa recta ascend limb IGF1+
capillary FABP5-RBP7-
capillary FABP5+RBP7+
glomerular
lymphatic CCL21+
lymphatic ACKR4-CCDC80+
artery
vein
capillary FABP5+RBP7-
capillary FABP5+RBP7lo
capillary FABP5+RBP7+
lymphatic CCL21+
artery
mean expression
ln(CP10K+1)
0
0.5
1
% of cells positive
12.5%
25%
50%
100%
cell type symbols
∞ = proliferating
? = unassigned/unknown
c. = cell
hormone source & target cell
putative source
putative target

Fig. 1 - continued

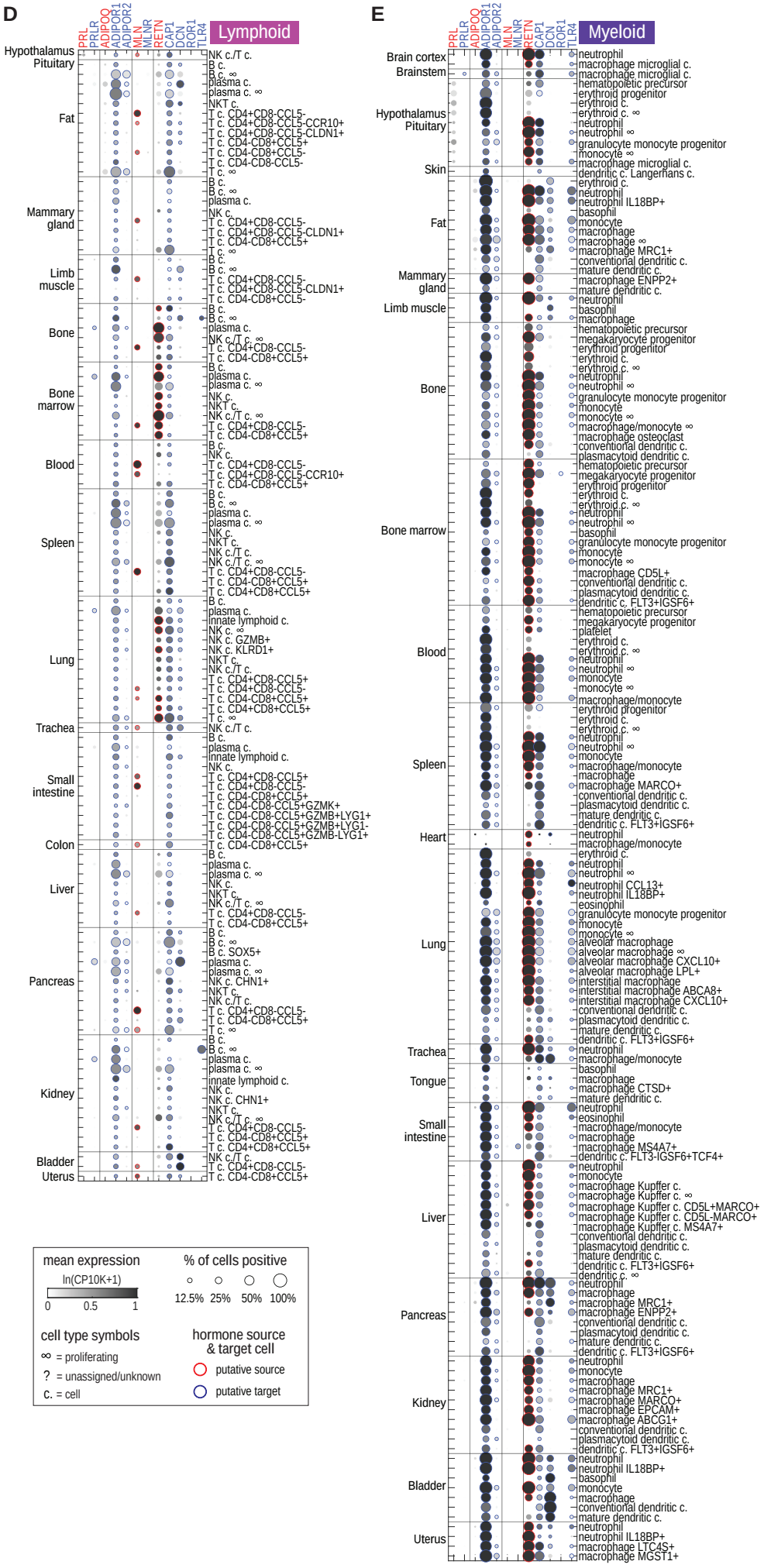

Fig. 2

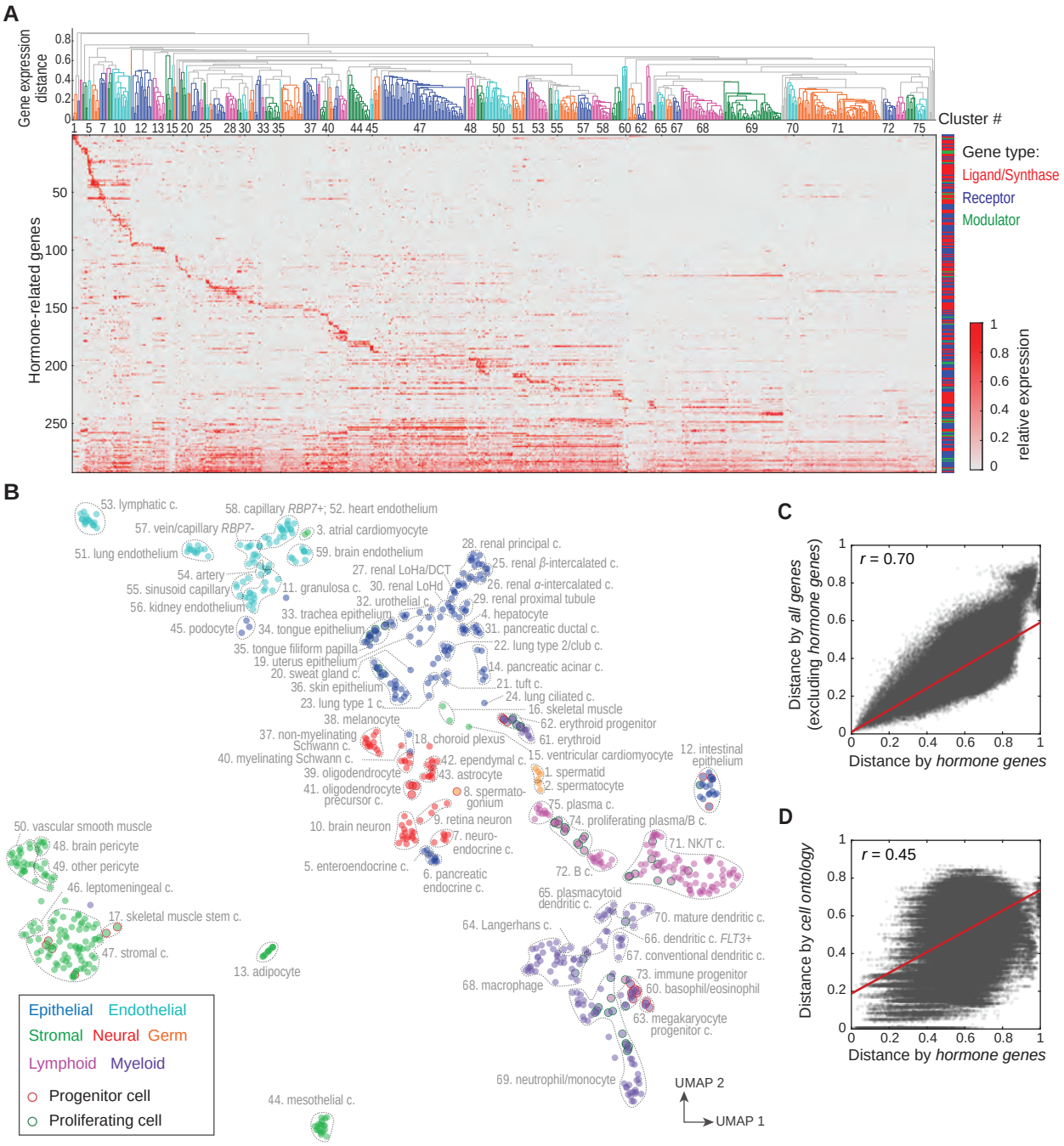
A
Gene expression distance
Cluster #
Hormone-related genes
Gene type:
Ligand/Synthase
Receptor
Modulator
relative expression
B
53. lymphatic c.
58. capillary RBP7+; 52. heart endothelium
57. vein/capillary RBP7-
3. atrial cardiomyocyte
51. lung endothelium
59. brain endothelium
28. renal principal c.
25. renal β-intercalated c.
27. renal LoHa/DCT
54. artery
55. sinusoid capillary
11. granulosa c.
30. renal LoHd
26. renal α-intercalated c.
56. kidney endothelium
32. urothelial c.
29. renal proximal tubule
33. trachea epithelium
4. hepatocyte
45. podocyte
34. tongue epithelium
31. pancreatic ductal c.
35. tongue filiform papilla
22. lung type 2/club c.
19. uterus epithelium
20. sweat gland c.
14. pancreatic acinar c.
36. skin epithelium
21. tuft c.
23. lung type 1 c.
24. lung ciliated c.
16. skeletal muscle
38. melanocyte
62. erythroid progenitor
37. non-myelinating Schwann c.
18. choroid plexus
61. erythroid
40. myelinating Schwann c.
15. ventricular cardiomyocyte
12. intestinal epithelium
42. ependymal c.
39. oligodendrocyte
43. astrocyte
1. spermatid
41. oligodendrocyte precursor c.
2. spermatocyte
8. spermato-gonium
75. plasma c.
50. vascular smooth muscle
10. brain neuron
9. retina neuron
74. proliferating plasma/B c.
48. brain pericyte
7. neuro-endocrine c.
71. NK/T c.
49. other pericyte
5. enteroendocrine c.
6. pancreatic endocrine c.
72. B c.
46. leptomeningeal c.
65. plasmacytoid dendritic c.
17. skeletal muscle stem c.
70. mature dendritic c.
64. Langerhans c.
66. dendritic c. FLT3+
47. stromal c.
67. conventional dendritic c.
13. adipocyte
73. immune progenitor
68. macrophage
60. basophil/eosinophil
63. megakaryocyte progenitor c.
Epithelial
Endothelial
Stromal
Neural
Germ
Lymphoid
Myeloid
Progenitor cell
Proliferating cell
69. neutrophil/monocyte
44. mesothelial c.
UMAP 2
UMAP 1
C
r = 0.70
Distance by all genes (excluding hormone genes)
Distance by hormone genes
D
r = 0.45
Distance by cell ontology
Distance by hormone genes

Fig. 3

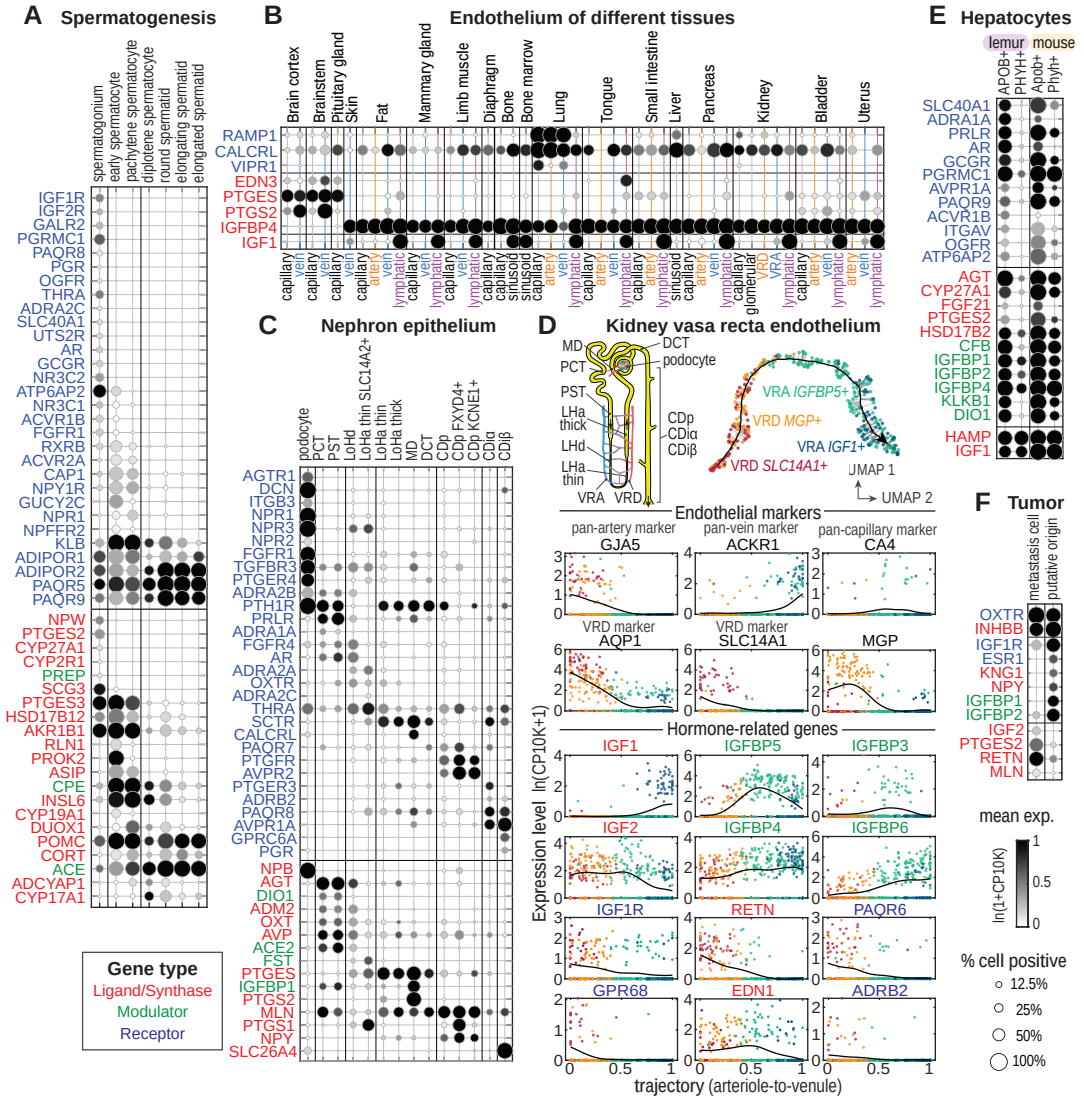
A Spermatogenesis
spermatogonium
early spermatocyte
pachytene spermatocyte
diplotene spermatocyte
round spermatid
elongating spermatid
elongated spermatid
IGF1R
IGF2R
GALR2
PGRMC1
PAQR8
PGR
OGFR
THRA
ADRA2C
SLC40A1
UTS2R
AR
GCGR
NR3C2
ATP6AP2
NR3C1
ACVR1B
FGFR1
RXRB
ACVR2A
CAP1
NPY1R
GUCY2C
NPR1
NPFFR2
KLB
ADIPOR1
ADIPOR2
PAQR5
PAQR9
NPW
PTGES2
CYP27A1
CYP2R1
PREP
SCG3
PTGES3
HSD17B12
AKR1B1
RLN1
PROK2
ASIP
CPE
INSL6
CYP19A1
DUOX1
POMC
CORT
ACE
ADCYAP1
CYP17A1
Gene type
Ligand/Synthase
Modulator
Receptor
B Endothelium of different tissues
Brain cortex
Brainstem
Pituitary gland
Skin
Fat
Mammary gland
Limb muscle
Diaphragm
Bone
Bone marrow
Lung
Tongue
Small intestine
Liver
Pancreas
Kidney
Bladder
Uterus
RAMP1
CALCRL
VIPR1
EDN3
PTGES
PTGS2
IGFBP4
IGF1
capillary
vein
artery
lymphatic
sinusoid
glomerular
VRD
VRA
C Nephron epithelium
podocyte
PCT
PST
LoHd
LoHa thin SLC14A2+
LoHa thin
LoHa thick
MD
DCT
CDp
CDp FXYD4+
CDp KCNE1+
CDiα
CDiβ
AGTR1
DCN
ITGB3
NPR1
NPR3
NPR2
FGFR1
TGFBR3
PTGER4
ADRA2B
PTH1R
PRLR
ADRA1A
FGFR4
AR
ADRA2A
OXTR
ADRA2C
THRA
SCTR
CALCRL
PAQR7
PTGFR
AVPR2
PTGER3
ADRB2
PAQR8
AVPR1A
GPRC6A
PGR
NPB
AGT
DIO1
ADM2
OXT
AVP
ACE2
FST
PTGES
IGFBP1
PTGS2
MLN
PTGS1
NPY
SLC26A4
D Kidney vasa recta endothelium
MD
DCT
PCT
podocyte
PST
LHa thick
LHd
LHa thin
VRA
VRD
CDp
CDiα
CDiβ
VRA IGFBP5+
VRD MGP+
VRA IGF1+
VRD SLC14A1+
UMAP 1
UMAP 2
Endothelial markers
pan-artery marker
pan-vein marker
pan-capillary marker
GJA5
ACKR1
CA4
VRD marker
AQP1
SLC14A1
MGP
Hormone-related genes
IGF1
IGFBP5
IGFBP3
IGF2
IGFBP4
IGFBP6
IGF1R
RETN
PAQR6
GPR68
EDN1
ADRB2
Expression level ln(CP10K+1)
trajectory (arteriole-to-venule)
E Hepatocytes
lemur
mouse
APOB+
PHYH+
Apob+
Phyh+
SLC40A1
ADRA1A
PRLR
AR
GCGR
PGRMC1
AVPR1A
PAQR9
ACVR1B
ITGAV
OGFR
ATP6AP2
AGT
CYP27A1
FGF21
PTGES2
HSD17B2
CFB
IGFBP1
IGFBP2
IGFBP4
KLKB1
DIO1
HAMP
IGF1
F Tumor
metastasis cell
putative origin
OXTR
INHBB
IGF1R
ESR1
KNG1
NPY
IGFBP1
IGFBP2
IGF2
PTGES2
RETN
MLN
mean exp.
ln(1+CP10K)
1
0.5
0
% cell positive
12.5%
25%
50%
100%

Fig. 4

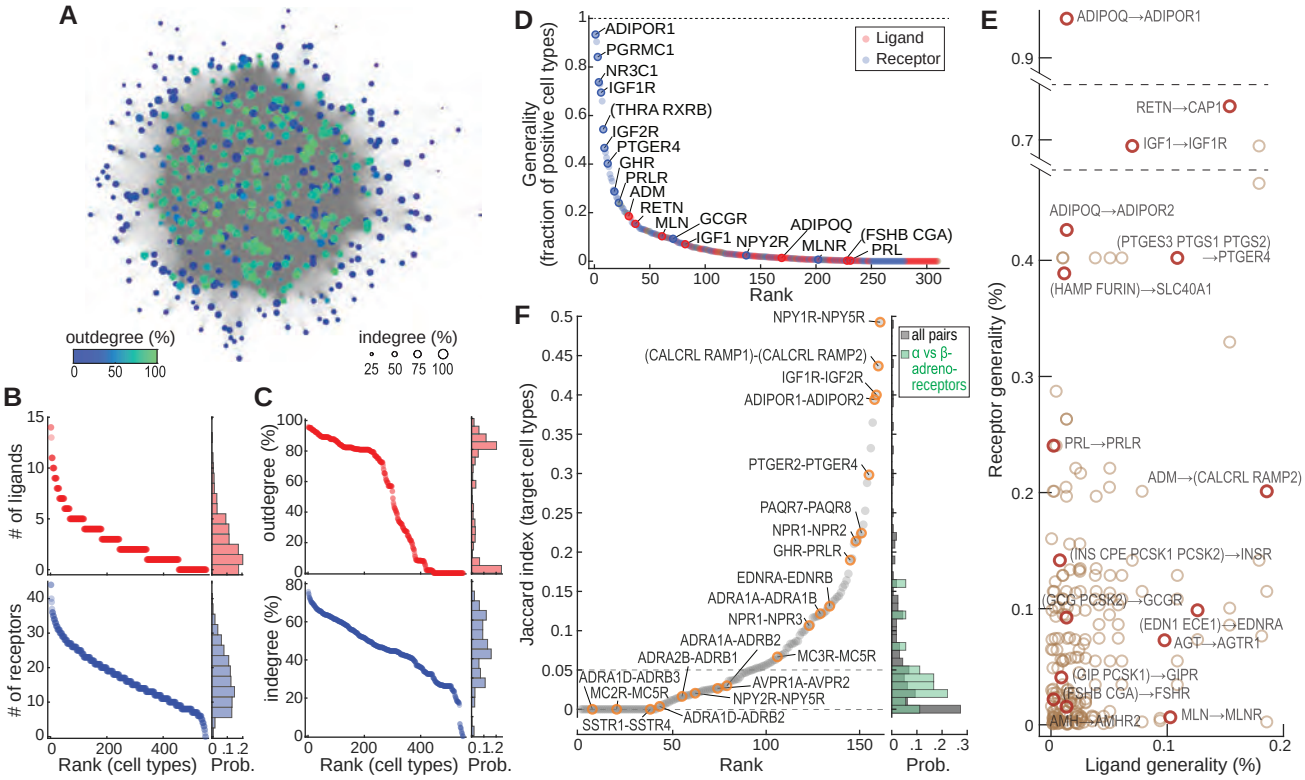
A
outdegree (%)
0 50 100
indegree (%)
25 50 75 100
B
# of ligands
# of receptors
Rank (cell types)
Prob.
C
outdegree (%)
indegree (%)
Rank (cell types)
Prob.
D
Generality (fraction of positive cell types)
Ligand
Receptor
ADIPOR1
PGRMC1
NR3C1
IGF1R
(THRA RXRB)
IGF2R
PTGER4
GHR
PRLR
ADM
RETN
MLN
GCGR
IGF1
NPY2R
ADIPOQ
MLNR
(FSHB CGA)
PRL
Rank
E
ADIPOQ→ADIPOR1
RETN→CAP1
IGF1→IGF1R
ADIPOQ→ADIPOR2
(PTGES3 PTGS1 PTGS2) →PTGER4
(HAMP FURIN)→SLC40A1
PRL→PRLR
ADM→(CALCRL RAMP2)
(INS CPE PCSK1 PCSK2)→INSR
(GCG PCSK2)→GCGR
(EDN1 ECE1)→EDNRA
AGT→AGTR1
(GIP PCSK1)→GIPR
(FSHB CGA)→FSHR
MLN→MLNR
AMH→AMHR2
Receptor generality (%)
Ligand generality (%)
F
Jaccard index (target cell types)
NPY1R-NPY5R
(CALCRL RAMP1)-(CALCRL RAMP2)
IGF1R-IGF2R
ADIPOR1-ADIPOR2
PTGER2-PTGER4
PAQR7-PAQR8
NPR1-NPR2
GHR-PRLR
EDNRA-EDNRB
ADRA1A-ADRA1B
NPR1-NPR3
ADRA1A-ADRB2
ADRA2B-ADRB1
MC3R-MC5R
ADRA1D-ADRB3
AVPR1A-AVPR2
MC2R-MC5R
NPY2R-NPY5R
ADRA1D-ADRB2
SSTR1-SSTR4
all pairs
α vs β-adreno-receptors
Rank
Prob.

Fig. 5

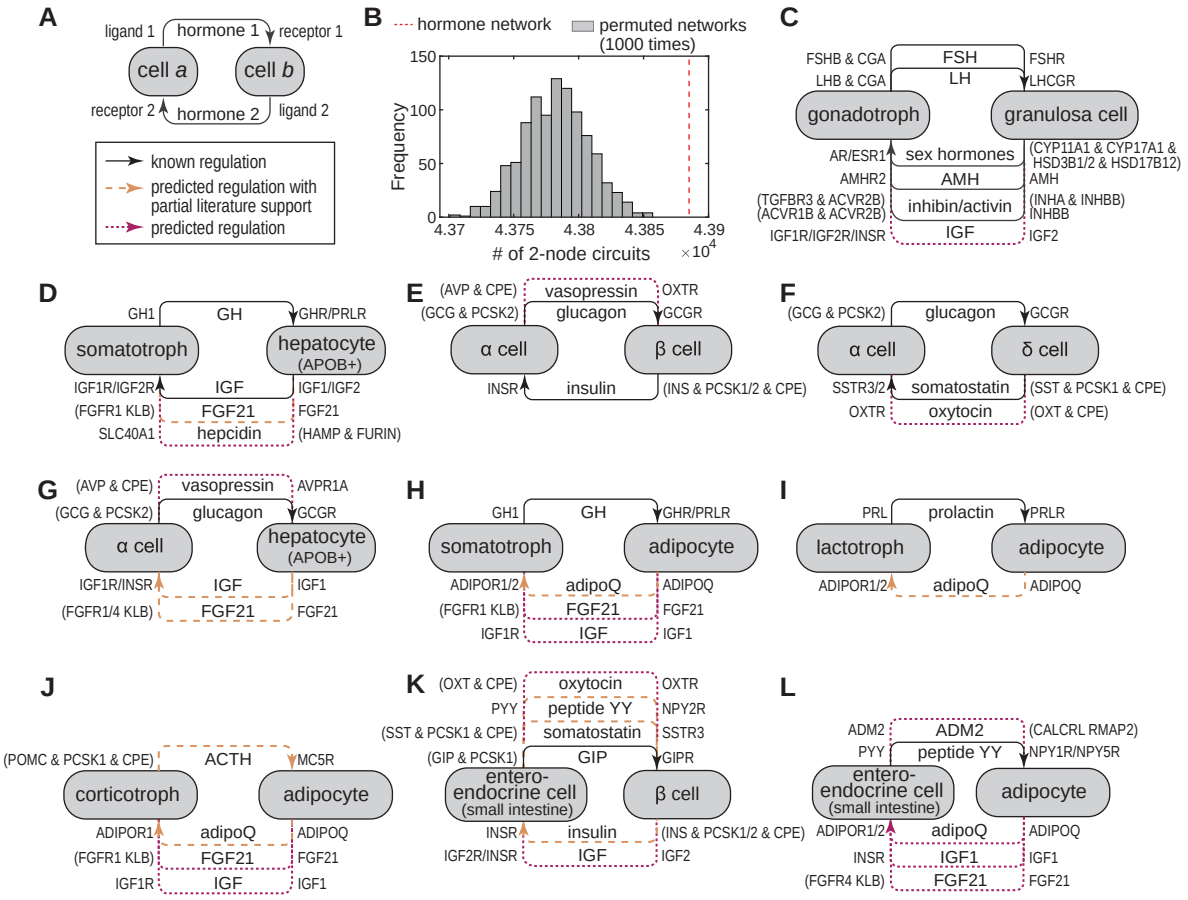
A
ligand 1
hormone 1
receptor 1
cell a
cell b
receptor 2
hormone 2
ligand 2
known regulation
predicted regulation with partial literature support
predicted regulation
B
hormone network
permuted networks (1000 times)
Frequency
150
100
50
0
4.37
4.375
4.38
4.385
4.39
# of 2-node circuits
×10^4
C
FSHB & CGA
LHB & CGA
FSH
LH
FSHR
LHCGR
gonadotroph
granulosa cell
AR/ESR1
AMHR2
sex hormones
AMH
(CYP11A1 & CYP17A1 & HSD3B1/2 & HSD17B12)
AMH
(TGFBR3 & ACVR2B)
(ACVR1B & ACVR2B)
inhibin/activin
(INHA & INHBB)
INHBB
IGF1R/IGF2R/INSR
IGF
IGF2
D
GH1
GH
GHR/PRLR
somatotroph
hepatocyte (APOB+)
IGF1R/IGF2R
IGF
IGF1/IGF2
(FGFR1 KLB)
FGF21
FGF21
SLC40A1
hepcidin
(HAMP & FURIN)
E
(AVP & CPE)
vasopressin
OXTR
(GCG & PCSK2)
glucagon
GCGR
α cell
β cell
INSR
insulin
(INS & PCSK1/2 & CPE)
F
(GCG & PCSK2)
glucagon
GCGR
α cell
δ cell
SSTR3/2
somatostatin
(SST & PCSK1 & CPE)
OXTR
oxytocin
(OXT & CPE)
G
(AVP & CPE)
vasopressin
AVPR1A
(GCG & PCSK2)
glucagon
GCGR
α cell
hepatocyte (APOB+)
IGF1R/INSR
IGF
IGF1
(FGFR1/4 KLB)
FGF21
FGF21
H
GH1
GH
GHR/PRLR
somatotroph
adipocyte
ADIPOR1/2
adipoQ
ADIPOQ
(FGFR1 KLB)
FGF21
FGF21
IGF1R
IGF
IGF1
I
PRL
prolactin
PRLR
lactotroph
adipocyte
ADIPOR1/2
adipoQ
ADIPOQ
J
(POMC & PCSK1 & CPE)
ACTH
MC5R
corticotroph
adipocyte
ADIPOR1
adipoQ
ADIPOQ
(FGFR1 KLB)
FGF21
FGF21
IGF1R
IGF
IGF1
K
(OXT & CPE)
oxytocin
OXTR
PYY
peptide YY
NPY2R
(SST & PCSK1 & CPE)
somatostatin
SSTR3
(GIP & PCSK1)
GIP
GIPR
entero-endocrine cell (small intestine)
β cell
INSR
insulin
(INS & PCSK1/2 & CPE)
IGF2R/INSR
IGF
IGF2
L
ADM2
ADM2
(CALCRL RMAP2)
PYY
peptide YY
NPY1R/NPY5R
entero-endocrine cell (small intestine)
adipocyte
ADIPOR1/2
adipoQ
ADIPOQ
INSR
IGF1
IGF1
(FGFR4 KLB)
FGF21
FGF21

Fig. 6

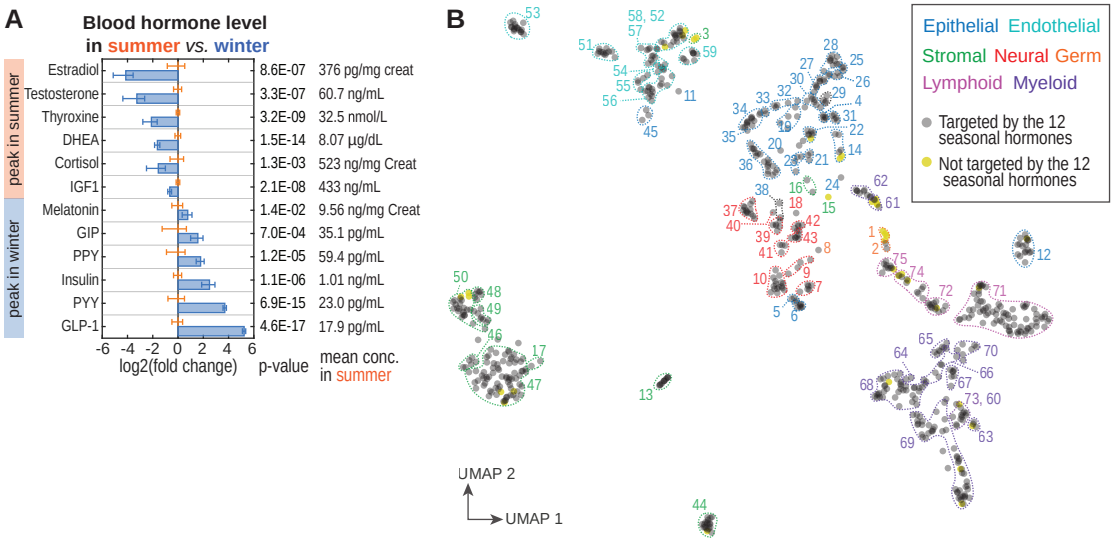
A
Blood hormone level
in summer vs. winter
peak in summer
peak in winter
Estradiol 8.6E-07 376 pg/mg creat
Testosterone 3.3E-07 60.7 ng/mL
Thyroxine 3.2E-09 32.5 nmol/L
DHEA 1.5E-14 8.07 µg/dL
Cortisol 1.3E-03 523 ng/mg Creat
IGF1 2.1E-08 433 ng/mL
Melatonin 1.4E-02 9.56 ng/mg Creat
GIP 7.0E-04 35.1 pg/mL
PPY 1.2E-05 59.4 pg/mL
Insulin 1.1E-06 1.01 ng/mL
PYY 6.9E-15 23.0 pg/mL
GLP-1 4.6E-17 17.9 pg/mL
-6 -4 -2 0 2 4 6
log2(fold change)
p-value
mean conc. in summer
B
Epithelial Endothelial
Stromal Neural Germ
Lymphoid Myeloid
Targeted by the 12 seasonal hormones
Not targeted by the 12 seasonal hormones
UMAP 2
UMAP 1

Fig. S2

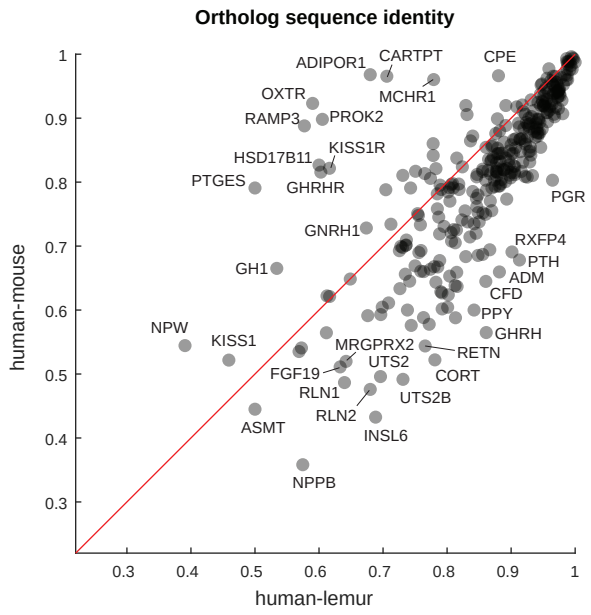
Ortholog sequence identity
human-mouse
human-lemur
1
0.9
0.8
0.7
0.6
0.5
0.4
0.3
0.3
0.4
0.5
0.6
0.7
0.8
0.9
1
ADIPOR1
CARTPT
CPE
MCHR1
OXTR
RAMP3
PROK2
KISS1R
HSD17B11
PTGES
GHRHR
PGR
GNRH1
RXFP4
PTH
GH1
ADM
CFD
PPY
NPW
GHRH
KISS1
MRGPRX2
RETN
UTS2
FGF19
CORT
RLN1
UTS2B
RLN2
ASMT
INSL6
NPPB

Fig. S3

By transcriptome (excluding hormone-related genes)

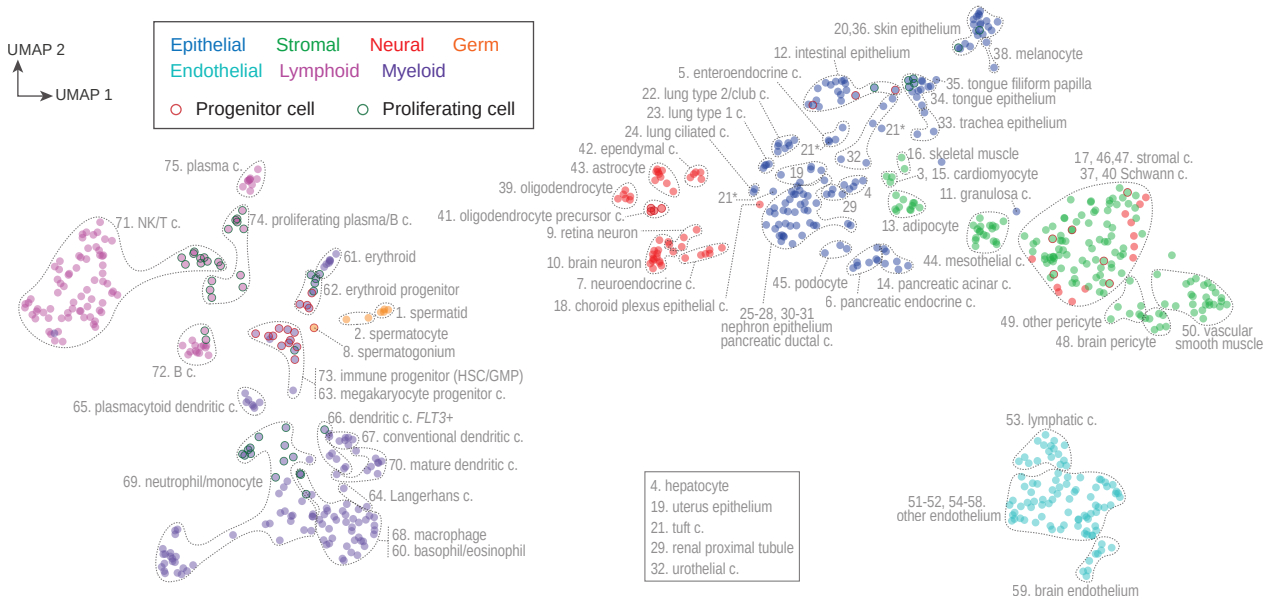

Fig. S4

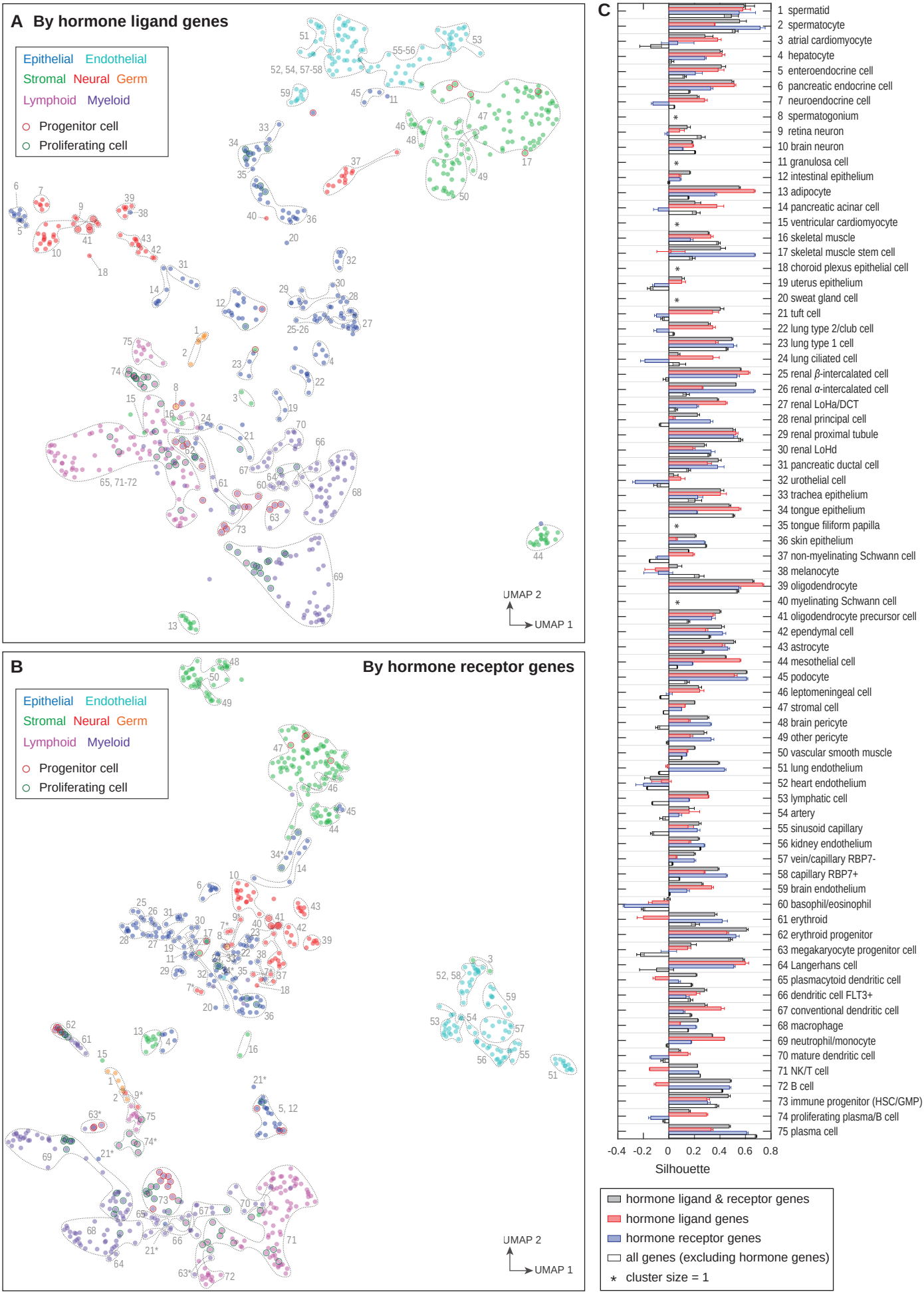
A By hormone ligand genes
Epithelial Endothelial
Stromal Neural Germ
Lymphoid Myeloid
Progenitor cell
Proliferating cell
UMAP 2
UMAP 1
B By hormone receptor genes
Epithelial Endothelial
Stromal Neural Germ
Lymphoid Myeloid
Progenitor cell
Proliferating cell
UMAP 2
UMAP 1
C
1 spermatid
2 spermatocyte
3 atrial cardiomyocyte
4 hepatocyte
5 enteroendocrine cell
6 pancreatic endocrine cell
7 neuroendocrine cell
8 spermatogonium
9 retina neuron
10 brain neuron
11 granulosa cell
12 intestinal epithelium
13 adipocyte
14 pancreatic acinar cell
15 ventricular cardiomyocyte
16 skeletal muscle
17 skeletal muscle stem cell
18 choroid plexus epithelial cell
19 uterus epithelium
20 sweat gland cell
21 tuft cell
22 lung type 2/club cell
23 lung type 1 cell
24 lung ciliated cell
25 renal β-intercalated cell
26 renal α-intercalated cell
27 renal LoHa/DCT
28 renal principal cell
29 renal proximal tubule
30 renal LoHd
31 pancreatic ductal cell
32 urothelial cell
33 trachea epithelium
34 tongue epithelium
35 tongue filiform papilla
36 skin epithelium
37 non-myelinating Schwann cell
38 melanocyte
39 oligodendrocyte
40 myelinating Schwann cell
41 oligodendrocyte precursor cell
42 ependymal cell
43 astrocyte
44 mesothelial cell
45 podocyte
46 leptomeningeal cell
47 stromal cell
48 brain pericyte
49 other pericyte
50 vascular smooth muscle
51 lung endothelium
52 heart endothelium
53 lymphatic cell
54 artery
55 sinusoid capillary
56 kidney endothelium
57 vein/capillary RBP7-
58 capillary RBP7+
59 brain endothelium
60 basophil/eosinophil
61 erythroid
62 erythroid progenitor
63 megakaryocyte progenitor cell
64 Langerhans cell
65 plasmacytoid dendritic cell
66 dendritic cell FLT3+
67 conventional dendritic cell
68 macrophage
69 neutrophil/monocyte
70 mature dendritic cell
71 NK/T cell
72 B cell
73 immune progenitor (HSC/GMP)
74 proliferating plasma/B cell
75 plasma cell
-0.4 -0.2 0 0.2 0.4 0.6 0.8
Silhouette
hormone ligand & receptor genes
hormone ligand genes
hormone receptor genes
all genes (excluding hormone genes)
* cluster size = 1

Fig. S5

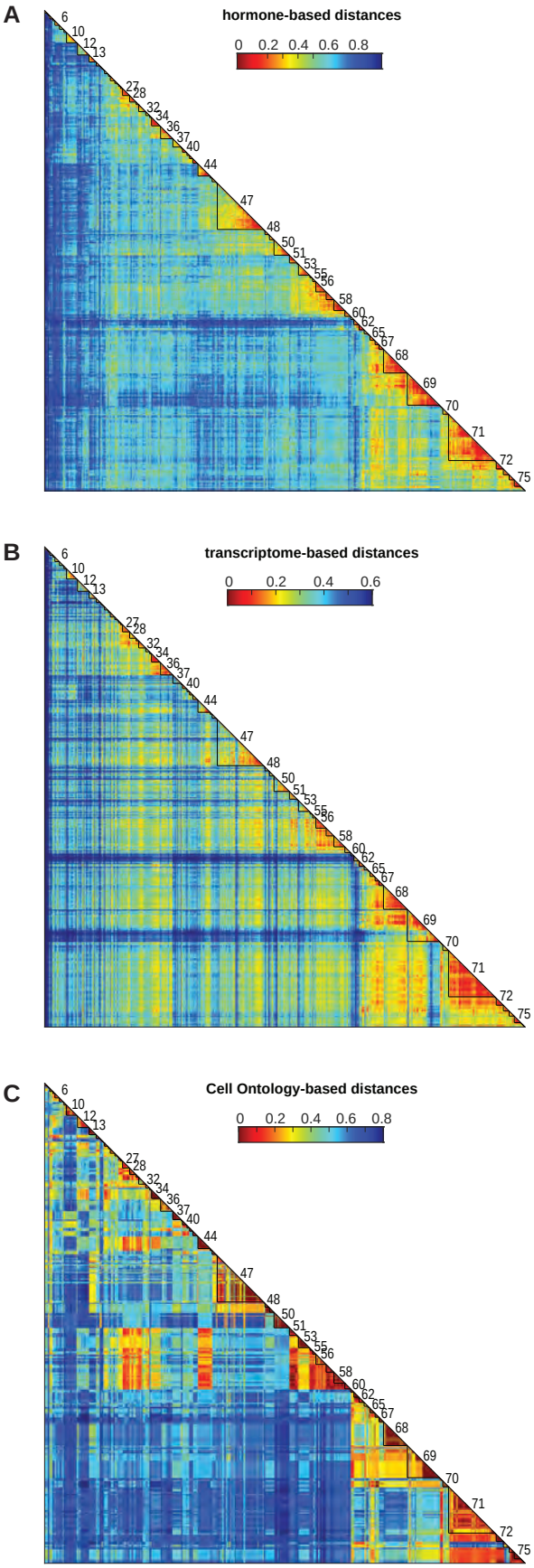
A
hormone-based distances
0 0.2 0.4 0.6 0.8
B
transcriptome-based distances
0 0.2 0.4 0.6
C
Cell Ontology-based distances
0 0.2 0.4 0.6 0.8
6 10 12 13 27 28 32 34 36 37 40 44 47 48 50 51 53 55 56 58 60 62 65 67 68 69 70 71 72 75

Fig. S6

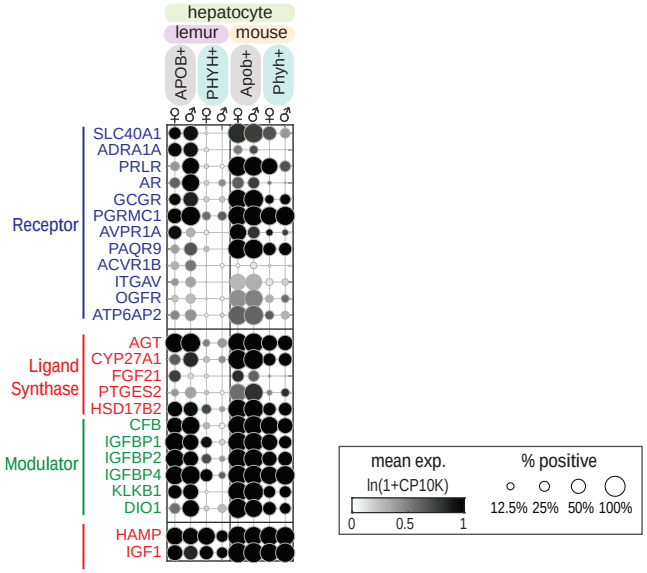
hepatocyte
lemur
mouse
APOB+
PHYH+
Apob+
Phyh+
♀ ♂ ♀ ♂ ♀ ♂ ♀ ♂
Receptor
SLC40A1
ADRA1A
PRLR
AR
GCGR
PGRMC1
AVPR1A
PAQR9
ACVR1B
ITGAV
OGFR
ATP6AP2
Ligand Synthase
AGT
CYP27A1
FGF21
PTGES2
HSD17B2
Modulator
CFB
IGFBP1
IGFBP2
IGFBP4
KLKB1
DIO1
HAMP
IGF1
mean exp.
ln(1+CP10K)
0
0.5
1
% positive
12.5%
25%
50%
100%

Fig. S7

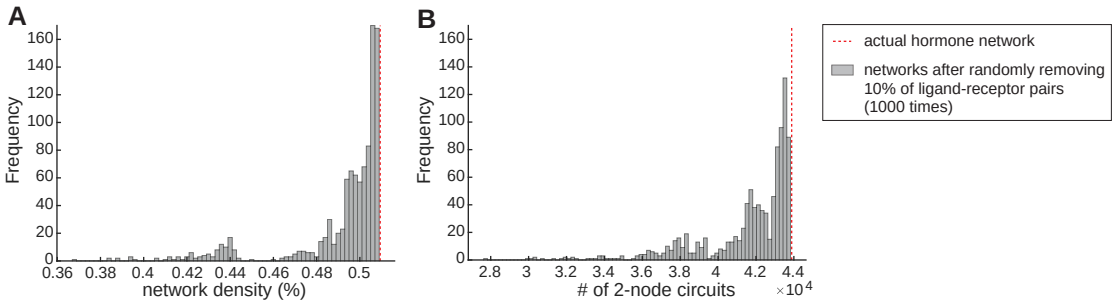
A
Frequency
network density (%)
B
Frequency
# of 2-node circuits
×10^4
actual hormone network
networks after randomly removing 10% of ligand-receptor pairs (1000 times)

Fig. S8

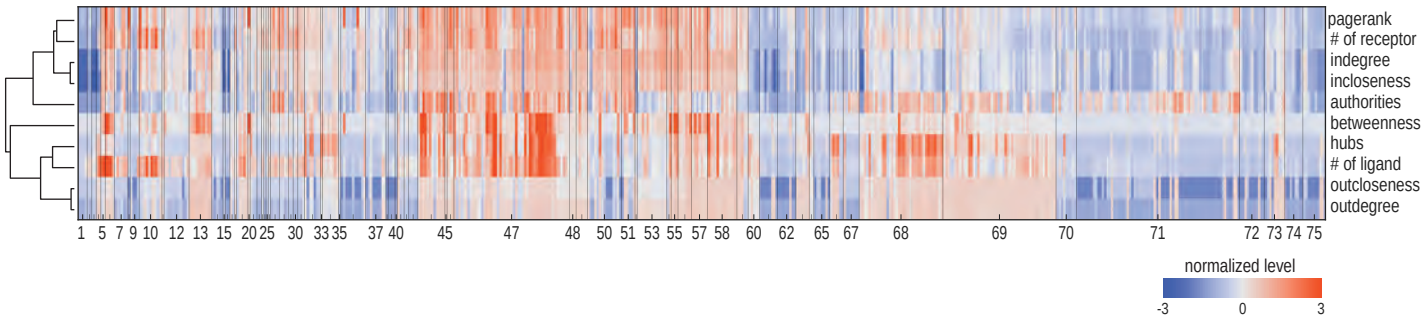
pagerank
# of receptor
indegree
incloseness
authorities
betweenness
hubs
# of ligand
outcloseness
outdegree
1 5 7 9 10 12 13 15 20 25 30 33 35 37 40 45 47 48 50 51 53 55 57 58 60 62 65 67 68 69 70 71 72 73 74 75
normalized level
-3
0
3

Fig. S9

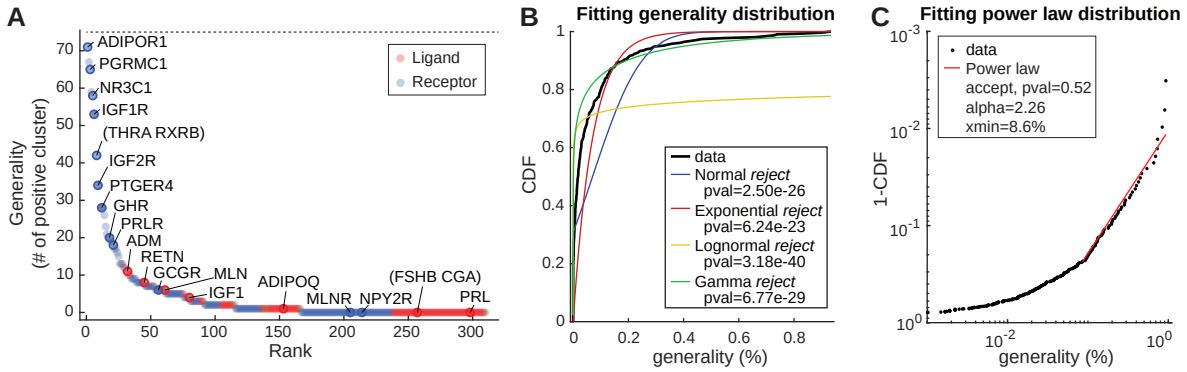
A
Generality
(# of positive cluster)
Rank
ADIPOR1
PGRMC1
NR3C1
IGF1R
(THRA RXRB)
IGF2R
PTGER4
GHR
PRLR
ADM
RETN
GCGR
MLN
IGF1
ADIPOQ
MLNR
NPY2R
(FSHB CGA)
PRL
Ligand
Receptor
B
Fitting generality distribution
CDF
generality (%)
data
Normal reject
pval=2.50e-26
Exponential reject
pval=6.24e-23
Lognormal reject
pval=3.18e-40
Gamma reject
pval=6.77e-29
C
Fitting power law distribution
1-CDF
generality (%)
data
Power law
accept, pval=0.52
alpha=2.26
xmin=8.6%

The Tabula Microcebus Consortium

Name	Email	Lab	Affiliations
Snigdha Agarwal	snigdha.agarwal@czbiohub.org	CZ Biohub	Chan Zuckerberg Biohub, San Francisco, CA, USA.
Aditi Agrawal	aditi.agrawal@czbiohub.org	CZ Biohub	Chan Zuckerberg Biohub, San Francisco, CA, USA.
Ahmad Al-Moujahed	ahmadm@stanford.edu	Albert Wu	Department of Ophthalmology, Stanford University School of Medicine, Stanford, CA, USA.
Alina Alam	alina.ara.alam@gmail.com	Charles Chan	Institute for Stem Cell Biology and Regenerative Medicine, Stanford University School of Medicine, Stanford, CA, USA.
Megan A. Albertelli	albertel@stanford.edu	Megan Albertelli	Department of Comparative Medicine, Stanford University School of Medicine, Stanford, CA, USA.
Paul Allegakoen	paul.allegakoen@ucsf.edu	Franklin Huang	Division of Hematology/Oncology, Department of Medicine, University of California San Francisco, San Francisco, CA, USA.
Thomas Ambrosi	ambrosi@stanford.edu	Charles Chan	Institute for Stem Cell Biology and Regenerative Medicine, Stanford University School of Medicine, Stanford, CA, USA.
Jane Antony	janetony@stanford.edu	Michael Clarke	Institute for Stem Cell Biology and Regenerative Medicine, Stanford University School of Medicine, Stanford, CA, USA.
Steven Artandi	sartandi@stanford.edu	Steven Artandi	Stanford Cancer Institute, Stanford University School of Medicine, Stanford, CA, USA.; Department of Medicine, Stanford University School of Medicine, Stanford, CA, USA.; Department of Biochemistry, Stanford University School of Medicine, Stanford, CA, USA.
Fabienne Aujard	fabienne.aujard@mnhn.fr	Fabienne Aujard	Adaptive Mechanisms and Evolution (MECADEV), UMR 7179, National Center for Scientific Research, National Museum of Natural History, Brunoy, France.
Kyle Awayan	kyle.awayan@czbiohub.org	CZ Biohub	Chan Zuckerberg Biohub, San Francisco, CA, USA.
Ankit Baghel	abaghel@stanford.edu	Philip Beachy	Department of Biology, Stanford University, Stanford, CA, USA.
Isaac Bakerman	isaacbakerman@email.arizona.edu	Patricia Nguyen	Department of Medicine, Division of Cardiovascular Medicine, Stanford University, Stanford, CA, USA.
Trygve E. Bakken	trygveb@alleninstitute.org	Allen Institute for Brain Science	Human Cell Types Department, Allen Institute for Brain Science, Seattle, WA, USA.
Jalal Baruni	baruni@stanford.edu	Mark Krasnow; Liqun Luo	Department of Anesthesiology, Perioperative and Pain Medicine, Stanford University School of Medicine, Stanford, CA, USA.; Department of Biochemistry, Stanford University School of Medicine, Stanford, CA, USA.; Department of Biology, Stanford University, Stanford, CA, USA.; Howard Hughes Medical Institute, USA.
Philip Beachy	pbeachy@stanford.edu	Philip Beachy	Institute for Stem Cell Biology and Regenerative Medicine, Stanford University School of Medicine, Stanford, CA, USA.; Department of Developmental Biology, Stanford University School of Medicine, Stanford, CA, USA.; Department of Urology, Stanford University School of Medicine, Stanford, CA, USA.; Department of Chemical and Systems Biology, Stanford University School of Medicine, Stanford, CA, USA.
Biter Bilen	biterbilen@gmail.com	Thomas Rando	Department of Neurology and Neurological Sciences, Stanford University School of Medicine, Stanford, CA, USA.
Olga Botvinnik	olga.botvinnik@gmail.com	CZ Biohub	Chan Zuckerberg Biohub, San Francisco, CA, USA.
Scott D. Boyd	sboyd1@stanford.edu	Scott Boyd	Department of Pathology, Stanford University School of Medicine, Stanford, CA, USA.
Deviana Burhan	deviana.burhan@ucsf.edu	Bruce Wang	Department of Medicine and Liver Center, University of California San Francisco, San Francisco, CA, USA.
Kerriann M. Casey	kmcasey@stanford.edu	Kerriann Casey	Department of Comparative Medicine, Stanford University School of Medicine, Stanford, CA, USA.
Charles Chan	chazchan@stanford.edu	Charles Chan	Institute for Stem Cell Biology and Regenerative Medicine, Stanford University School of Medicine, Stanford, CA, USA.
Charles A. Chang	changca@stanford.edu	Seung Kim	Department of Developmental Biology, Stanford University School of Medicine, Stanford, CA, USA.; Stanford Diabetes Research Center, Stanford, CA, USA.
Stephen Chang	scthree@stanford.edu	Mark Krasnow	Department of Biochemistry, Stanford University School of Medicine, Stanford, CA, USA.; Department of Medicine, Division of Cardiovascular Medicine, Stanford University, Stanford, CA, USA.; Howard Hughes Medical Institute, USA.
Ming Chen	ming2017@stanford.edu	Douglas Vollrath	Department of Genetics, Stanford University School of Medicine, Stanford, CA, USA.
Michael F. Clarke	mfclarke@stanford.edu	Michael Clarke	Institute for Stem Cell Biology and Regenerative Medicine, Stanford University School of Medicine, Stanford, CA, USA.
Sheela Crasta	sheelat@stanford.edu	CZ Biohub	Chan Zuckerberg Biohub, San Francisco, CA, USA.

Rebecca Culver	becca.culver@gmail.com	Kerwyn Casey Huang	Department of Genetics, Stanford University School of Medicine, Stanford, CA, USA.
Jessica D'Addabbo	jcdaddab@stanford.edu	Patricia Nguyen	Division of Cardiovascular Medicine, Stanford University, Stanford, CA, USA.; Stanford Cardiovascular Institute, Stanford, CA, USA.
Spyros Darmanis	spyros.darmanis@czbiohub.org	CZ Biohub	Chan Zuckerberg Biohub, San Francisco, CA, USA.
Roozbeh Dehghannasiri	rdehghan@stanford.edu	Julia Salzman	Department of Biochemistry, Stanford University School of Medicine, Stanford, CA, USA.; Department of Biomedical Data Science, Stanford University, Stanford, CA, USA.
Song-Lin Ding	songd@alleninstitute.org	Allen Institute for Brain Science	Human Cell Types Department, Allen Institute for Brain Science, Seattle, WA, USA.
Connor V. Duffy	cvduffy@stanford.edu	Silvana Konermann	Department of Genetics, Stanford University School of Medicine, Stanford, CA, USA.; Howard Hughes Medical Institute, USA.
Jacques Epelbaum	jacques.epelbaum@inserm.fr	Jacques Epelbaum	Adaptive Mechanisms and Evolution (MECADEV), UMR 7179, National Center for Scientific Research, National Museum of Natural History, Brunoy, France.; Unité Mixte de Recherche en Santé 894 INSERM, Centre de Psychiatrie et Neurosciences, Université Paris Descartes, Sorbonne, Paris, France
F. Hernán Espinoza	hespinoz@stanford.edu	Mark Krasnow	Department of Biochemistry, Stanford University School of Medicine, Stanford, CA, USA.; Howard Hughes Medical Institute, USA.
Camille Ezran	camillee@stanford.edu	Mark Krasnow	Department of Biochemistry, Stanford University School of Medicine, Stanford, CA, USA.; Howard Hughes Medical Institute, USA.
Jean Farup	jean@biomed.au.dk	Thomas Rando	Department of Neurology and Neurological Sciences, Stanford University School of Medicine, Stanford, CA, USA.; Department of Biomedicine, Aarhus University, Aarhus, Denmark.
James E. Ferrell, Jr.	james.ferrell@stanford.edu	James Ferrell	Department of Chemical and Systems Biology, Stanford University School of Medicine, Stanford, CA, USA.; Department of Biochemistry, Stanford University School of Medicine, Stanford, CA, USA.
Hannah K. Frank	hkfrank@tulane.edu	Scott Boyd	Department of Pathology, Stanford University School of Medicine, Stanford, CA, USA.; Department of Ecology and Evolutionary Biology, Tulane University, New Orleans, LA, USA.
Margaret Fuller	mtfuller@stanford.edu	Margaret Fuller	Department of Developmental Biology, Stanford University School of Medicine, Stanford, CA, USA.; Department of Genetics, Stanford University School of Medicine, Stanford, CA, USA.
Astrid Gillich	agillich@stanford.edu	Mark Krasnow	Department of Biochemistry, Stanford University School of Medicine, Stanford, CA, USA.; Howard Hughes Medical Institute, USA.
Elias Godoy	eligodoy@stanford.edu	Stanford Veterinary Service Center	Department of Comparative Medicine, Stanford University School of Medicine, Stanford, CA, USA.
Dita Gratzinger	ditag@stanford.edu	Dita Gratzinger	Department of Pathology, Stanford University School of Medicine, Stanford, CA, USA.
Lisbeth A. Guethlein	libbyg@stanford.edu	Peter Parham	Department of Structural Biology, Stanford University School of Medicine, Stanford, CA, USA.; Department of Microbiology and Immunology, Stanford University School of Medicine, Stanford, CA, USA.
Yan Hang	yanh@stanford.edu	Seung Kim	Department of Developmental Biology, Stanford University School of Medicine, Stanford, CA, USA.; Stanford Diabetes Research Center, Stanford, CA, USA.
Kazuteru Hasegawa	kazuteru@stanford.edu	Steven Artandi	Stanford Cancer Institute, Stanford University School of Medicine, Stanford, CA, USA.; Department of Medicine, Stanford University School of Medicine, Stanford, CA, USA.; Department of Biochemistry, Stanford University School of Medicine, Stanford, CA, USA.
Rebecca D. Hodge	rebeccah@alleninstitute.org	Allen Institute for Brain Science	Human Cell Types Department, Allen Institute for Brain Science, Seattle, WA, USA.
Malachia Hoover	malachia@stanford.edu	Charles Chan	Institute for Stem Cell Biology and Regenerative Medicine, Stanford University School of Medicine, Stanford, CA, USA.
Franklin W. Huang	franklin.huang@ucsf.edu	Franklin Huang	Division of Hematology/Oncology, Department of Medicine, University of California San Francisco, San Francisco, CA, USA.
Kerwyn C. Huang	kchuang@stanford.edu	Kerwyn Casey Huang	Department of Bioengineering, Stanford University, Stanford, CA, USA.; Department of Microbiology and Immunology, Stanford University School of Medicine, Stanford, CA, USA.; Chan Zuckerberg Biohub, San Francisco, CA, USA.
Shelly Huynh	shelly.huynh@czbiohub.org	CZ Biohub	Chan Zuckerberg Biohub, San Francisco, CA, USA.

Taichi Isobe	tisobe.kyushu@gmail.com	Michael Clarke	Department of Oncology and Social Medicine, Kyushu University, Japan.
Carly Israel	carly.israel@yale.edu	CZ Biohub	Chan Zuckerberg Biohub, San Francisco, CA, USA.
SoRi Jang	sorijang@stanford.edu	Mark Krasnow	Department of Biochemistry, Stanford University School of Medicine, Stanford, CA, USA.; Howard Hughes Medical Institute, USA.
Qiuyu Jing	qjingab@connect.ust.hk	Angela Wu	Division of Life Science, Hong Kong University of Science and Technology, Hong Kong SAR, China.
Robert C. Jones	jonesbob@stanford.edu	Stephen Quake	Department of Bioengineering, Stanford University, Stanford, CA, USA.
Jengmin Kang	jminkang@stanford.edu	Thomas Rando	Department of Neurology and Neurological Sciences, Stanford University School of Medicine, Stanford, CA, USA.
Caitlin J. Karanewsky	ckaranew@stanford.edu	Mark Krasnow	Department of Biochemistry, Stanford University School of Medicine, Stanford, CA, USA.; Howard Hughes Medical Institute, USA.
Jim Karkanias	jim.karkanias@czbiohub.org	CZ Biohub	Chan Zuckerberg Biohub, San Francisco, CA, USA.
Justus Kebschull	justus@kebschull.me	Justus Kebschull	Department of Biomedical Engineering, Johns Hopkins School of Medicine, Baltimore, MD, USA.
Aaron Kershner	kershner@stanford.edu	Philip Beachy	Department of Biochemistry, Stanford University School of Medicine, Stanford, CA, USA.; Institute of Stem Cell Biology and Regenerative Medicine, Stanford University School of Medicine, Stanford, CA, USA.
Lily Kim	lilykim@stanford.edu	Douglas Vollrath	Department of Genetics, Stanford University School of Medicine, Stanford, CA, USA.
Seung K. Kim	seungkim@stanford.edu	Seung Kim	Department of Developmental Biology, Stanford University School of Medicine, Stanford, CA, USA.; Stanford Diabetes Research Center, Stanford, CA, USA.; JDRF Center of Excellence, Stanford, CA, USA.; Department of Medicine, Stanford University School of Medicine, Stanford, CA, USA.
E. Christopher Kirk	eckirk@austin.utexas.edu	E. Christopher Kirk	Department of Anthropology, University of Texas at Austin, Austin, TX, USA.
Winston Koh	Winston_koh@imcb.a-star.edu.sg	Molecular Engineering Lab	Institute of Bioengineering and Bioimaging, Agency of Science Technology and Research, Singapore; Bioinformatics Institute, Agency of Science Technology and Research, Singapore
Silvana Konermann	silvanak@stanford.edu	Silvana Konermann	Department of Biochemistry, Stanford University School of Medicine, Stanford, CA, USA.; Howard Hughes Medical Institute, USA.
William Kong	wwkong@stanford.edu	Philip Beachy	Institute for Stem Cell Biology and Regenerative Medicine, Stanford University School of Medicine, Stanford, CA, USA.
Mark A. Krasnow	krasnow@stanford.edu	Mark Krasnow	Department of Biochemistry, Stanford University School of Medicine, Stanford, CA, USA.; Howard Hughes Medical Institute, USA.
Christin Kuo	ckuo@stanford.edu	Christin Kuo	Department of Pediatrics, Stanford University School of Medicine, Stanford, CA, USA.
Corinne Lautier	corinne.lautier@umontpellier.fr	Corinne Lautier	MMDN, University of Montpellier, EPHE-PSL, INSERM, Montpellier, France.
Song Eun Lee	songlee@stanford.edu	Tony Wyss-Coray	Department of Neurology and Neurological Sciences, Stanford University School of Medicine, Stanford, CA, USA.; Wu Tsai Neurosciences Institute, Stanford, CA, USA.
Ed S. Lein	edl@alleninstitute.org	Allen Institute for Brain Science	Human Cell Types Department, Allen Institute for Brain Science, Seattle, WA, USA.
Rebecca Lewis	rjlewis@austin.utexas.edu	Rebecca Lewis	Department of Anthropology, University of Texas at Austin, Austin, TX, USA.
Peng Li	penglium@umich.edu	Mark Krasnow	Department of Biochemistry, Stanford University School of Medicine, Stanford, CA, USA.; Howard Hughes Medical Institute, USA.
Shengda Lin	shengda_lin@zju.edu.cn	Steven Artandi; Shengda Lin	Zhejiang Provincial Key Laboratory for Cancer Molecular Cell Biology, Life Sciences Institute, Zhejiang University, Hangzhou, Zhejiang, China.
Shixuan Liu	shixuan@stanford.edu	Mark Krasnow; James Ferrell	Department of Chemical and Systems Biology, Stanford University School of Medicine, Stanford, CA, USA.; Department of Biochemistry, Stanford University School of Medicine, Stanford, CA, USA.; Howard Hughes Medical Institute, USA.
Yin Liu	yinl@stanford.edu	Mark Krasnow	Department of Biochemistry, Stanford University School of Medicine, Stanford, CA, USA.; Howard Hughes Medical Institute, USA.
Gabriel Loeb	gabriel.loeb@ucsf.edu	Gabriel Loeb	Division of Nephrology, Department of Medicine, University of California San Francisco, San Francisco, CA, USA.
Jonathan Z. Long	jzlong@stanford.edu	Jonathan Long	Department of Pathology, Stanford University School of Medicine, Stanford, CA, USA.; Stanford ChEM-H, Stanford, CA, USA.
Wan-Jin Lu	wjlu@stanford.edu	Philip Beachy	Institute for Stem Cell Biology and Regenerative Medicine, Stanford University School of Medicine, Stanford, CA, USA.

Katherine Lucot	kllucot@stanford.edu	Tom Montine	Department of Pathology, Stanford University School of Medicine, Stanford, CA, USA.
Liqun Luo	lluo@stanford.edu	Liqun Luo	Department of Biology, Stanford University, Stanford, CA, USA.; Howard Hughes Medical Institute, USA.
Aaron McGeever	aaron.mcgeever@czbiohub.org	CZ Biohub	Chan Zuckerberg Biohub, San Francisco, CA, USA.
Ross Metzger	rmetzger@stanford.edu	Ross Metzger	Department of Pediatrics, Stanford University School of Medicine, Stanford, CA, USA.; Division of Cardiology, Stanford University School of Medicine, Stanford, CA, USA.
Jingsi Ming	jsming@fem.ecnu.edu.cn	Can Yang; Jingsi Ming	Academy of Statistics and Interdisciplinary Sciences, KLATASDS-MOE, East China Normal University, Shanghai, China.; Department of Mathematics, Hong Kong University of Science and Technology, Hong Kong SAR, China.
Tom Montine	tmontine@stanford.edu	Tom Montine	Department of Pathology, Stanford University School of Medicine, Stanford, CA, USA.
Antoine de Morree	demorree@stanford.edu	Thomas Rando	Department of Neurology and Neurological Sciences, Stanford University School of Medicine, Stanford, CA, USA.; Department of Biomedicine, Aarhus University, Aarhus, Denmark.
Maurizio Morri	morri@stanford.edu	CZ Biohub	Chan Zuckerberg Biohub, San Francisco, CA, USA.
Karim Mrouj	karim.mrouj@stanford.edu	Philip Beachy	Institute for Stem Cell Biology and Regenerative Medicine, Stanford University School of Medicine, Stanford, CA, USA.
Shravani Mukherjee	smukherj@stanford.edu	Albert Wu	Department of Ophthalmology, Stanford University School of Medicine, Stanford, CA, USA.
Ahmad Nabhan	anabhan123@gmail.com	Mark Krasnow	Department of Biochemistry, Stanford University School of Medicine, Stanford, CA, USA.; Howard Hughes Medical Institute, USA.
Saba Nafees	saba.nafees@czbiohub.org	CZ Biohub	Chan Zuckerberg Biohub, San Francisco, CA, USA.
Norma Neff	norma.neff@czbiohub.org	CZ Biohub	Chan Zuckerberg Biohub, San Francisco, CA, USA.
Patrick Neuhöfer	pneuhoef@stanford.edu	Steve Artandi	Stanford Cancer Institute, Stanford University School of Medicine, Stanford, CA, USA.; Department of Medicine, Stanford University School of Medicine, Stanford, CA, USA.; Department of Biochemistry, Stanford University School of Medicine, Stanford, CA, USA.
Patricia Nguyen	pknguyen@stanford.edu	Patricia Nguyen	Department of Medicine, Stanford University School of Medicine, Stanford, CA, USA.; Stanford Cardiovascular Institute, Stanford, CA, USA.; Division of Cardiovascular Medicine, Stanford University, Stanford, CA, USA.
Jennifer Okamoto	jenokamoto@gmail.com	CZ Biohub	Chan Zuckerberg Biohub, San Francisco, CA, USA.
Julia Olivieri	jolivier@stanford.edu	Julia Salzman	Institute for Computational and Mathematical Engineering, Stanford University, Stanford, CA, USA.
Youcef Ouadah	yzouadah@caltech.edu	Mark Krasnow	Department of Biochemistry, Stanford University School of Medicine, Stanford, CA, USA.; Program in Cancer Biology, Stanford University School of Medicine, Stanford, CA, USA.
Honor Paine	honor.paine@ucsf.edu	Bruce Wang	Department of Medicine and Liver Center, University of California San Francisco, San Francisco, CA, USA.
Peter Parham	peropa@stanford.edu	Peter Parham	Department of Structural Biology, Stanford University School of Medicine, Stanford, CA, USA.; Department of Microbiology and Immunology, Stanford University School of Medicine, Stanford, CA, USA.
Jozeph L. Pendleton	zephpen@stanford.edu	Mark Krasnow	Department of Biochemistry, Stanford University School of Medicine, Stanford, CA, USA.; Howard Hughes Medical Institute, USA.
Lolita Penland	lpenland@calicolabs.com	CZ Biohub	Chan Zuckerberg Biohub, San Francisco, CA, USA.
Martine Perret	martine.perret@mnhn.fr	Martine Perret	Adaptive Mechanisms and Evolution (MECADEV), UMR 7179, National Center for Scientific Research, National Museum of Natural History, Brunoy, France.
Angela Oliveira Pisco	angela.pisco@czbiohub.org	CZ Biohub	Chan Zuckerberg Biohub, San Francisco, CA, USA.
Zhen Qi	zhenqi@stanford.edu	Michael Clarke	Institute for Stem Cell Biology and Regenerative Medicine, Stanford University School of Medicine, Stanford, CA, USA.
Stephen R. Quake	steve@czbiohub.org; steve@quake-lab.org	Stephen Quake; CZ Biohub	Department of Bioengineering, Stanford University, Stanford, CA, USA.; Chan Zuckerberg Biohub, San Francisco, CA, USA.; Department of Applied Physics, Stanford University, Stanford, CA, USA.
Ute Radespiel	ute.radespiel@tiho-hannover.de	Ute Radespiel	Institute of Zoology, University of Veterinary Medicine Hannover, Germany.
Thomas A. Rando	rando@stanford.edu	Thomas Rando	Department of Neurology and Neurological Sciences, Stanford University School of Medicine, Stanford, CA, USA.

Hajanirina Noëline Ravelonjanahary	hajanravel@gmail.com	Mark Krasnow	Department of Animal Biology, Faculty of Science, University of Antananarivo, Antananarivo 101, BP 566, Madagascar.
Andriamahery Razafindrakoto	amaherix@gmail.com	Mark Krasnow	Department of Animal Biology, Faculty of Science, University of Antananarivo, Antananarivo 101, BP 566, Madagascar.
Julia Salzman	horence@stanford.edu	Julia Salzman	Department of Biochemistry, Stanford University School of Medicine, Stanford, CA, USA.; Department of Biomedical Data Science, Stanford University, Stanford, CA, USA.
Nicholas Schaum	ndschaum@gmail.com	Tony Wyss-Coray	Department of Neurology and Neurological Sciences, Stanford University School of Medicine, Stanford, CA, USA.
Robert Schopler	bobby.schopler@duke.edu	Duke Lemur Center	Duke Lemur Center, Durham, NC, USA.
Bronwyn Scott	bronwyns@stanford.edu	Albert Wu	Department of Ophthalmology, Stanford University School of Medicine, Stanford, CA, USA.
Liza Shapiro	liza.shapiro@austin.utexas.edu	Liza Shapiro	Department of Anthropology, University of Texas at Austin, Austin, TX, USA.
Hosu Sin	hosu@stanford.edu	Margaret Fuller	Department of Developmental Biology, Stanford University School of Medicine, Stanford, CA, USA.
Rahul Sinha	sinhar@stanford.edu	Irving Weissman	Stanford Institute for Stem Cell Biology and Regenerative Medicine, Stanford, CA, USA.
Rene Sit	rene.sit@czbiohub.org	CZ Biohub	Chan Zuckerberg Biohub, San Francisco, CA, USA.
Geoff Stanley	gmstanle@stanford.edu	Stephen Quake	Department of Bioengineering, Stanford University, Stanford, CA, USA.
Lubert Stryer	stryer@stanford.edu	Lubert Stryer	Department of Neurobiology, Stanford University School of Medicine, Stanford, CA, USA.
Varun Ramanan Subramaniam	varunramanan608@gmail.com	Albert Wu	Department of Ophthalmology, Stanford University School of Medicine, Stanford, CA, USA.
Aditi Swarup	aswarup@stanford.edu	Albert Wu	Department of Ophthalmology, Stanford University School of Medicine, Stanford, CA, USA.
Weilun Tan	weilun.tan@czbiohub.org	CZ Biohub	Chan Zuckerberg Biohub, San Francisco, CA, USA.
Alexander Tarashansky	tarashanst@gmail.com; alexander@tarashansky.com	Bo Wang; CZ Biohub	Department of Bioengineering, Stanford University, Stanford, CA, USA.; Chan Zuckerberg Biohub, San Francisco, CA, USA.
Aris Taychameekiatchai	aris.taychameekiatchai@ucsf.edu	Bruce Wang	Department of Medicine and Liver Center, University of California San Francisco, San Francisco, CA, USA.
Jérémy Terrien	jeremy.terrien@mnhn.fr	Jérémy Terrien	Adaptive Mechanisms and Evolution (MECADEV), UMR 7179, National Center for Scientific Research, National Museum of Natural History, Brunoy, France.
Kyle J. Travaglini	ktrav@stanford.edu	Mark Krasnow	Department of Biochemistry, Stanford University School of Medicine, Stanford, CA, USA.; Howard Hughes Medical Institute, USA.
Andoni Urtasun	a.urtasun.arricaberri@gmail.com	Thomas Rando	Department of Neurology and Neurological Sciences, Stanford University School of Medicine, Stanford, CA, USA.
Sivakamasundari V	sivav@stanford.edu	Philip Beachy	Institute for Stem Cell Biology and Regenerative Medicine, Stanford University School of Medicine, Stanford, CA, USA.
Avin Veerakumar	avinv@stanford.edu	Mark Krasnow	Department of Biochemistry, Stanford University School of Medicine, Stanford, CA, USA.; Department of Bioengineering, Stanford University, Stanford, CA, USA.; Medical Scientist Training Program, Stanford University School of Medicine, Stanford, CA, USA.; Howard Hughes Medical Institute, USA.
Venkata N. P. Vemuri	pranathi.vemuri@czbiohub.org	CZ Biohub	Chan Zuckerberg Biohub, San Francisco, CA, USA.
Jean-Michel Verdier	jean-michel.verdier@ephe.psl.eu	Jean-Michel Verdier	MMDN, University of Montpellier, EPHE-PSL, INSERM, Montpellier, France.
Iwijn De Vlaminck	vlaminck@cornell.edu; idevlaminck@gmail.com	Iwijn De Vlaminck	Nancy E. and Peter C. Meinig School of Biomedical Engineering, Cornell University, Ithaca, NY, USA.
Douglas Vollrath	vollrath@stanford.edu	Douglas Vollrath	Department of Genetics, Stanford University School of Medicine, Stanford, CA, USA.
Bo Wang	wangbo@stanford.edu	Bo Wang	Department of Bioengineering, Stanford University, Stanford, CA, USA.
Bruce Wang	bruce.wang@ucsf.edu	Bruce Wang	Department of Medicine and Liver Center, University of California San Francisco, San Francisco, CA, USA.
Gefei Wang	gwangas@connect.ust.hk	Can Yang	Department of Mathematics, Hong Kong University of Science and Technology, Hong Kong SAR, China.
Michael F.Z. Wang	fw262@cornell.edu	Iwijn De Vlaminck	Nancy E. and Peter C. Meinig School of Biomedical Engineering, Cornell University, Ithaca, NY, USA.; Department of Computational Biology, Cornell University, Ithaca, NY, USA.
Sheng Wang	swang@cs.washington.edu	Sheng Wang	Paul G. Allen School of Computer Science & Engineering, University of Washington, Seattle, WA, USA.
James Webber	james.webber@czbiohub.org	CZ Biohub	Chan Zuckerberg Biohub, San Francisco, CA, USA.

Hannah Weinstein	hnw2105@cumc.columbia.edu	Franklin Huang	Division of Hematology/Oncology, Department of Medicine, University of California San Francisco, San Francisco, CA, USA.; Helen Diller Family Comprehensive Cancer Center, University of California San Francisco, San Francisco, CA, USA.; Bakar Computational Health Sciences Institute, University of California San Francisco, San Francisco, CA, USA.
Irving L. Weissman	irv@stanford.edu	Irving Weissman	Stanford Institute for Stem Cell Biology and Regenerative Medicine, Stanford, CA, USA.
Amanda L. Wiggenhorn	awiggen@stanford.edu	Jonathan Long	Department of Pathology, Stanford University School of Medicine, Stanford, CA, USA.; Department of Chemistry, Stanford University, Stanford, CA, USA.
Cathy V. Williams	cathy.williams@duke.edu	Duke Lemur Center	Duke Lemur Center, Durham, NC, USA.
Patricia Wright	Patricia.Wright@Stonybrook.edu; patchapplewright@gmail.com	Patricia Wright	Department of Anthropology, Stony Brook University, NY, USA.
Albert Y. Wu	awu1@stanford.edu	Albert Wu	Department of Ophthalmology, Stanford University School of Medicine, Stanford, CA, USA.
Angela Wu	angelawu@ust.hk	Angela Wu	Division of Life Science, Hong Kong University of Science and Technology, Hong Kong SAR, China.; Department of Chemical and Biological Engineering, Hong Kong University of Science and Technology, Hong Kong SAR, China.; Center for Aging Science, Hong Kong University of Science and Technology, Hong Kong SAR, China.
Tony Wyss-Coray	twc@stanford.edu	Tony Wyss-Coray	Department of Neurology and Neurological Sciences, Stanford University School of Medicine, Stanford, CA, USA.; Wu Tsai Neurosciences Institute, Stanford, CA, USA.
Bao Xiang	bxli@stanford.edu	Albert Wu	Department of Ophthalmology, Stanford University School of Medicine, Stanford, CA, USA.
Jia Yan	rose.yan@czbiohub.org	CZ Biohub	Chan Zuckerberg Biohub, San Francisco, CA, USA.
Can Yang	macyang@ust.hk	Can Yang	Department of Mathematics, Hong Kong University of Science and Technology, Hong Kong SAR, China.
Jinxurong Yang	jyang@diagnoa.com	Angela Wu	Division of Life Science, Hong Kong University of Science and Technology, Hong Kong SAR, China.
Anne D. Yoder	anne.yoder@duke.edu	Anne Yoder	Department of Biology, University Program in Genetics & Genomics, Duke University, Durham, NC, USA.
Brian Yu	brian.yu@czbiohub.org	CZ Biohub	Chan Zuckerberg Biohub, San Francisco, CA, USA.
Andrea R. Yung	andreay@stanford.edu	Mark Krasnow	Department of Biochemistry, Stanford University School of Medicine, Stanford, CA, USA.; Howard Hughes Medical Institute, USA.
Yue Zhang	helen18@stanford.edu	Mark Krasnow	Department of Biology, Stanford University, Stanford, CA, USA.; Howard Hughes Medical Institute, USA.
Jia Zhao	jzhaoaz@connect.ust.hk	Can Yang	Department of Mathematics, Hong Kong University of Science and Technology, Hong Kong SAR, China.
Zicheng Zhao	zczhao@stanford.edu; rezczhao@gmail.com	Megan Albertelli; Mark Krasnow	Department of Comparative Medicine, Stanford University School of Medicine, Stanford, CA, USA.; Howard Hughes Medical Institute, USA.